POLITECNICO DI TORINO

Master's Degree in Civil Engineering

Master's Degree Thesis

Numerical Modelling of Double-O-Tube Tunnelling in Stiff Clays

Supervisors:

Prof. **Lidija ZDRAVKOVIC**
Prof. **Marco BARLA**

Candidate:

Mattia VATTUONE

Alla mia famiglia che mi ha insegnato a volare e a Federica con cui ho condiviso ogni gioia, dolore, sacrificio e successo di questo mio percorso.

Abstract

A preliminary numerical investigation of the effects in terms of tunnelling-induced ground movements in short- and long-term due to the construction of a Double-O-Tube tunnel in London clay beneath Hyde Park is presented. The model is calibrated against oedometer and undrained triaxial tests on intact samples of London Clay using a kinematic hardening soil model (named M2-SKH). The adoption of this advanced constitutive model is justified through the simulation of some drained and undrained triaxial tests on normal-consolidated and over-consolidated samples. The results are compared to a recent analysis of the excavation of the new Crossrail twin tunnels, which provides excellent predictions of the measurements obtained with the available field monitoring data. The influence of the permeability of the lining significantly affects the short- and long-term predictions. The use of this technique not only allows a more efficient use of the underground space and a reduction in construction time, but also limits the negative effects due to the interaction between twin tunnels. The extension of the surface area affected by vertical settlements is very similar to that obtained by excavating the twin tunnels, but the values are slightly smaller. These encouraging results show that DOT shield tunnelling technology can be convenient compared to traditional techniques even when applied in stiff heavily overconsolidated clays.

Acknowledgment

First of all, I would like to thank the institutions of Imperial College London, the Universitè Grenoble Alpes and the Politecnico di Torino for allowing me to carry out these months of internship in which the following master thesis was prepared. In particular thanks to Prof. Lidija Zdravkovic and Prof. Cino Viggiani, thanks to whom I was able to carry out this project. Thanks to Ph.D student Ding Zhou who has always encouraged and followed me in my work. A special thanks to my academic tutor Prof. Marco Barla and my academic advisor Prof. Cecilia Surace for having supported me during my thesis period despite a very serious covid-induced disruption. I would like to thank all the guys who helped me in this path with technical advice and suggestions, in particular a special thanks to Wenjie, Giuseppe, Sara, Eli, Tom, Tara, Kika and Tokio. Thanks to all the members of the Imperial College geotechnical research group who welcomed me immediately into this adventure and with whom I shared pleasant moments inside and outside the working environment. An endless thank you to my family and to my girlfriend Federica who has always supported me in these years and to all my friends, a constant and indispensable presence to face every challenge in the best way.

Contents

List of Figures

List of Tables

Chapter 1

INTRODUCTION

1.1 Research description and objectives

This master thesis is an integral part of a current research project carried out within the geotechnics section of Imperial College London. Double-O-Tube (DOT) shield tunnelling technology was developed relatively recently in Japan and has been successfully used in several projects in eastern Asia including the construction of six sections of the Shanghai Metro in China. The main objective of this report is to investigate the short- and long-term effects in terms of tunnelling-induced ground movements that the use of this technique would produce in the particular geological conditions of central London, in heavily overconsolidated stiff clays.

Specifically, approaching the problem from a numerical point of view, the idea is to evaluate the results by comparing them with the trends obtained from the simulation of the excavation of the new Crossrail standard twin tunnels at the extensive monitored Hyde Park site. Consolidated coupled analyses are performed using the Imperial College Finite Element Program ICFEP applying advanced soil constitutive models including the two surfaces kinematic hardening soil model used to simulate the mechanical behaviour of London clay.

1.2 Thesis Overview

In chapter 2 the topic of this thesis is framed in the currently available literary context. Specifically, a first paragraph aims to introduce the DOT tunnelling technique and explain why its application in the London background may make sense. A series of increasingly complex empirical theories have tried over the years to describe the response of soil and pre-existing tunnels to the construction of a new tunnel, however, providing a too generalized point of view. The advent of numerical analysis has represented a big step forward allowing to reach much more precise results. Focusing on the response given by the

tunnelling in stiff overconsolidated London clay, Chapter 2 reports on the updates that have gradually made it possible to predict more and more accurate results up to those directly applied in this thesis.

Chapter 3 describes the process that led to the use of an advanced kinematic hardening 'bubble' model to describe the behaviour of London stiff overconsolidated clays. The characteristics of the model were analysed by running simulations of drained and undrained triaxial tests on stiff clay samples such as London's and soft clay samples such as Shanghai ones.

Chapter 4 reports the results of the numerical modelling of the excavation of the new Crossrail twin tunnels at the extensive monitored Hyde Park site. The analysis was carried out with the intention of reproducing and analysing the results obtained on previous versions of a more recent version of ICFEP and extending them over the long term by applying the latest available updates so as to provide a firm reference point for the next analysis.

Chapter 5 shows the results of the numerical analysis of a DOT tunnel in Hyde Park and compares the results with those previously obtained using the traditional twin tunnel technique. The entire analysis and in particular the dimensions of the tunnel are designed using the parameters of the previous analysis in order to produce results that are as comparable as possible.

The conclusions regarding the use of this new technique with respect to the one adopted are summarized in chapter 6 which also reports some thoughts regarding where further future research could focus.

Chapter 2

LITERATURE REVIEW

2.1 Context

2.1.1 Historical background

In parallel with the progressive development of large high-density urban centres, a radical rethinking of transport infrastructure was necessary in order to overcome traffic congestion and respond to the growing demand for a fast service network allowing people to move rapidly from one place to another one of the cities. The construction of tunnels in an urban environment and the development of underground networks has made possible to solve this problem.

Historically, the city of London has been an important forge for the advancement of the most modern excavation techniques. Brunel's Thames Tunnel was the first tunnel to be built under a navigable river and its construction was made possible by the use of the first rudimentary registered shield tunnel between 1825 and 1843. Since the world's first underground line was built in London using the destructive cut-and-cover technique by hand, the track of the Metropolitan line between Paddington and Farringdon Street which opened in 1863, more and more sophisticated excavation techniques have been adopted. The idea of Brunel was further enhanced by Barlow's intuition to build a cylindrical shield that allowed Greathead to quickly build in 1869 the Tower Subway, the second tunnel under the River Thames. As explained by West (1988) and Diamond & Kassel (2018), the real revolution of the Greathead shield was the possibility of erecting the bolted cast iron segments of lining, against which the shield was pushed forward with the help of hydraulic jacks, in the same time as the face excavation progressed.

This intuition allowed the construction of first underground bored tunnels underneath London's buildings around 1880 and remains at the basis of the most modern tunnel construction techniques. Excavation in north London was easier thanks to the characteristics of London Clay which is a consolidated and an

impermeable material that guarantees a good short-term resistance. However, it was clear from the beginning how the operation could be risky due to the settlement of the soil and on the impact on the surrounding structures over time. This problem still represents one of the main challenges of modern tunnelling (Mair, 1998).

2.1.2 Current construction techniques

The modern excavation techniques used in the London underground are summed up in Potts & Zdravkovic (2001) providing a global image of the range of technologies available in the world of tunnelling.
Today's evolution of the Greathead shield is represented by the closed face tunnelling machines better known as TBMs. The excavation proceeds by means of a rotating mechanical head that leverages on the lining which is gradually installed as the work proceeds. The different types of these machines are used according to the geological conditions of the site. The two main versions, the Slurry Shield and the Earth Pressure Balance (EPB) Shield, were used during the excavation of the DLR Lewisham Extension (Sugiyama *et al.*, 1999) and currently in the realization of the Crossrail (Black *et al.*, 2015).

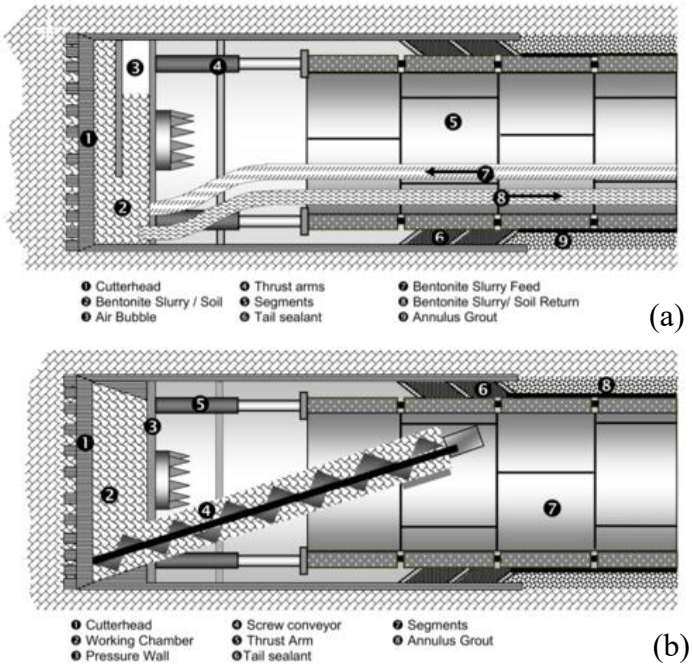

Fig. 2.1: *Rapresentations of TBMs machine: (a) Slurry Shield; (b) Earth Pressure Balance Shield (EFNARC, 2005)*

Fig. 2.1 shows a representation of these two types of machines. The idea is to apply a certain pressure to the tunnel face in order to limit the related ground

movements as much as possible. The first technique involves the injection of a slurry mixture of bentonite and spoils within the cutting bulkhead, the returning bentonite is separated from the mixture and pumped back into the chamber behind the cutter head. The Slurry Shield is suitable to operate in sites with very variable lithography, in soft ground and in high interstitial water pressures conditions. On the other hand, the Earth Pressure Balance machines exploit the excavated material to balance the pressure exerted by the ground against the tunnel face by collecting it inside a sealed excavation chamber. A screw conveyor removes the material in relation to the forward speed, on the type of soil in which it operates and how much the soil movements must be limited.

Sprayed Concrete Lining (SCL) is another type of technique that is usually used in soft ground. This method is reported as the New Austrian Tunnelling Method (NATM) and has been used in London in the construction of Crossrail stations. The technique involves the construction of a pilot tunnel and the continuation of the extension in subsequent phases with the use of sprayed reinforced concrete as a temporary support. Its ductility to many types of geotechnical conditions makes it perfect for the construction of non-circular tunnels, cross passages, platforms and short tunnels, but unlike TBMs, it does not guarantee control over soil movements.

The use of the most varied and modern tunnelling techniques in London's subsoil, summarised above, has enabled the city to meet the challenge of keeping pace with other major cities on the planet by building a transport system that would allow its citizens to move easily from one side of the city to the other. The challenge for the future is to continue to keep up with the times and to be able to improve. In the world of tunnelling this means being able, in the shortest possible time, to dig tunnels that limit as much as possible the movement of the ground ensuring the stability of the structure and of the surrounding buildings in the short and the long term trying to limit costs as much as possible.

2.1.3 Double-O-Tube shield tunnelling

A relatively recent type of technology that has never been used in London before is the Double-O-Tube (DOT) shield tunnelling. This technique was developed in Japan in the early 80's and then patented in 1987 after that the first prototype tunnel was built on site (Moriya, 2000). Starting from those years in Japan there was a growth in the construction of special shaped tunnels aimed at minimizing the use of underground space and realized through the use of special TBMs (Kuzuno *et al*., 1996). The DOT shield is a type of Earth Pressure Balance (EPB) Shield that exploits the combined action of two spoke cutterheads rotating in opposite directions to create a tunnel originated by the partial overlapping of two distinct circular sections (Fig. 2.2). Digging a single tunnel compared to two

separate bored tunnels has the advantage of reducing construction time, making cross-passages unnecessary and minimizing the impact on surrounding buildings (Chow, 2006). The first double-O tunnel was built in 1988 along the national road N.54 in Hiroshima, Japan. Although Japan continues to exercise leadership in the development of this technology, in recent years these machines have been used also in the construction of six sections of the Shanghai Metro in China (He *et al*., 2009) and on the construction of the Mass Rapid Transit system in Taipei, Taiwan (Fang *et al*., 2012).

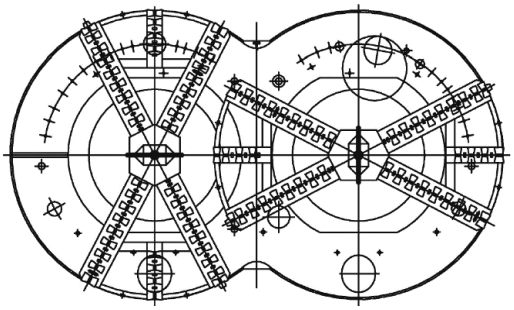

Fig. 2.2: *Section of the double circular shield used in Shanghai (He et al., 2009)*

Specifically, as can be seen from the previous image and described in Fang *et al.* (2012) each rotating head is equipped with four radial principals spoke and two auxiliaries spoke, four lateral copy cutters are used to correct the rolling of the shield. The tunnel lining consists of 11 segments erected in position by two independent erectors as the excavation proceeds and connected to each other by straight steel bolts. In particular, the central segments, called large and small seagull for their peculiar shapes and located above and below the pillar, are reversed from ring to ring. Above the upper seagull and below the lower seagull there are grouting holes made to facilitate the containment of the ground movements related to the tail void closure. The backfill grouting is performed manually through precast holes in the lining segments. Fig. 2.3 shows the section of the tunnel lining.

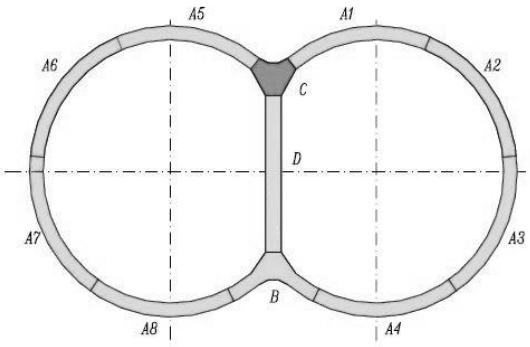

Fig. 2.3: *Section of the lining in Shanghai DOT tunnel (Chow, 2006)*

2.2 Soil movements due to tunnelling

2.2.1 Ground volume loss

This sub-paragraph describes the mechanism of ground volume loss due to tunnelling. As explained in Potts & Zdravkovic (2001), the excavation of a tunnel generates an immediate release of stress on the surrounding ground which results in a phenomenon of soil rearrangement. Soil tends to move towards the tunnel until a new equilibrium configuration is reached. From a practical point of view, if the excavated volume coincided with the design volume of the final tunnel, these movements would not leave time to erect the linings. Therefore, in order to overcome this technical problem, it is necessary to excavate an extra portion of soil in addition to the final volume. Assuming to be in undrained conditions, this difference in volume is equal to the integral of the surface settlement trough. The percentage given by the ratio between the excavated volume and the final theoretical volume is conventional called volume loss (V_L).

The analysis of soil movements, caused by a loss of volume related to the adopted shield tunnelling technique, reveals four main local phenomena that affect the short term response (Attewell, 1978): the *face loss* due to the release of the stress at the excavation front, which may cause the settlement at the surface ahead of the face; *shield loss* movements related to the radial displacements caused by the overcutting of the rotating head with respect to the size of the shield; the *tail void loss* which is due to the gap between the final part of the shield and the lining; and the generally small *lining deflections* that occur after grout injections in the space between the lining and the ground. Fig. 2.4 shows the various contributions.

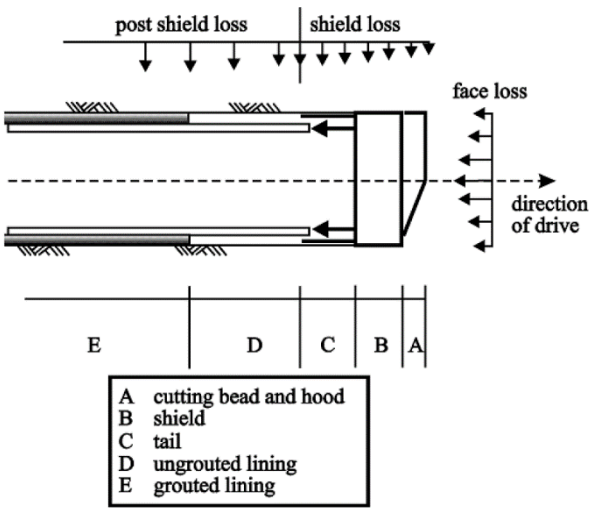

Fig. 2.4: *Ground movements induced by TBMs (Potts&Zdravkovic, 2001)*

In long term, further deformations are caused by the soil consolidation process. This is especially true in the case of clayey soils with the gradual dissipation of interstitial overpressures. Soil movements are influenced by the drainage effect of the tunnel related to the permeability of the lining. The settlement varies depending on the type of soil and on the use of different machines. Slurry Shields or Earth Pressure Balance greatly limit face loss phenomena, while Sprayed Concrete Lining does not include losses due to shield loss or tail void loss.

A separate more in-depth discussion can be made for the DOT tunnels. The initial consideration is that the actual data and available studies associated to this particular excavation technique in large cities are still limited to very few real cases compared to conventional circular shield tunnelling and mainly in soft clay conditions. Nevertheless, it is possible to report a further series of important observations from previous research related to the ground volume loss.

Although in general the mechanism of volume loss can be traced back to the reasons given above for generic Earth Pressure Balance TBMs, in this case the two cutter heads are spoked so it is more difficult to effectively balance the supporting pressure controlled by the speed of screw to earth pressure. According to Chow (2006), during the excavation this imbalance can lead to significant variations of the face volume loss generating surface settlements or in some cases heaves. Again, the space between the spoked cutter heads and the shield would represent a further cause of volume loss. Another factor to be taken into consideration is the opposite and synchronous rotation of the two cutting heads which generates the accumulation of lumps of soil at the groove causing an initial swelling which will turn into settlement over time.

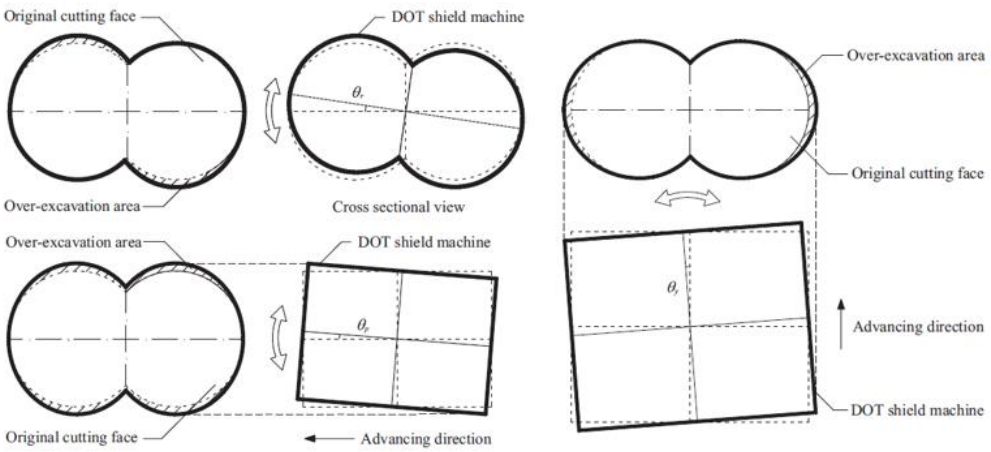

Fig. 2.5: *Over-excavated area caused by rolling, yawing and pitching in DOT tunnel (Ren et al., 2018).*

Frequent changes in trajectory are noticed during the tunnel excavation due to the asymmetrical longitudinal or transversal machine set-up on one side to the other or torque imbalances due to variable soil properties. The reasons and ways to correct the trajectory of DOT tunnels have been the subject of several studies (Zhang, 2004; Shen *et al.*, 2009, Ren *et al.*, 2018). As can be seen from Fig. 2.5, any deviation from the main trajectory, whether due to rolling, yawing or pitching, is associated with ground volume loss. The correction that can be made through back filling grouting cannot compensate too large deviations, so it is essential to always remain within a certain control range.

After dealing with the generalities and causes that contribute to the ground volume loss due to tunnelling, from an engineering point of view, it is essential to be able to define relationships that make it possible to quantify its entity a priori. Over time a series of different empirical formulations have been developed for the single circular shield tunnels in clays starting from those of Schmidt (1969), Glossop (1978) and Hurrell (1985) based on the parameter of the stability ratio N defined by Broms & Bennermark (1967) (Fig. 2.6):

$$N = \frac{\sigma_v - \sigma_t}{S_u}$$

Where σ_v is the total earth pressure at the axis of the tunnel, σ_t the tunnel supporting pressure and S_u the undrained shear strength of clays.

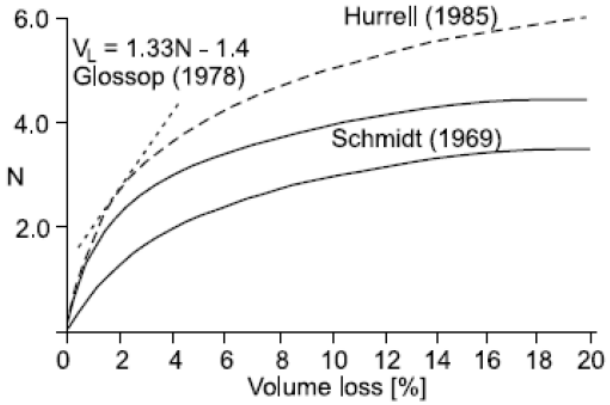

Fig. 2.6: *Relationship between the volume loss* $\boldsymbol{V_L}$ *and the stability ratio N (Lake et al., 1992)*

Further improvements have been made by Mair *et al.* (1981) and O'Reilly (1988) who parameterized the volume losses in relation to the load factor LF by analysing the results of a series of centrifugal tests considering that:

$$LF = \frac{N}{N_{TC}}$$

Where N is the stability ratio at working condition and N_{TC} at failure.

In 1999 Macklin formulated the following relationship integrating a series of recent experimental results:

$$V_L = 0.23e^{4.4(LF)}$$

In the context of the London clays, in situ analyses reveal low V_L values. Generally, for open face shield tunnels they are in the range of 1-2% with some exceptions reported over the years such as those measured in the greenfield site of St. James Park (Standing *et al.*, 1996), in which the parameters of the numerical analysis reported in the following chapters were calibrated and V_L were measured between 2.9% and 3.3%. This unexpected result was attributed by subsequent research (Standing & Burland, 2006) as due to particular geological factors and to the fast speed of excavation of the Jubilee Line Extension bored holes. Referring to the use of EPB TBMs, the ratio still drops to values between 0.25% and 1%.

Compared to previous reports relating to single circular shield tunnels, the calculation of the volume loss for DOT tunnels is more complex. However, through the superposition method it is possible to define a value by combining the results referred to two partially overlapping single tunnels considering the particular shape of the new gap between shield and lining (Ren *et al*., 2018). The contribution of the variations of trajectory can be assessed through expansion coefficients with respect to the angle of deviation. In soft clay it may even be relevant to consider the loss of effectiveness of the injected grout slurry. A formula that considers all this series of factors has been proposed by Ren *et al*. (2018):

$$V_L = (\Delta V + \Delta V_P + \Delta V_Y + \Delta V_R + \eta V_S)/V_{DOT}$$

Where ΔV is the gap volume between the DOT shield machine and the linings, ΔV_P, ΔV_Y and ΔV_R are the over-excavated volume due to pitch, yawing and rolling, η is a reduction coefficient, V_S the grouting volume of slurry and V_{DOT} the volume of the final DOT tunnel.

2.2.2 Ground surface settlement

Volume losses due to tunnelling result in the formation of ground settlement troughs. The challenge of predicting the magnitudes of these surface settlements through mathematical formulations is one of the most important problems in geotechnical engineering. The reference system on which the problem is based is illustrated in Fig. 2.7.

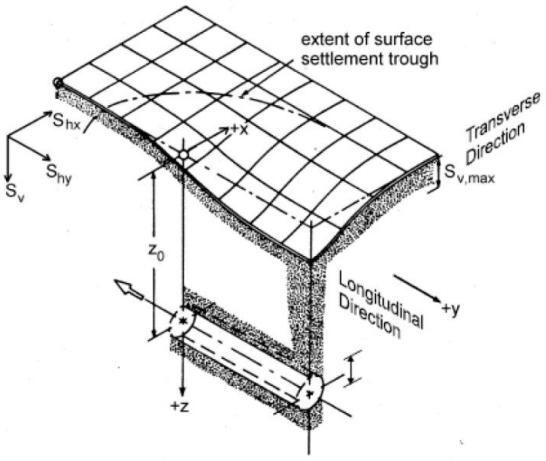

Fig. 2.7: *Representation of the three-dimensional settlement trough problem (Attewell et al., 1986)*

The first contribution was made by Peck (1969) who formulated an empirical formulation according to which transversal failure can be described through the form of a Gaussian function:

$$S_v(x) = S_{v,max} e^{-\frac{x^2}{2i_x^2}}$$

Where $S_{v,max}$ is the maximum surface settlement above the tunnel centre axis, x is the offset distance from the tunnel centreline and i_x the distance between the inflection point of the trough function and the centreline which is the standard deviation of the Gaussian equation.

For tunnels excavated in different types of materials Peck related the width of the subsidence to the depth of the excavation by measuring the relationship between the dimensionless parameters i/R and z/2R where R is the radius of the tunnel and z is the depth. From the integral of this function it is possible to obtain the volume loss for linear length V_s from which in undrained condition it is easy to obtain the percentage of the ground volume loss:

$$V_s = \sqrt{2\pi} i_x S_{v,max} \approx 2.5 i_x S_{v,max}$$

$$V_L = \frac{V_s}{V_t} \cdot 100\% \qquad V_t = \frac{\pi D^2}{4}$$

Where V_t is the volume of the final tunnel for linear length and D the diameter of the tunnel.

From the combination of the above equations, the following formula, describing the trend of the transverse settlement trough for a single circular shield tunnel as shown in Fig. 2.8 can be obtained:

$$S_v(x) = \sqrt{\frac{\pi}{2}} \frac{V_L D^2}{4 i_x} e^{-\frac{x^2}{2 i_x^2}}$$

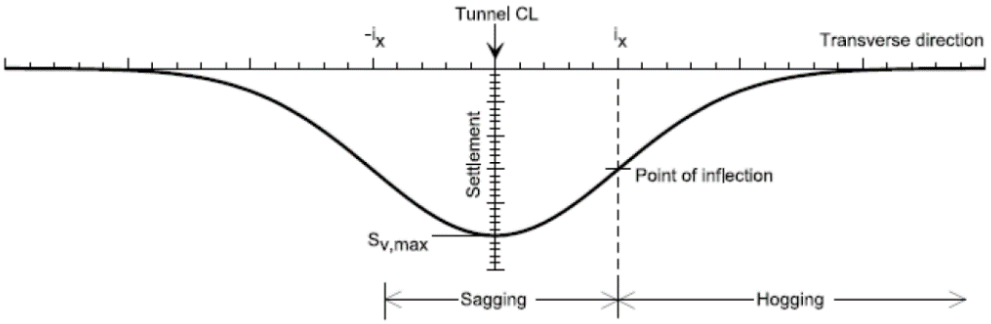

Fig. 2.8: *Transversal surface settlement (Franzius, 2004)*

Further experimental investigations, such as those described by O'Reilly & New (1982) investigated more in depth the correlation between i_x and other parameters such as the tunnel axis depth z_0 and have defined the following formulation for London clays considering small diameter tunnels at shallow depths (z_0<20m):

$$i_x = 0.43 z_0 + 1.1$$

Or more simply, considering for clays K values very close to 0.5, such as:

$$i_x = K z_0$$

The other part of the problem concerns the horizontal displacements. The formulation developed by O'Reilly & New (1982) considers the horizontal component of the field of vector displacements pointing towards the centreline of the tunnel described as:

$$S_{hx} = -\frac{x S_v(x)}{z_0}$$

From which the function of horizontal strains $\varepsilon_{hx}(x)$ can be easily derived:

$$\varepsilon_{hx}(x) = \frac{S_v(x)}{z_0} \left(\frac{x^2}{i_x^2} - 1 \right)$$

Fig. 2.9 below shows the distribution of horizontal displacements and strains. The displacements directed towards the central axis of the tunnel and the tensile strains are assumed to be positive:

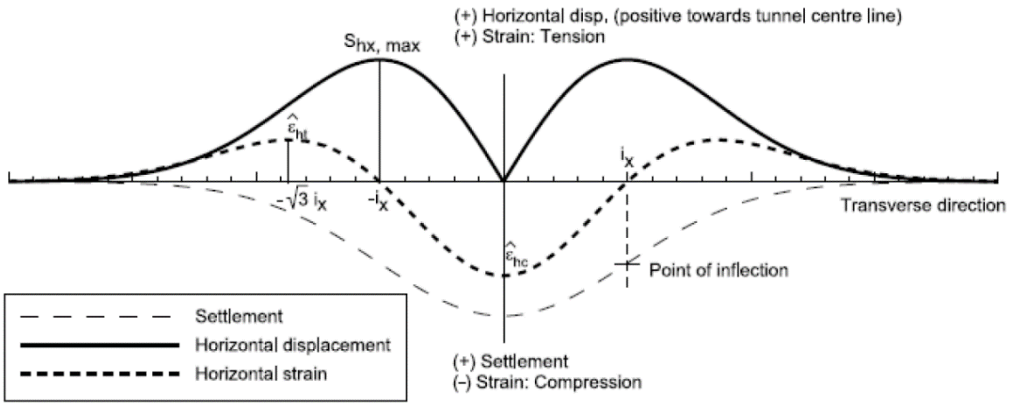

Fig. 2.9: *Transversal surface vertical and horizontal displacements (Franzius, 2004)*

The problem of longitudinal surface settlement was addressed by Attewell & Woodman (1982). The empirical formulation describing the phenomenon as a function of y is expressed in terms of cumulative probability ϕ and respect to the maximum value of the Gaussian transverse settlement:

$$S_v(y)_{x=0} = S_{v,max}\phi\left(\frac{y}{i_y}\right)$$

Which can be explicit in form:

$$S_{hy}(y)_{x=0} = \frac{V_L D^2}{8z_0} e^{-\frac{y^2}{2i^2}}$$

In London clay, the percentage of surface settlement at the face of the tunnel in relation to $S_{v,max}$ was computed to be between 30% and 50% depending on the used excavation technique (Fig. 2.10). In many cases the value i_y is assumed to be equal to the value i_x although subsequent research (Attewell *et al.*, 1986) has shown that in many cases i_x is wider than i_y.

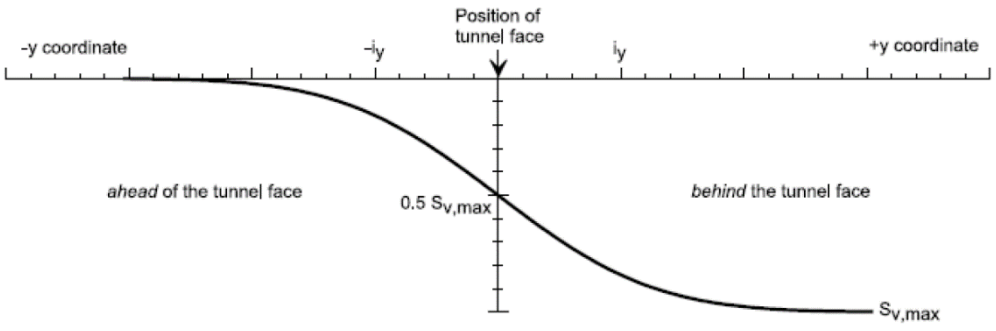

Fig. 2.10: *Longitudinal surface settlement (Franzius, 2004)*

The DOT tunnelling technique requires a different treatment. The empirical theories available refer to the formulations seen so far for single circular tunnels and are based on two different lines of thought.

The equal area method reported in Zhang (2007) suggests to approximate DOT shield soil displacements to those generated by an equivalent circular shield tunnel with radius R_{eq}. The transformation is carried out through the analysis of in situ data by calculating $V_{s,DOT}$ per linear length and placing it equal to the integral of the settlement trough due to the circular tunnel of equivalent radius R_{eq}. The cross-section area of the DOT tunnel is placed equal to that of the equivalent single circular tunnel (Fig. 2.11). In this way it is possible to obtain the approximate Gaussian function of the transversal settlement using the i_x obtained through Peck's adimensional graphs and calculating $S_{v,max}$ from the inverse relation of V_s.

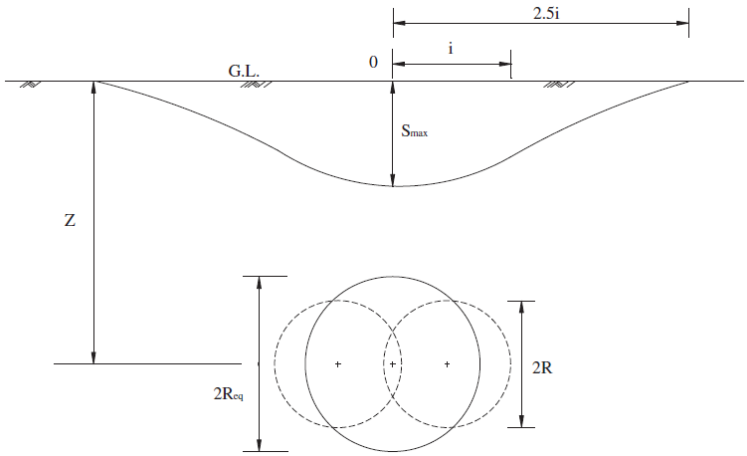

Fig. 2.11: *Ground surface settlement with the equal area method (Fang et al., 2012)*

The other method has been discussed by Fang *et al.* (1994) and is applicable in the particular case of negligible interactions between two tunnels, i.e. when the two tunnels are built parallel and at the same time. This superposition method assumes the surface settlement equal to the sum of the settlement associated with 1st tunnel plus those associated with 2nd tunnel. Under symmetrical conditions this means that each tunnel suffers a ground volume loss of 50% of the total. Fig. 2.12 shows the surface settlement associated with each tunnel and their sum.

These theories refer to ideal situations. In reality, the field of displacements is practically always influenced by external interactions, by the inhomogeneous characteristics of the soil, by phenomena related to viscosity and plasticity. The region closest to the tunnel is affected by soil plasticisation phenomena whose extent may vary depending on the type of soil and the excavation method, so that the relationship between the volume of surface settlement trough and the ground

volume loss at the level of the tunnel is much more complex than the theories described above. However, from the in situ analyses (Zhou et al., 2005), the deviations from the main trend attributable to the phenomena described above seem to play a secondary role and in general the Gaussian distribution is very well suited to describe the trend of transverse surface subsidence induced by the DOT tunnel.

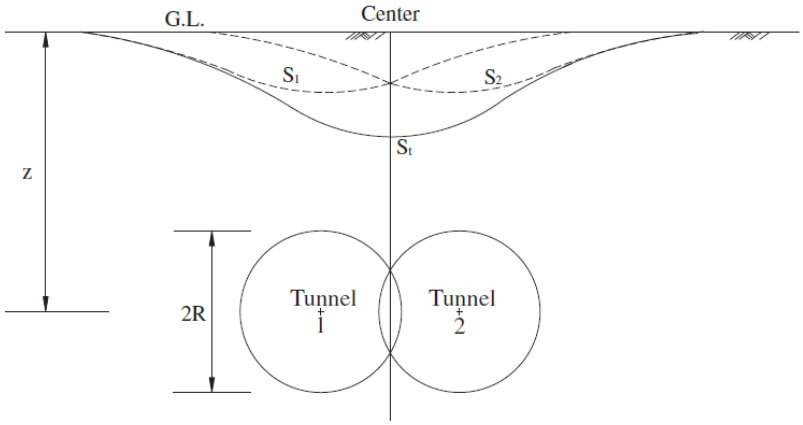

Fig 2.12: *Ground surface settlement with the superposition method (Fang, et al., 2012)*

2.2.3 Subsurface ground movements

Surface settlements represent only the most tangible effect of underground movements induced by tunnelling. To understand internal phenomena such as interactions between underground structures, it is necessary to develop the problem of movements related to depth.

A first expression is obtained by replacing z_0 with the term $z - z_0$ within the equation of i_x (O'Reilly & New, 1982) described in the previous sub-paragraph:

$$i_z = K(z - z_0)$$

Where z is the desired depth at which the Gaussian transversal settlement is obtained with K values close or equal to 0.5.

However, in contrast to what was previously hypothesized, the experimental results obtained from subsequent research (Mair *et al*., 1993) have shown that the width of the settlement trough decreases much more gradually as the depth increases according to the following interpolation law:

$$\frac{i_z}{z_0} = 0.175 + 0.325(1 - \frac{z}{z_0})$$

The comparison between the two functions can be appreciated in Fig. 2.13.

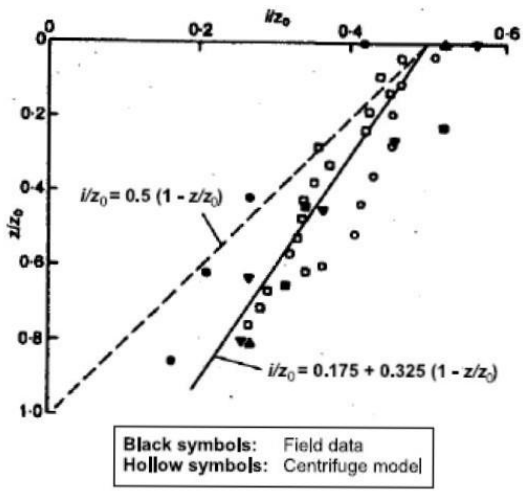

Fig. 2.13: *Trends of the trough width parameter* $\boldsymbol{i_z}$ *in relation to the depth (Mair et al., 1993)*

So, the new expression of K turns out to be:

$$K = 0.325 + \frac{0.175}{1 - \frac{z}{z_0}}$$

In 2008 the Geotechnical Consulting Group in London derived an improved expression related to the tunnel invert level z_{inv} through in situ data analysis. The results are more reliable the closer z is to the level of the tunnel crown. The relationship in which m is equal to 0.5 is as follows:

$$i_z = i_{surf}\left(\frac{z_{inv} - z}{z_{inv}}\right)$$

Where i_{surf} is the width parameter at the surface.

In the same research the issue of horizontal displacements is addressed. As a result, the displacement vectors are assumed to be directed towards a point of sink located at a distance Δz_{ps} below the axis of the tunnel:

$$\Delta z_{ps} = \left(\frac{1}{m} - 1\right)(z_0 - z_s)$$

Where z_s is the distance of the considered horizontal line from the ground level.

2.3 Numerical analysis of tunnelling in stiff clays

The empirical solutions seen above are a good tool to understand and roughly quantify the mechanism of soil movements due to tunnelling. However, their use is linked to several stringent conditions that make them unsuitable to deal with engineering problems according to modern design criteria. Their use can only be useful in a preliminary study phase, while the main role is played by numerical analysis which is a tool that allows to overcome the shortcomings of the empirical laws.

The advantages of numerical analysis and specifically of the finite element method compared to approximations of closed-form solutions and simple methods such as limit analysis are numerous. First of all, it is possible to simulate complex geometries such as DOT tunnel in multi-layers geometry without having to use the equal area or superposition method. Another great advantage is the possibility to simulate the entire construction process and analyse its effects from short to long term in relation to the implemented parameters. The real behaviour of the soil can be simulated according to the materials and by adopting different types of constitutive model available to incorporate its geological history. In the context of tunnelling the response of the lining elements can be obtained, for example, evaluating the effects of particular types of joints on the global structure. In addition, the problem can easily take into account the effects of interstitial pressures, reproducing the effects of a flow of water described in the coupled theory. Last but not least, a really useful advantage of the finite element method is to be able to take into account the effects of interactions between underground structures.

This paragraph will analyse in detail those theoretical aspects concerning the finite element method useful to be able to carry out the Imperial College Finite Element Program ICFEP simulations contained in this thesis drawing on previous research and the theoretical notions provided by the manuals (Potts & Zdravkovic, 1999, 2001).

2.3.1 Simulation of the construction process

Although modern technology makes it possible to simulate the construction process even on a three-dimensional level, most numerical analyses are still carried out two-dimensionally. In fact, performing complex numerical analyses can be very costly from a computational and economic point of view. This means having to make assumptions in order to modelling in plane strain.

After generating a mesh grid suitable for analysing the problem, it is necessary to set the initial conditions of the terrain simulating the effects of its geological history. At this point, the elements involved in the excavation of the

tunnel can be removed and the conditions at the edge adapted. Boundary conditions are one of the essential elements to perform a finite element numerical analysis. The loading and flow conditions act on the right-hand side of the global equilibrium equation, while the boundary conditions on displacements and water pressures on the left-side. Specifically, there are several ways to model the excavation of a tunnel such as:

- The *gap method* (Rowe *et al*., 1983) in which the initial and final position of the tunnel is given a priori. The gap represents the associated ground volume loss and is given by the difference between the diameters of the initial and final tunnel. Once the elements of the excavation are removed the nodes of the elements at the edge of the tunnel are free to move until the final configuration is reached. This state marks the beginning of the soil-lining interaction phase.
- Also in the *convergence confinement method* (Panet & Guenot, 1982) the ground volume loss is known a priori. Before the start of the modelled excavation the internal effort gradually decays proportionally to λ. This variable varies incrementally from 0 until a fixed value λ_d is reached. This point marks the construction of the lining and the beginning of the resulting soil-lining stresses.
- The *progressive softening method* (Swoboda, 1979) was developed in order to simulate the excavation technique of the New Austrian Tunnelling Method (NATM). Similarly to the λ method, in this case the stiffness of the soil is proportionally reduced in relation to β before the sequential removal of the excavated elements.
- The *volume loss control method* (Addenbrooke *et al*., 1996) refers to the value of the ground volume loss. The approach is equivalent to the λ method: the nodal internal forces are reduced in order to simulate the excavation process until a final ground volume loss value is reached (Fig. 2.14). This method has been used in most of the research conducted by the Imperial College and will be adopted also in this case. As previously seen, the ground volume loss is an important parameter that is increasingly used as a design request in the tunnelling projects.

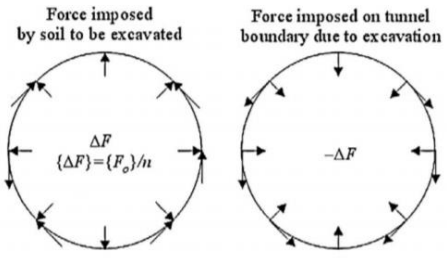

Fig. 2.14: *Modelling of solid elements excavation (Potts & Zdravkovic, 2001)*

2.3.2 Short term response

Plausible predictions of the numerical analysis performed in the stiff over consolidated clay in London, as detailed in Chapter 3, require the adoption of models that can at least reproduce the pre-failure non linearity. Despite this, the road to obtaining results that could be the representation of the real in situ data was long. Swallower and wider surface settlements functions than real trough were often achieved.

The calibration of the model adopted in the numerical simulations of this research was carried out by Avgerinos *et al* (2016) with reference to the results of the in situ analysis in the greenfield section of Jubilee Line Extension beneath St. James's Park (Standing *et al*., 1996). As previously reported on this location, unusually high values of ground volume loss equal to 3.3% were measured.

Experimental evidence on over consolidated London clay samples immediately revealed markedly non-linear and inelastic behaviour in the small strain range (Jardine, 1984; Burland, 1990). From a numerical point of view, the importance of considering non-linearity pre-yield in order to predict a better trend of transversal surface settlement in short-term due to tunnelling than the linear elastic case was demonstrated by Addenbrooke *et al*. (1997). Fig. 2.15 shows the result of his numerical analysis, the forecasts of the non-linear elastic models developed by Jardine *et al*. (1986) J4, and by Puzrin & Burland (1998) L4, are still far from describing the trend of the data collected in situ, but show a clear improvement compared to the simple linear elastic perfectly plastic Mohr-Coulomb case.

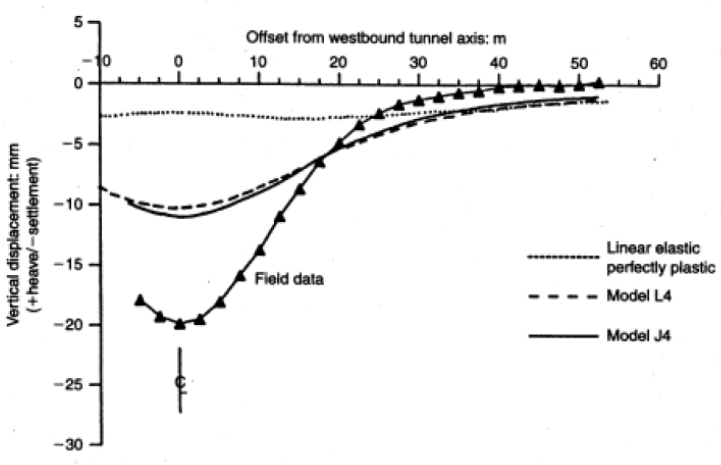

Fig. 2.15: *Surface Settlement profiles with different pre-yiled models for excavation of the Westbound tunnel at St. James's Park (Addenbrooke et al., 1997)*

Addenbrook *et al*. (1996) also helped to demonstrate the impact of the coefficient of earth pressure at rest K_0 on surface settlement predictions.

Numerical results revealed that the lower the K_0 values surrounding the tunnel, the deeper and narrower the trough function. In situ analysis showed that as the excavation progressed, the effective stress ratio increased in the upper and lower vicinity of the tunnel, while it decreased at the sides (Potts & Zdravkovic, 1999). On the other hand, anisotropic transverse stiffness within realistic values did not seem to have much influence on the trend of settlements.

The modified kinematic hardening models introduced by Grammatikopoulou (2004) allowed the integration in the numerical analysis of the London clay stress history on which its rigidity depends. On St. James's Park case the geological history includes the removal of 200m of London clay and the following deposition of made ground and alluvium layers. The results of her researches showed that increasingly sophisticated kinematic hardening models applied at the Saint James's Park site led to greater and narrower predictions than Addenbrooke et al (1997) ones, but again still far from the results obtained on the field (Fig. 2.16). This improvement was confirmed by Masin & Herle (2005) who compared different constitutive models applied to a NATM tunnel in London Clay and concluded how important it's to take into account the dependence of stiffness on stress path direction and its geological history to obtain better results.

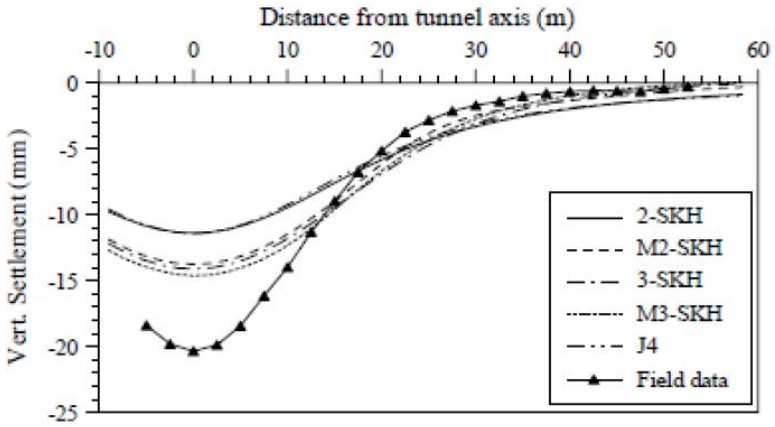

Fig. 2.16: *Comparison between surface settlement troughs using different models (Grammatikopoulou, 2004)*

A decisive contribution was given by the research of Hight *et al.* (2007) and Gasparre *et al.* (2007a,2007b,2008) who, through the analysis of experimental data, concluded that the elastic stiffness ranges were much lower than those previously used and that the history of stress in more advanced models influenced stiffness only before touching the Y2 surface. In his numerical model Gonzalez *et al.* (2012) continued the development of research demonstrating

how important it is to structure the constitutive model of the geological profile, but he didn't include in the model the effects of its geological history.
In the last available contribution of Avgerinos *et al.* (2014) to which this thesis refers, it was possible to achieve a good degree of approximation between numerical result and in-situ detection highlighting the importance of the link between stiffness degradation and strains. His research compares four numerical analyses, calibrated on experimental data obtained from oedometric and undrained triaxial tests considering the values related to elastic stiffness precedents and antecedents to the measurements on London Clay samples from Heathrow terminal 5 (Gasparre, 2005; Hight *et al.*, 2007). The response is controlled by the shear behaviour of the material and different calibrations lead to different results in K_0 profiles and in the yield stress ratio YSR. Avgerinos *et al.* (2016) concludes that short-term predictions do not seem to be influenced by the initial elastic stiffness, but more by the unloading percentage. From the graph in Fig. 2.17 it is clear that the best predictions in this case are those calibrated by the triaxial test without integrating the experimental results of the oedometer unloading path. Rather than the initial stiffness, it is the distribution of stiffness that becomes relevant in the short-term behaviour.

Analysis	Volume loss from radial displacement: %	Unloading: %
Low triaxial	3·39	13·5
High triaxial	3·38	23·5
Low both	3·40	26·5
High both	3·37	37·0

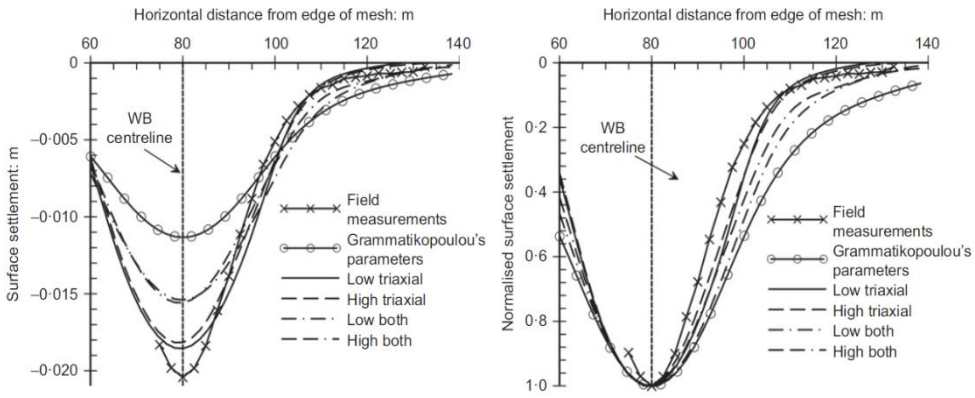

Fig. 2.17: *Surface and normalised surface settlements profile due to WB tunnel excavation for the four different analysis (Avgerinos et al., 2014)*

The importance of the stiffness degradation curve in the bubble model is supported by a subsequent analysis in which, through the variation of a

parameter associated directly with the rate of stiffness degradation after the elastic range, the strong influence it has on the K_0 profile is demonstrated.

The subsurface soil displacements are also captured quite well for all four cases. The maximum vertical displacement is located just above the crown of the tunnel because the stiffness degradation degrades to almost equal value for all calibrations. While below the invert, heave is predicted. Calibration based on both triaxial and oedometric data predicts slightly underestimated vertical displacements compared to in situ measurements, while results are excellent when only triaxial results are taken into account, especially if low. The horizontal displacements of numerical analyses, except in the first 20 metres depth where in situ data are unrealistic, retrace quite well the trend of the measured data (Fig. 2.18).

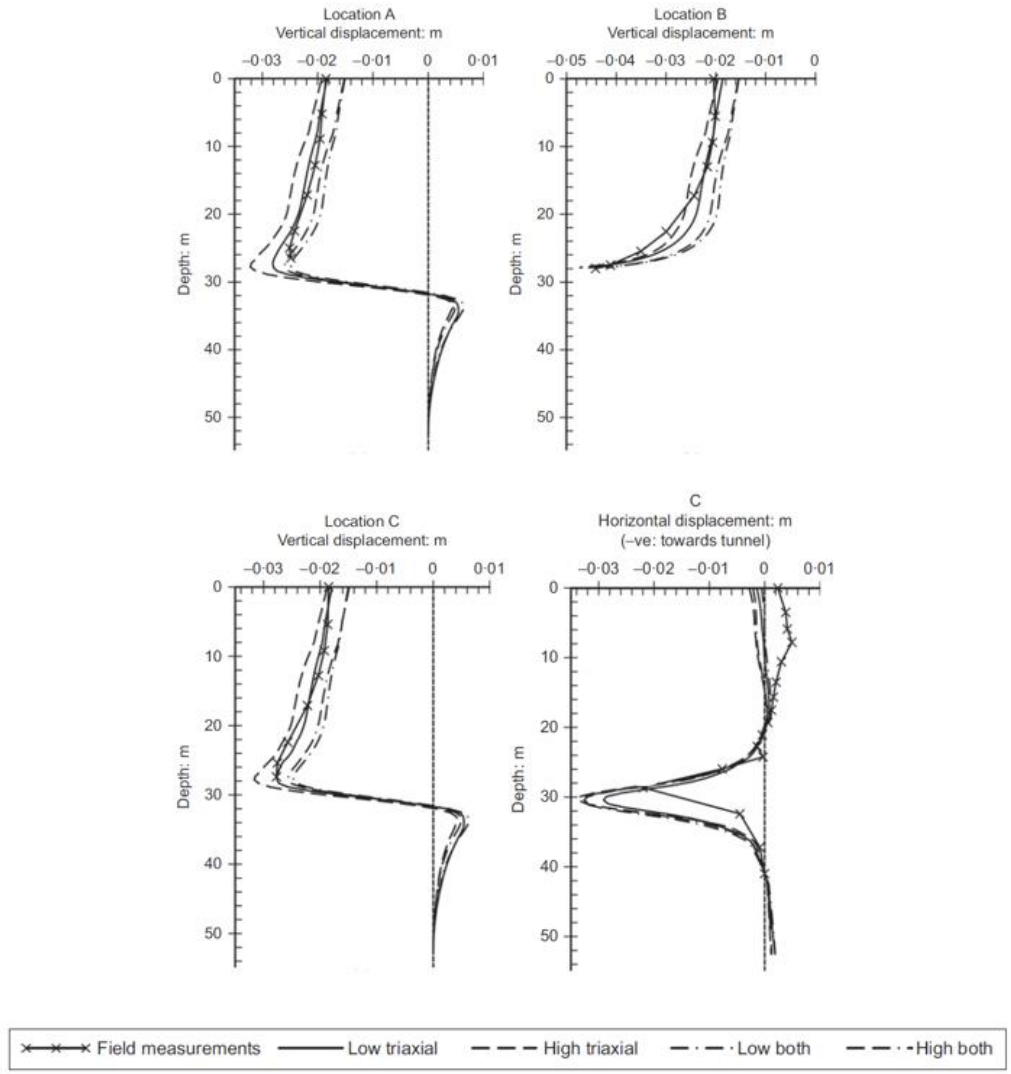

Fig. 2.18: *Distribution of the vertical and horizontal displacements with depth due to WB tunnel excavation in different locations (Avgerinos et al., 2014)*

2.3.3 Long term response

Long-term stability is one of the requirements of tunnel design. This type of survey represents one of the biggest challenges in geotechnical engineering because there are few field data available and the errors that are mitigated in the short term accumulate more and more over time.

Long-term soil movements are affected by the process of dissipation of the pore water overpressures altered as a result of tunnel excavation. The mechanical response of the soil is influenced, according to Mair & Taylor (1997), by the permeability and compressibility of the soil, by the relationship between the pre- and post-excavation conditions of the water pressures and by the permeability of the soil-lining interface which alters the hydraulic boundary condition of the site.

Observing the in-situ revelations Mair (1998) concluded that long term-surface settlements become wider and deeper than the short-term ones. Since the first analyses at St. James's Park (Nyren, 1998) a marked increase in long-term surface settlement emerged, after two years the trough had already doubled. From the comparison between the settlements of the St. James's site and Elizabeth House at Waterloo (Fig. 2.19) it emerges that the magnitude of vertical movements at St. James's after 11 years was five times higher than the other site. Mair (2008) attributed these differences to the different initial distribution of water pressures at the two sites and to the differences in permeability between the two interfaces soil-linings. At St. James's Park where the lining consists of not grouted expanded concrete segments the permeability is higher than the sprayed concrete with secondary reinforced concrete layer at Elizabeth House, Waterloo.

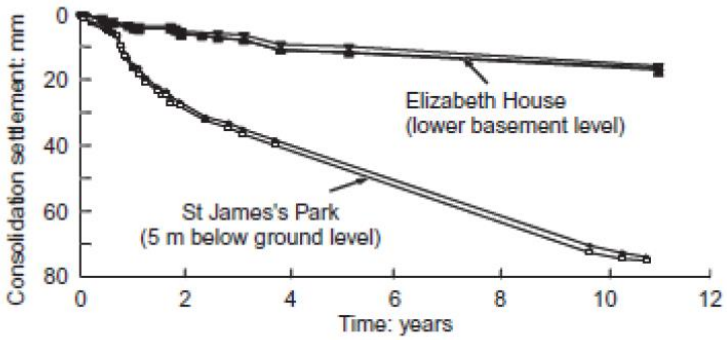

Fig. 2.19: *Comparison of consolidation settlements at St.James's Park and Elizabeth House (Mair, 2008)*

The short-term results of the numerical analysis of Avgerinos *et al*. (2014), mentioned in the previous sub-paragraph, have been extended by him to the long term and they are shown in Fig. 2.20. In this case it can be seen that the data better approximate the trend of in situ settlements when obtained by calibration on the experimental results of both triaxial and oedometer tests. In terms of

maximum settlement values, the numerical results reflect well the real data values. There is discrepancy in the values at the wings of the settlement trough, the numerical predictions are narrower than the in-situ measurements.

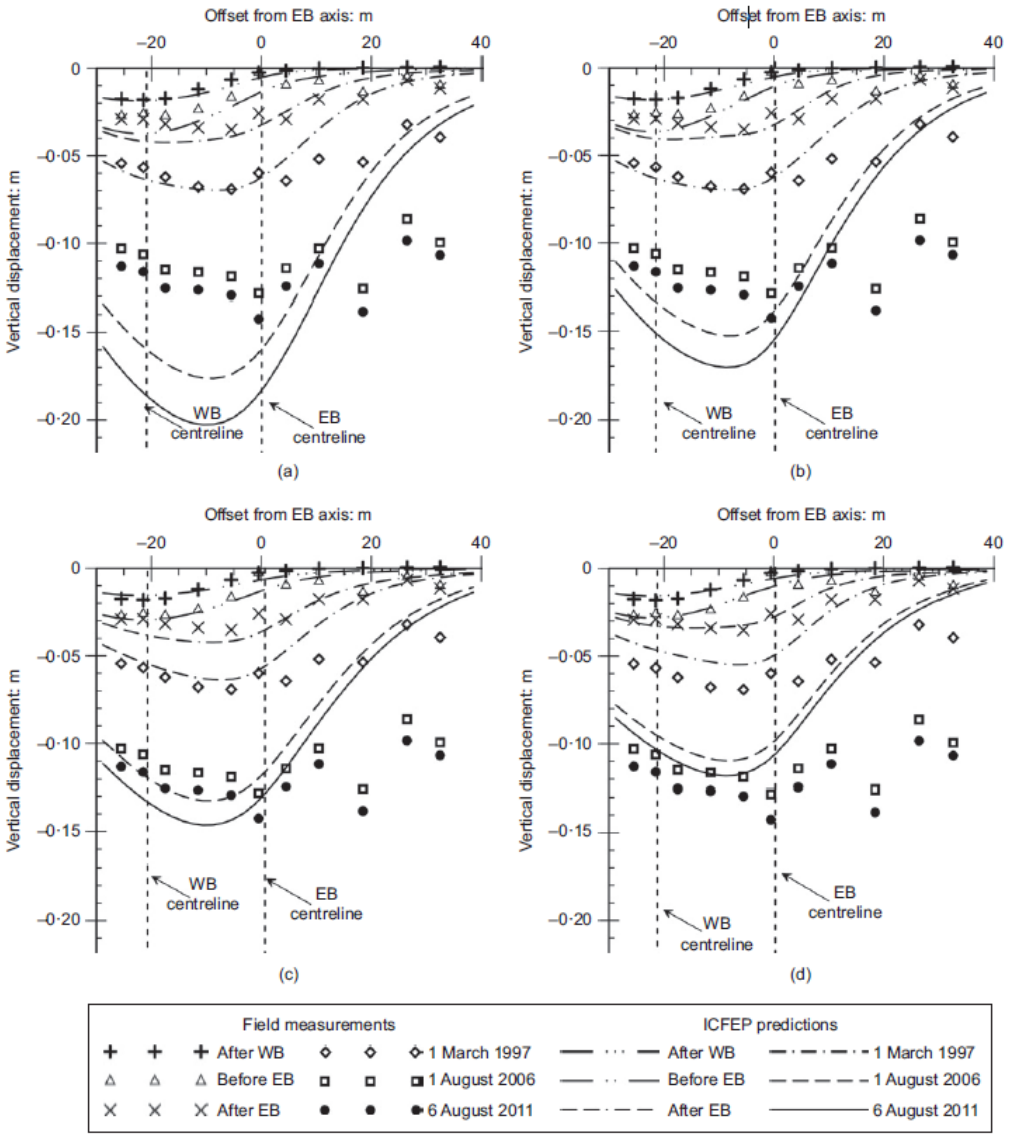

Fig. 2.20: *Long-term settlement profiles for: (a) low triaxial; (b) high triaxial; (c) low both; (d) high both calibration cases (Avgerinos et al., 2014)*

Addressing the issue of subsurface displacement, from the monitoring of the WB tunnel at the St. James site, in accordance with the research of Wongsaroj *et al.* (2007), the long-term strains can be grouped in three different zones: the upper zone of the tunnel crown within 5 meters is subject to swelling, the extended lateral zone is subject to consolidation, while the rest of the ground

behaves like a rigid body moving downwards. This phenomenon was also found in the subsequent construction of the EB tunnel as shown in Fig. 2.21.

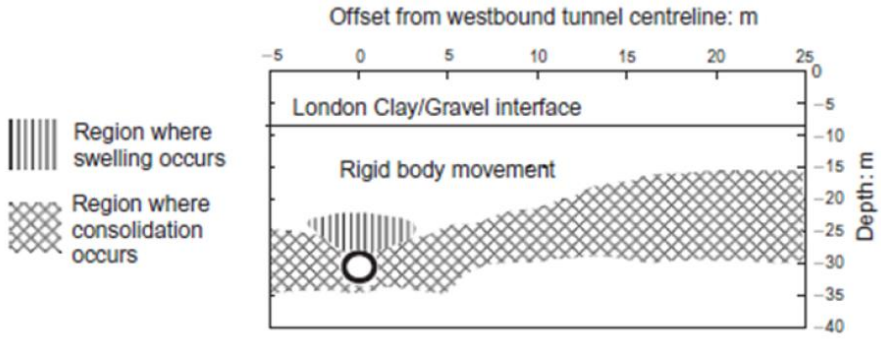

Fig. 2.21: *Schematic diagram indicating zones of different response during consolidation (Wongsaroj et al., 2007)*

In general over the long term as far as the lining behaviour is concerned, even considering minimum permeability values in poorly permeable clay such as London clay, there is an increase in the hoop thrust as the consolidation process proceeds, especially at the crown of the tunnel. The numerical analyses of Shin *et al.* (2002) and Mair (2008) correlate the variations of the hoop forces to the permeability of the soil-lining interface. In case the lining was completely permeable the variations on thrust hoops would be negligible, but this would lead to the occurrence of tunnel squats (Fig. 2.22). On the contrary, the impermeability would result in an increase of stresses in the lining, without deformations. In practice, taking into account that permeability is a parameter difficult to quantify, it is used to take into account a partial permeability that is able to predict both the contribution of the ground surface definitely given by the deformations of the tunnel and the increase of the hoop forces on the tunnel itself as commonly found by in situ analysis.

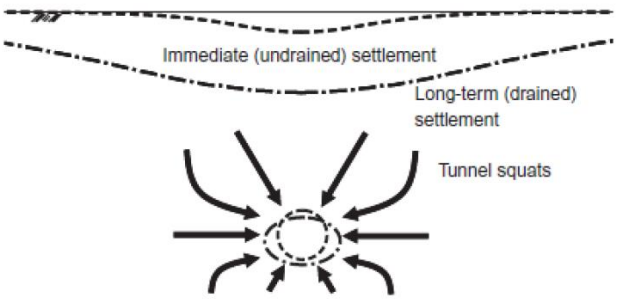

Fig. 2.22: *Qualitative response of soil and tunnel lining in the long term for tunnel lining being completely permeable (Mair, 2008)*

From Wongsaroj *et al*. (2007), Mair (2008) and Avgerinos *et al.* (2016) it emerges how important it is to also take into account the anisotropic stiffness of the ground, higher horizontal permeability values compared to the vertical one as in the case of St. James's Park contribute to make the ground surface settlement wider and in agreement with the in situ measurements (Fig. 2.23). It is concluded that the more the lining is permeable and the higher the anisotropy of the ground, the lower the hoop thrust and the higher the squatted tunnel.

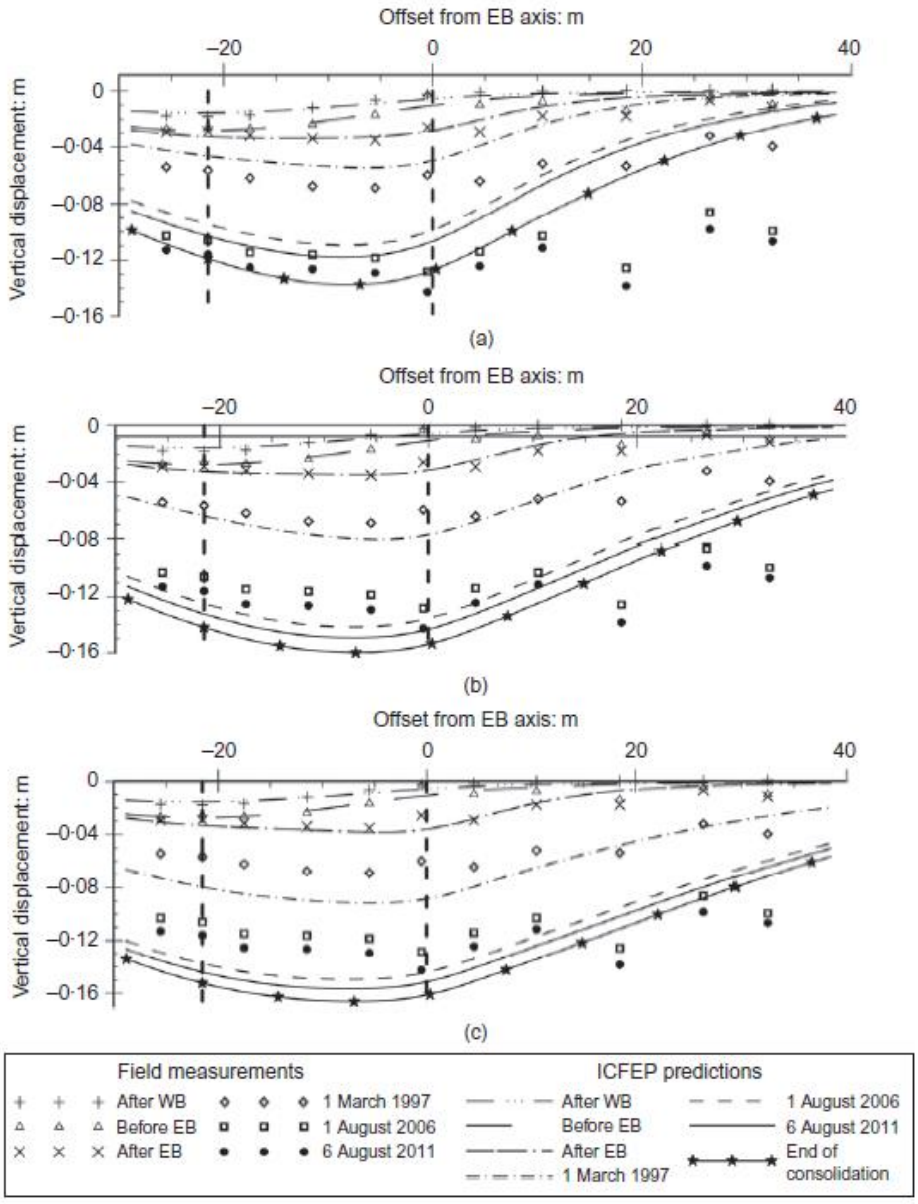

Fig. 2.23: *Profile of vertical movements for: (a) 2; (b) 25; (c) 100 degrees of anisotropy of permeability sub-unit A3 in St. James's Park site (Avgerinos et al., 2016)*

2.3.4 Interaction between twin tunnels

Below large cities in an increasingly densely built underground environment, the problem of interactions between different structures is increasingly relevant. This thesis analyses in detail the Crossrail case study at Hyde Park where twin tunnels are built parallel at different times. In this kind of situation, the analytical and empirical formulations are difficult to apply; great importance is given to the few in situ surveys of pre-existing cases on which the reliability of numerical models is tested.

The phenomenon is well described by Addenbrooke & Potts (2001) which investigates the effects of the interaction between two twin tunnels in London Clays as their spatial and temporal construction distances varies. The results are well integrated with in situ data. The geometry of the model is described in Fig. 2.24:

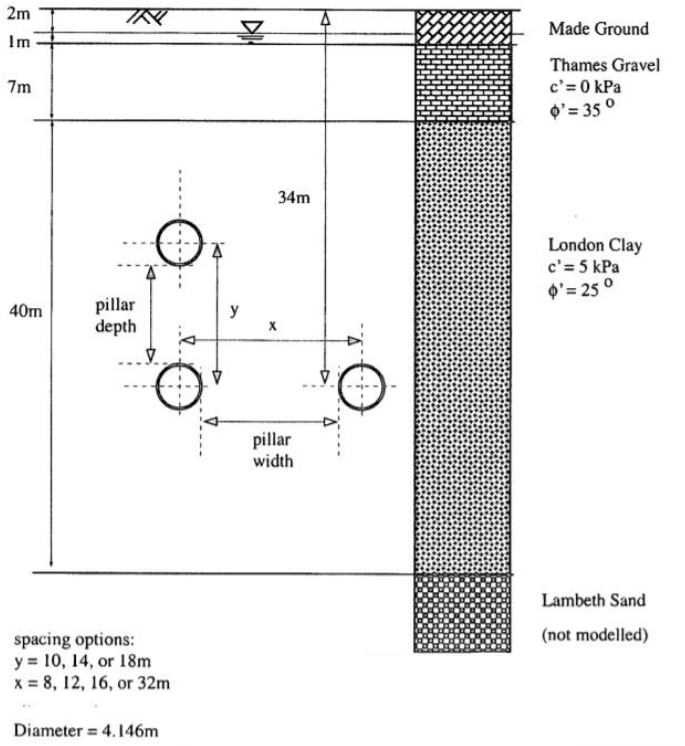

Fig. 2.24: *Side by side and piggy back geometry of the model (Addenbrooke & Potts, 2001)*

The first set of analyses in which the two tunnels are dug in parallel at a temporal distance of 3 weeks from each other reveals the tendency of the existing tunnel to move towards the newly constructed tunnel. In a strongly over consolidated soil this is manifested in the squatting induction of the lining with the increase of the horizontal diameter deformations compared to the vertical

ones. The greater the horizontal distance between tunnels and the smaller is the interaction between the two. The analysis shows that for pillar widths greater than 7 times the diameter the effects of subsurface displacements are negligible. An inverse argument is made for the configuration of the two tunnels vertically, the pre-existing tunnel will tend to be lengthening vertically assuming an egg shape. In this configuration the interactions are negligible for pillar depth greater than 3 diameters. The distortions are lower when the second tunnel is built above the pre-existing tunnel than below. The results are shown in the following graphs:

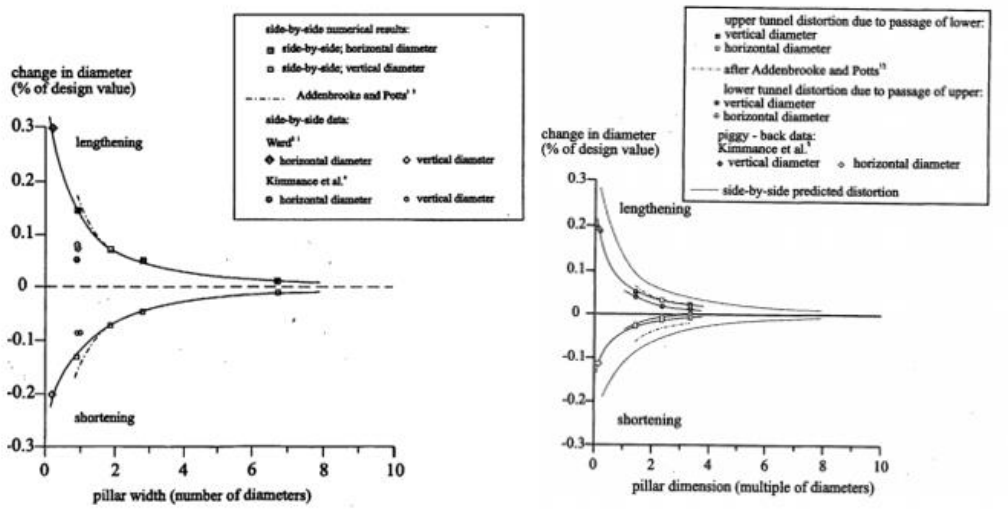

Fig. 2.25: *Deformations of the 1st tunnel in response to 2nd tunnel for side by side geometry (on the left) and piggy back geometry (on the right) (Addenbrooke&Potts, 2001)*

From the research by Avgerinos *et al.* (2016) in St. James's Park site it can be seen that the maximum surface displacement above the EB tunnel is shifted about 5 metres towards the pre-existing WB tunnel. This is in accordance with what has been previously described.

The effect of the interaction between the tunnels in the consolidation process is not negligible, the movements of the ground following the excavation of the second tunnel are affected by the plasticisation phenomena caused by the excavation of the first. This can produce undesirable effects such as lining distortions. In this regard, one of the great advantages of the DOT tunnels excavation method is to cancel these temporal interaction effects present in twin tunnels.

Chapter 3

THE CHOICE OF A CONSTITUTIVE MODEL

The aim of this project is to simulate the effects of the recent Double-O-Tube (DOT) shield tunnelling technique in the ground conditions of the central London. As seen in the Literature Review chapter, the use of this technology has been successfully adopted for about twenty tunnelling projects in eastern Asia, more precisely in Japan, China and Taiwan. In particular, this study refers to the current research projects in which this type of technique has been adopted to soft clay ground conditions in Shanghai (Zhou & Zdravkovic, 2020). This chapter investigates the use of two constitutive models in the simulation of the mechanical behaviour of an over-consolidated stiff clay such as London Clay. One constitutive model is an advanced kinematic hardening 'bubble' constitutive model and the other is a standard modified Cam clay model that is generally better suited to describe the mechanical behaviour of a soft clay. The effectiveness and the modelling characteristics of the two surfaces kinematic hardening soil model (Grammatikopoulou, 2004), the 'bubble' model, were tested by simulating a triaxial test using the Imperial College Finite Element Program ICFEP (Potts & Zdravkovic, 1999; 2001) on two samples of soft and stiff clay and by comparing the results with those obtained simulating the same tests using the modified Cam clay model (Roscoe & Burland, 1968).

3.1 Geological considerations

This paragraph tries to provide a brief descriptive framework of the different soft ground conditions in London compared to those in Shanghai. The aim is to highlight the impact of initial conditions and geological history on the choice of the most suitable constitutive model to describe the mechanical behaviour of a clay.

3.1.1 Soft ground condition in Shanghai

The metropolis of Shanghai is located at the mouth of the Yangtze River and is built on top of a soft deltaic deposit consisting of a multi-aquifer-aquitard system. The underground is built within a layer of very soft clay with high water content. According to Shen *et al.* (2014) this material is characterized by high compressibility, low permeability and low shear strength. This geological structure (Fig. 3.1) leads to a widespread problem of soil subsidence which is aggravated by the massive withdrawal of water from the aquifers. From previous research (Zhou & Zdravkovic, 2020), modified Cam clay is considered appropriate to simulate the mechanical behaviour of normally consolidated and slightly over-consolidated soft clay such as Shanghai clay in which the consolidation took place gradually in parallel with the deposition of the overlying alluvial layers.

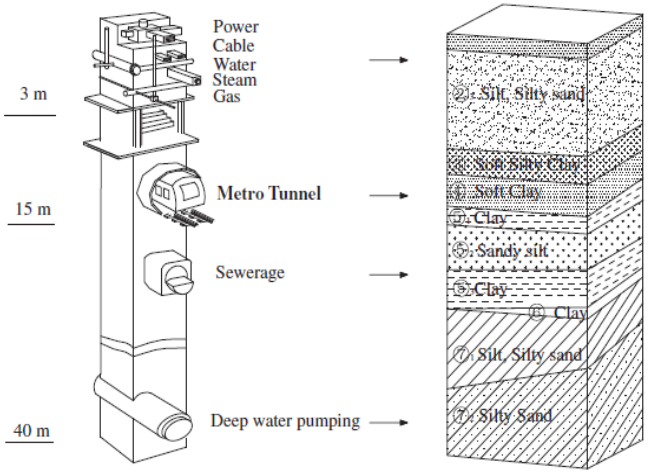

Fig. 3.1: *Cross sectional view of the underground spaces in Shanghai (Shen et al.,2014)*

3.1.2 Soft ground condition in London

The complexity of the geological history of London Clay, through which a large part of the subway was built, requires a more in-depth analysis. London Clay foundation is a marine geological formation divided into 5 different divisions classified from A to E. Each division is associated with a transgressive and regressive cyclical phase of the sea at a time when this region was occupied by a shallow sea basin and has a "coarsening upward" grain distribution (King, 1981). As reported in detail in Royse *et al.* (2012), the height of this layer of clay varies from few meters in the westernmost region to 200m in the easternmost ones. Over time the London Basin has been affected by repeated glacial and interglacial cycles and erosive phenomena have brought the old layers of clay to

the surface. The fluctuations of the River Thames have reshaped the area by alternating the more superficial clay deposits with gravel terraces and alluvial sediments (Fig. 3.2).

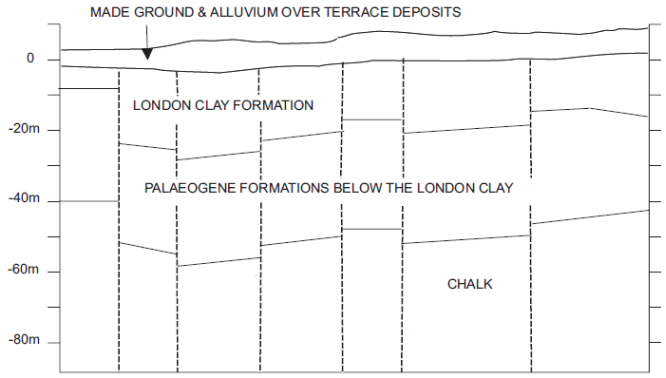

Fig. 3.2: *A schematic lithographic section showing the effect given by the presence of faults (Royse et al., 2012)*

The properties of unweathering London Clay reflect its complex history of loads: this material is stiff to very stiff and has a high degree of over-consolidation. Permeability is low and generally the water content decreases with increasing depth and density (Standing, 2018). Changes in volume are closely related to the water content, drying can cause a significant reduction in volume, whereas an increase in the amount of water causes the swelling of the clay. Although in the past this phenomenon during dry seasons has caused problems of damage to the foundations of buildings due to surface cyclic settlements, London Clay proved to be ideal for underground tunnelling. As seen in the Literature Review chapter, generally the slow and gradual expansion towards the excavation gives the time to mount the lining safely without the need for any major precautions (Mair, 1998). However, the very slow consolidation process due to the low permeability of London Clay requires long-term forecasts. The comparison between experimental data and the numerical results mentioned in the Literature Review chapter shown the importance of using advanced constitutive models such as two surfaces kinematic hardening soil model (Grammatikopoulou, 2004) in order to obtain plausible predictions.

3.2 Critical State models

The theory of the Critical State is the very first conceptual framework that links strength and stiffness of soils to their current volume. According to Lancellotta (2012) the central idea of the theory can be summarised in the following consideration: volume variations play an equally important role as

effective stresses and it is the relationship between initial state and critical state that characterizes the mechanical response of a soil element.

The challenge was to find an ideal conceptual qualitative theory able to collect the essential aspects of the elasto-plastic nature of the soil response that could overcome the limits of the previous theories by establishing a reference framework. The problems of ultimate limit state, starting from the solutions of practical interest of Coulomb (1776) and Rankine (1857) renounced the ambition of being able to describe the influence of load history on soil by assuming a perfectly plastic behaviour at failure. However, these theories constituted a first step on the road to understanding the key role of plasticity in describing the mechanical behaviour of geomaterials. The Drucker & Prager (1952) yield criterion and the associated plastic flow criterion tried to characterize the frictional behaviour of soil by developing the Von Mises yield criterion and the Mohr-Coulomb yield surface, but they struggled to put together all the aspects that emerged from the experimental data. Only at the end of the 50's, starting from the intuition of Drucker *et al*. (1957) that suggested the existence of a yield strength surface controlled by volume variations and through the analysis of data from a series of shear tests and triaxial tests performed at Imperial College (Henkel, 1960), the theory of the critical state was formulated by researchers at Cambridge University in Roscoe *et al.* (1958). They postulated the existence of a state boundary surface that envelops all the physically possible states detectable by the variables (p', q, v) where p' is the mean effective stress, q is a deviatoric stress and v is the specific volume in the soil. The conditions of no volume change at the end of different effective stress paths are reached at large deformations and represents the critical state condition that form the Critical State Line (CSL), indicated in the Fig. 3.3 by the double dark line.

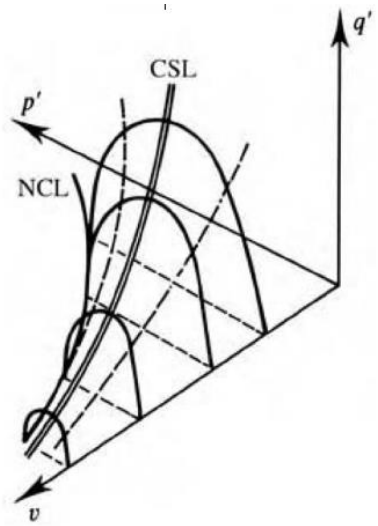

Fig. 3.3: *State Boundary Surface (Atkinson,2007)*

3.2.1 Cam Clay and Modified Cam Clay models

The Cam Clay (Roscoe *et al*., 1963; Schofield, 1968) and the Modified Cam-Clay (Roscoe & Burland, 1968) models were the first two models based on the critical state theory. They take as a reference an elasto-plastic hardening law (Calladine, 1963) assuming a logarithmic relationship between the mean stress and the specific volume under isotropic stress in perfectly drained condition. This simplification with respect to soils' real behaviour (Fig. 3.4) made it possible to define the direct relationship between the specific volume and mean effective stress during isotropic consolidation and swelling as:

$v_1 = v + \lambda \ln(p')$ *virgin consolidation line*
$v_s = v + k \ln(p')$ *swelling line*

Where v is the specific volume and p' the mean effective stress and v_1, λ and k are characteristic properties of the soil.

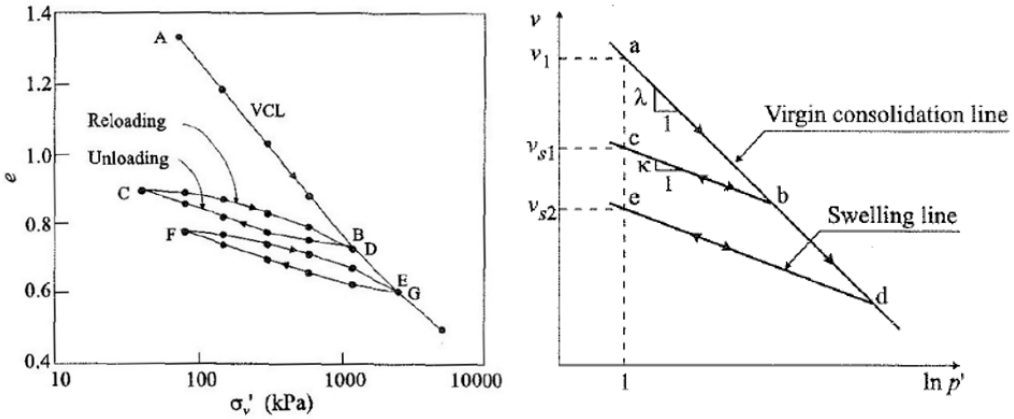

Fig. 3.4: *Oedometric test result on Pappadai clay (Cotecchia,1996) compared to the behaviour assumed by the Cam Clay models (Potts&Zdravkovic,1999)*

The constitutive law establishes a plastic (irreversible) volume change along the virgin consolidation line and an elastic (reversible) volume change along the swelling lines. Virgin consolidation line is seen as an upper limit of the soil state along which the soil can be defined as normally consolidated and below which it is considered to be over-consolidated.

The attainment of the three-dimensional state boundary surface in p'- J - v space, postulated by the critical state theory, is a generalisation two-dimensional yield loci existing above each of the swelling lines, as projected on the plane (p', J) and shown in Fig. 3.5. The yield functions of the tow first critical state models are described by the following equations:

$$F = \frac{J}{p' M_j} + \ln\left(\frac{p'}{p'_0}\right) = 0 \qquad Cam\ Clay$$

$$F = (\frac{J}{p'M_j})^2 - \left(\frac{p'}{p'_0} - 1\right) = 0 \qquad Modified\ Cam\ Clay$$

Where p' is the mean effective stress, J is the deviatoric invariant easily obtainable from the deviatoric stress q, p'_0 the intersection point between the virgin consolidation line with the current swelling line and M_j the slope of the CSL.

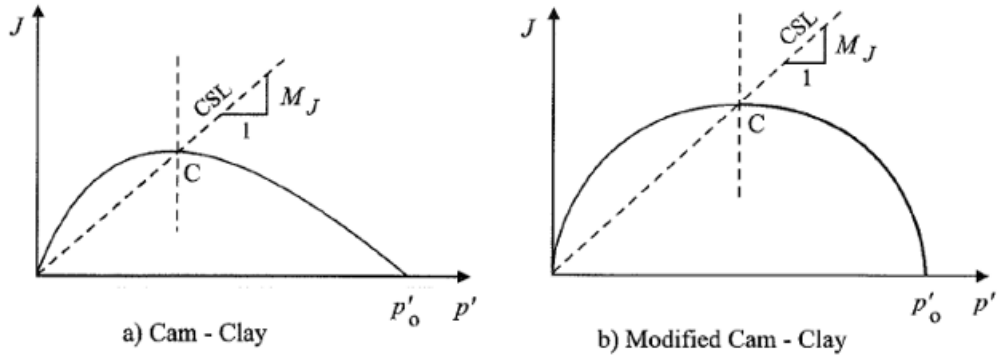

Fig. 3.5: : *Projection of the yield surface on the the plane (p',J) (Potts&Zdravkovic,1999).*

The calculation of the volumetric and shear components of the deformation gradient in the elastic phase can be expressed with the following matrix description:

$$\begin{Bmatrix}\delta\varepsilon_v^e\\ \delta\varepsilon_s^e\end{Bmatrix} = \begin{bmatrix}1/K' & 0\\ 0 & 1/3G'\end{bmatrix}\begin{Bmatrix}\delta p'\\ \delta q\end{Bmatrix}$$

Where K' is the elastic bulk modulus and G' the shear modulus related to the Poisson coefficient which can be assumed constant:

$$K' = \frac{vp'}{k} \qquad G = \frac{3(1-2v)}{2(1+v)}K'$$

The isotropic hardening law is another basic ingredient to define these elasto-plastic models because it establishes the relationship between p'_0 variations and plastic deformation and it is expressed by the relation:

$$\delta p'_0 = \frac{vp'_0}{\lambda - k}\delta\varepsilon_v^p$$

Where the new variable compared to the previous equations is the plastic volumetric strain ε_v^p.

Since the direction of the vector of the strain increment is directed as the gradient of the state bounding surface function and plastic strain increment normal to the surface, it can be inferred that the flow rule is associated and the

yielding surface plays the role of plastic potential. For practical and theoretical reasons related to the continuity of the yielding/potential surface in p_0' and for a more reasonable stress prediction, the use of the Modified Cam Clay model is preferred to the original Cam Clay model. The deduction is that the five parameters required for a numerical analysis are: v_1, k, λ, M_j and G or υ.

3.2.2 Extension to the deviatoric space

Often in the numerical analyses the stress state is definied in a more general description by the triplets of the principal effective stresses. The generalization of the Modified Cam Clay yielding and potential surfaces on tridimensional principal effective stresses space is an ellipsoid built around the positive octant trisector (Fig. 3.6). In this configuration the critical state surface take the shape of a cone with a constant value of J/p' cutting the ellipsoid at the poles (Drucker, 1953). Therefore, the projection on the deviatoric plane perpendicular to the axis of the ellipsoid is a circle.

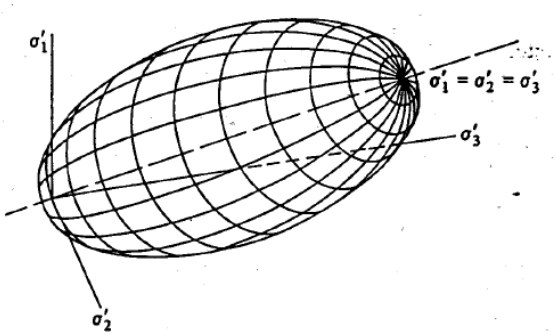

Fig. 3.6: *Ellipsoidal yield surface of the Modified Cam Clay model in the principal effective stresses space (Wood,1990)*

However, the original shape of the Cam models in the deviatoric plane was shown to be inadequate for modelling soils, in particular if performing plane-strain analyses. ICFEP capabilities have advanced this by enabling also a Mohr-Coulomb hexagon for the shape of the yield surface in the deviatoric plane, as well as the general shape of Van Eekelen (1980) which can reproduce the Lade's or Matsuoka-Nakai's surfaces that are experimentally derived.

The Mohr-Coulomb hexagonal yielding function is obtained from the equation:

$$g(\theta) = \frac{sin\varphi'_{cs}}{cos\theta + \frac{sin\theta sin\varphi'_{cs}}{\sqrt{3}}}$$

Where φ'_{cs} is the critical state angle of shearing resistance and θ is the Lode's angle.

Considering a conventional triaxial test the domain of the deviatoric space is restricted to the planes characterized by a Lode's angle equal to $\pm 30°$. This is due to the assumption that two values of the principal stresses must always coincide (Fig. 3.7). Although this test makes a description of the problem convenient in terms of (p, q), the generalized case requires the use of the deviator invariant J at q. The equations of the yield functions of the Cam models on tridimensional principal effective stresses space become:

$$F = \frac{J}{p' g(\theta)} + \ln\left(\frac{p'}{p'_0}\right) = 0 \qquad Cam\ Clay$$

$$F = \left(\frac{J}{p' g(\theta)}\right)^2 - \left(\frac{p'}{p'_0} - 1\right) = 0 \qquad Modified\ Cam\ Clay$$

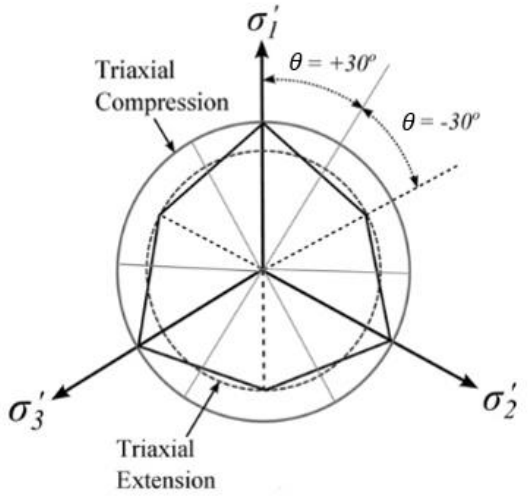

Fig. 3.7: *Deviatoric plane for a conventional triaxial test compared to the Mohr-Coulomb criterion and the external circle*

3.3 Bubble models

In contrast to what stated in the Cam clay models, there are dissipative phenomena already inside the state bounding surface that are reflected with a progressive decay of the stiffness with the proceeding of the strain level. A realistic pre-failure soil behaviour considers elastic non-linearity hand in hand with the plasticization of geomaterials from the early small strain stages (Fig. 3.8). For this reason, it is necessary to increase the level of sophistication by using an advanced constitutive model. In bubble models this improvement is

achieved by introducing one or more kinematic yielding surfaces inside the state bounding surface.

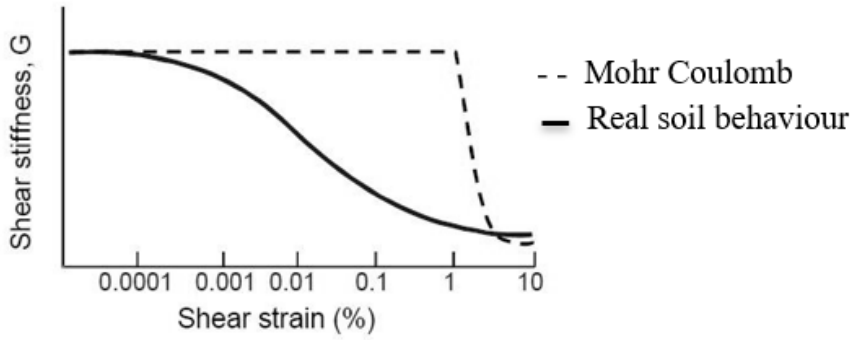

Fig. 3.8: *Scaling of the shear modulus comparison (Atkinson&Sallfors,1991)*

The bubble model developed by Al-Tabbaa (Al-Tabbaa, 1987; Al-Tabbaa & Wood, 1989) circumscribes the purely elastic behaviour in early very small strains stages to the region inside the small kinematic yield surface called bubble. The size of this volume is proportional to that of the bounding surface through a coefficient R. When the bubble border is reached, the behavior becomes elasto-plastic, the bubble starts to move, and the strains can grow until the stress-path reaches the bounding surface. An additional load would result in the joint movement of the two surfaces using the same principles theorized for the Modified Cam Clay model. Whenever there is a change in the direction of the stress path with a return within the bubble a certain value of the initial elastic stiffness is restored. The size of both surfaces varies dynamically in proportion to the variation of the plastic strains. A further improvement of the model was implemented by Stallebrass and Taylor (1997) with the addition of a second kinematic surface simulating the effects of recent stress history.

3.3.1 Modified two surface kinematic hardening soil model

The model developed by Al-Tabbaa & Wood (1989) has been integrated into the catalogue of available ICFEP models by Grammatikopoulou (2004) under the name M2-SKH. The kinematic and bounding surface can take the shape of the ellipsoid of the MCC model (Fig. 3.9a). However, in addition, Grammatikopoulou model is improved compared to previously cited models by allowing versatile shapes of the yield surface in deviatoric plane in the same way as for the MCC model (Fig. 3.9b). The term “modified” refers to the adoption of a yield criterion that allows to introduce a smooth elasto plastic transition between the elastic and the elasto plastic phase by imposing in this point yield modulus equal to infinity. (Grammatikopoulou *et al*, 2006).

The memory of a geomaterial contains fundamental information to correctly define its mechanical response. A big advantage of the bubble models is to be able to consider the anisotropic variation of stiffness according to the history of load. As can be seen from Fig. 3.9b, the bubble is not centered isotropically and it is free to move kinematically. In this way it is truly possible to succeed in predicting plausible values of the anisotropic stiffness.

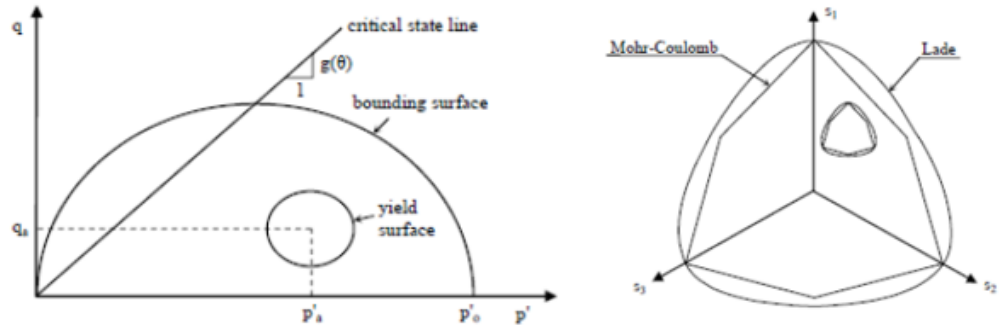

(a) (b)

Fig. 3.9: *(a) M2 -SKH model on the triaxial plane; (b) different possible shapes in the deviatoric plane (Grammatikopoulou, 2004)*

As already reported, the equations of the inner yield and bounding surfaces are based on the ellipse of the Modified Cam Clay model and are reformulated as follow:

$$F = \left(p' - \frac{p_0'}{2}\right)^2 + \frac{J}{{M_j}^2} - \frac{{p_0'}^2}{4} = 0 \qquad bounding\ surface$$

$$F = (p' - p_\alpha')^2 + \left(\frac{J - J_\alpha}{M_j}\right)^2 - R^2\frac{{p_0'}^2}{4} = 0 \qquad kinematic\ surface$$

Where p_α' and J_α are the centre of the bubble and R is the ratio of the size of the bubble to that of the bounding surfaces.

Other points remain in common with the Modified Cam Clay model. The elastic behavior in the bubble is described from the same isotropic elastic constitutive equations, the motion is related to the usual hardening/softening law and the flow rate remains associated. The slight difference is that compared to the Modified Cam Clay model, where the behaviour along the virgin consolidation and swelling lines is linear in relation to $v - lnp'$, in this model the relation is linear when $lnv - lnp'$. So, the bulk stiffness and the hardening law become:

$$K = \frac{p'}{k^*} \qquad\qquad \delta p_0' = \frac{p_0'}{\lambda^* - k^*}\delta\varepsilon_v^p$$

Where the asterisk with respect to the previous notation is intended precisely to underline this distinction.

The translation rule regulates the movements of the bubble and directs each state point on the kinematic surface along the vector β towards the associated point on the bounding surface ensuring that the bubble becomes tangential and completely enclosed within the bounding surface itself. This motion is associated with the variation in the size of the bubble in relation to the plastic deformation described by the hardening law. The hardening modulus is calibrated from the configuration in which the two surfaces are in contact and varies depending by the approach and by the distance between the bubble and the bounding surface. Looking at Fig. 3.10 to understand the meaning of the different variables, the translation rule is described by the following equation:

$$\begin{Bmatrix} \delta p'_\alpha \\ \delta J_\alpha \end{Bmatrix} = \frac{\delta p'_0}{p'_0} \begin{Bmatrix} p'_\alpha \\ J_\alpha \end{Bmatrix} + S\beta = \frac{\delta p'_0}{p'_0} \begin{Bmatrix} p'_\alpha \\ J_\alpha \end{Bmatrix} + S \begin{Bmatrix} \frac{p' - p'_\alpha}{R} - \left(p' - \frac{p'_\alpha}{2} \right) \\ \frac{J - J_\alpha}{R} - J \end{Bmatrix}$$

Where β is the vector from C to D, the first term is related to the variation of the size of the bubble and the second term to the translation on β, the scalar S is obtained by substituting this equation into the consistency condition of the kinematic surface and using the equation of the kinematic surface itself.

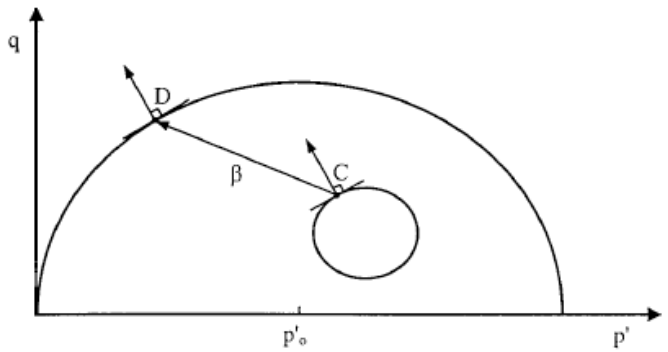

Fig. 3.10: *Relative translation of the kinematic yield surface along the vector* $\boldsymbol{\beta}$ *(Grammatikopoulou, 2004)*

The parameters required to initiate a numerical analysis considering the shape of the ellipsoid developed in the MCC model are 7: v_1, k^*, λ^*, M_j, R, μ and the coefficient in the hardening term α (Grammatikopoulou, 2004).

3.4 Triaxial test simulations

The triaxial test is the most common of geotechnical laboratory tests. It is used to simulate the mechanical response of deformable material specimen and to derive the associated mechanical properties. The interaction between liquid phase flow and solid phase deformations is reported by the coupled theory. The possibility to controlled drainage conditions and to measure water pressure makes it possible to describe the stress-strain relationship in terms of effective stresses. In this case the simulation is expressed in terms of fully drained and undrained conditions. The drained condition in clays occurs when the load is applied very slowly. The strains of the solid phase are independent from the variation of the water pore pressure. Under undrained conditions, water flow is prevented, the volume remains constant and excess pore water pressures are inextricably linked to the development of the deviatoric strains. The other important variable is related to the clay over-consolidation ratio. During a triaxial test the sample is normally consolidated and isotropically discharged to simulate in situ conditions. Considering samples consolidated at the same confining pressure p', each different degree of over-consolidation is associated with a different specific volume.

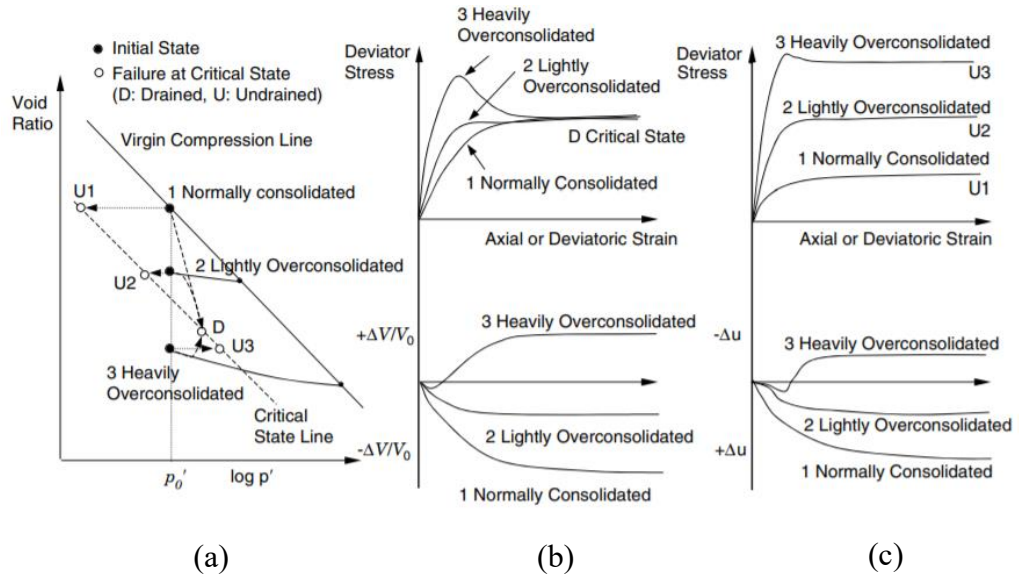

(a) (b) (c)

Fig. 3.11: *Stress-strain relationship of normally consolidated, lightly overconsolidate and heavily overconsolidated clays: (a) void ratio versus mean effective stress, (b) drained tests, and (c) undrained tests (Mitchell&Soga,2005).*

Fig. 3.11 shows the mechanical behaviour of clays in relation to the type of test (drained or undrained) and to the different degree of over consolidation. In the drained test on normal consolidated or slightly consolidated soft clay is

shown a ductile behaviour associated with a volume contraction. The achievement of the yield surface is followed by a hardening phase. In contrast for a heavily over-consolidated clay, the behaviour is rigid until the yield point is reached and progressively branches off toward the critical condition. The softening phase is associated with an increase in volume. In undrained tests the volume remains constant, from the same initial p' the more the specimen will be over-consolidated the more tension will be necessary to reach the yield point. A test performed on normal consolidated or slightly consolidated soft clay generates a positive interstitial overpressure. In contrast, shear on heavily over consolidated clays produces a negative interstitial pressure once the peak state is reached.

The results of a series of simulations of triaxial consolidated drained and undrained tests obtained through the Imperial College Finite Element Program ICFEP are reported below. The objective is to verify the theoretical concepts previously exposed on a practical level by comparing the numerical results of the modified Cam clay model with those obtained from the advanced modified two surface kinematic hardening soil model in terms of stress path on the triaxial plane (p', J) and of stress-strain (J, ε_a) and stiffness (ε_a, G) curves. The reference specimen is analysed considering an 8-node quadrilateral solid element with initial stresses at $\sigma'_h = 75$ kPa and $\sigma'_v = 100$ kPa. This is equivalent to consider an initial p' value of 83.33 kPa and j equal to 14.434 kPa. The properties of the material will be defined later in relation to the used model. The boundary conditions constrain the vertical displacements to the nodes on the lower side and the horizontal displacements on the left side of the square to zero. The first 100 increments are associated with a negative vertical imposed displacement of 0.1 mm, then moving to a value of -1 mm.

3.4.1 Triaxial test simulations using MCC model

The following table shows the values of the parameters used in MCC simulations considering two different cases with OCR=2 and OCR=4:

v_1	k	λ	g(Θ=30°)	μ
3.2	0.008	0.1	0.743	0.2

Tab. 3.1: *Material parameters implemented in ICFEP for the simulation of MCC triaxial tests*

At the first, it is presented the stress path on the triaxial plane $p' - J$ (Fig. 3.12). In the drained test, the trend expressed in terms of effective mean stresses coincides with the trend of total effective stresses. Therefore, the gap between the trend of the drained test and the trend in terms of mean effective stresses of

the undrained test represents the evolution of the excess pore water pressures. In the particular condition with OCR=2 the initial state remains below the line of the critical state so that in the undrained triaxial test the behaviour is practically considerable elastic perfectly plastic. The case with OCR=4 is more similar to the London Clay condition. From the following graph, the softening behaviour after yielding with the development of negative excess pore water pressures is very well visible. At the same initial p' value corresponds a higher value of the yield stress compared to the case with OCR=2.

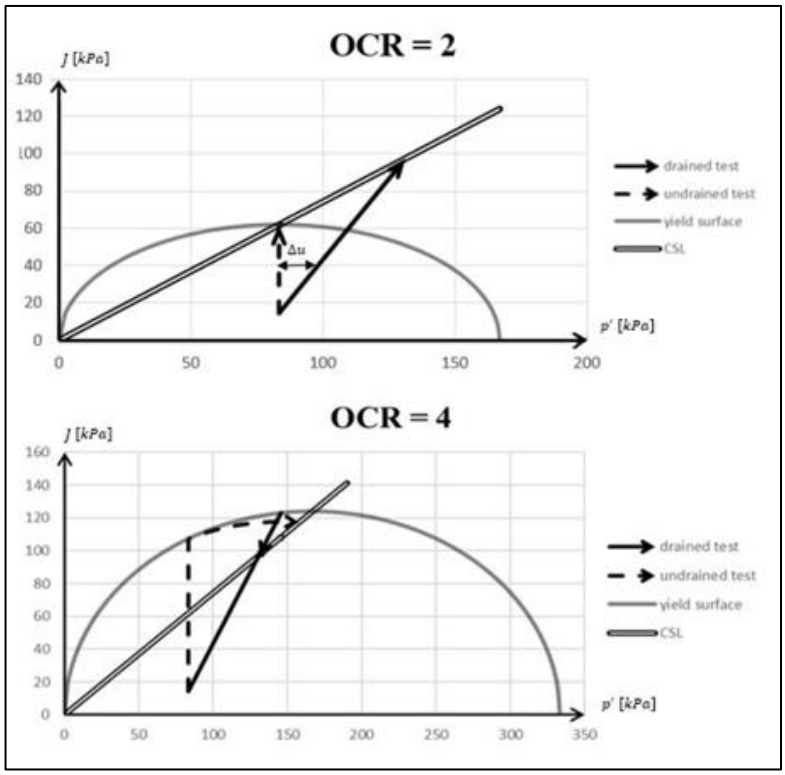

Fig. 3.12: *Stress-path on the triaxial plane* ($\boldsymbol{p'}$,$\boldsymbol{J}$) *using MCC model*

From the numerical simulation on the drained triaxial test, shown in Fig. 3.13, it is possible to appreciate the contribution of dilatancy on the mechanical behaviour of soils with different degree of over-consolidation. In the case with OCR=2 the critical state is reached through progressive volume compression, while in the case heavily over-consolidated with OCR=4 when the peak state is reached, there is a negative reversal of the volumic strains and the material softens toward the critical state.

In the undrained test it is appreciable how undrained resistance increases as the degree of overconsolidation increases. From the trend of the case with OCR=4 in Fig. 3.14 it is also observable a peculiar aspect of the heavily over-

consolidated clays: the mechanical instability that they exhibit once the peak condition is reached, leading to a sudden slight drop in J values.

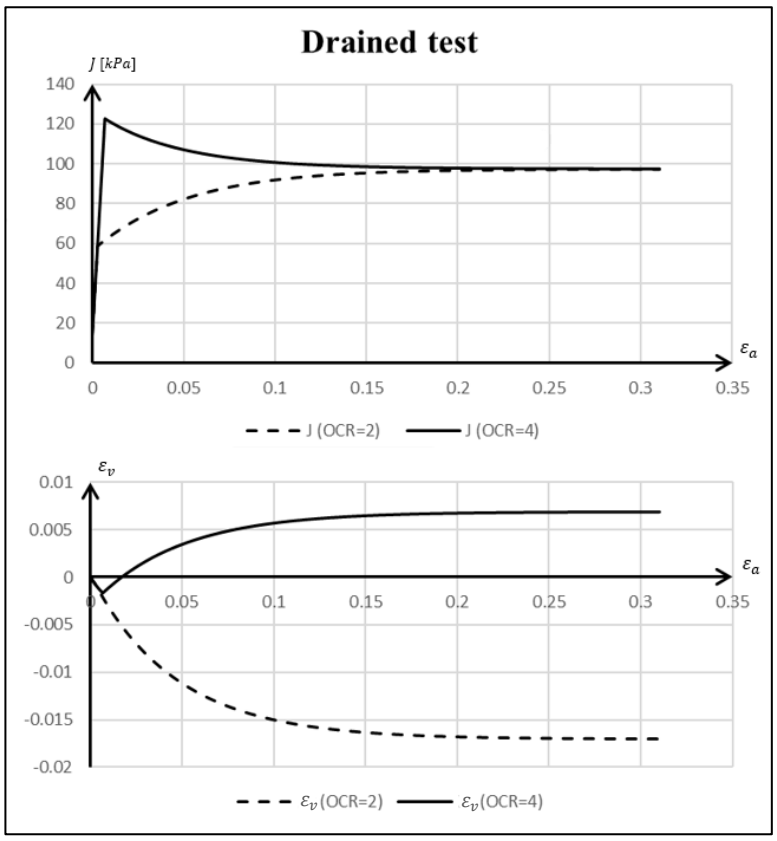

Fig. 3.13: *Stress-strain path related to volume changes in drained triaxial test using MCC model*

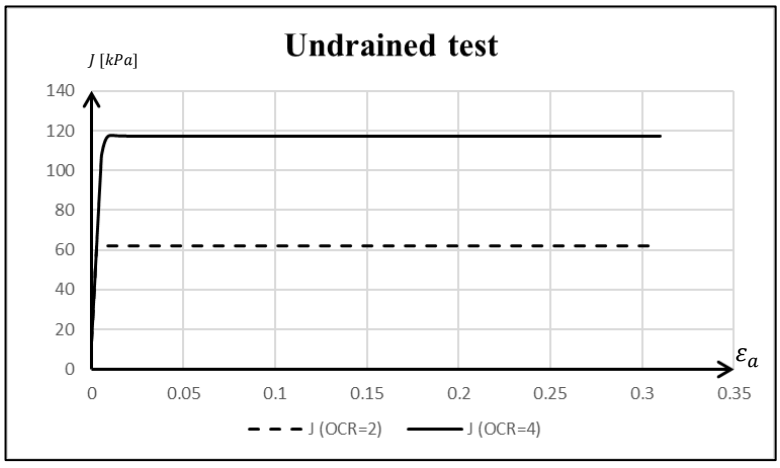

Fig. 3.14: *Stress-strain path in undrained triaxial test using MCC model*

3.4.2 Triaxial test simulations using M2-SKH model

As in previous simulations, the tests are performed considering two different cases with OCR=2 and OCR=4. The following table shows the values of the 7 parameters required to initiate a numerical analysis, considering the shape of the ellipsoid developed in the MCC model, used in M2-SKH simulations:

v_1	k^*	λ^*	g(Θ=30°)	μ	R	α
-3.2	-0.008	-0.1	0.743	0.2	0.02	15

Tab. 3.2: *Material parameters implemented in ICFEP for the simulation of M2-SKH triaxial tests*

The drained and undrained tests of the two cases are shown in Fig. 3.15. In order to correctly visualize the stress-path trends in relation to the dynamics of the inner and outer surfaces, the viewable configurations are associated with a given iteration number.

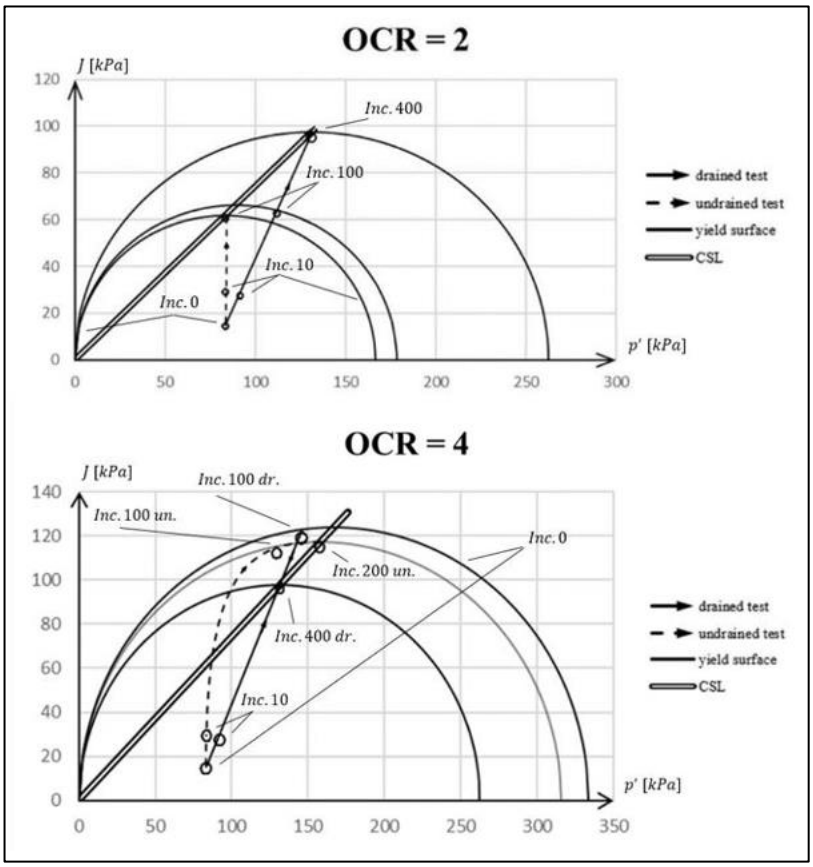

Fig. 3.15: *Stress-path on the triaxial plane* $(\boldsymbol{p'}, \boldsymbol{J})$ *using M2-SKH model*

From the previous test, the dynamic and proportionate increase in the size of the bubble and of the bounding surface is observed. Along the drained path it is noticeable how the size of the bubble and of the bounding surface remain constant until the yield point is reached and then shrink. The undrained stress-path on the triaxial plane (p', J) of the case with OCR=2 can be superimposed with that obtained with the MCC model. In contrast, by simulating the stiffer specimen with OCR=4 a completely different trend is obtained. Unlike the case obtained using the MCC, softening doesn't occur, the critical state is achieved through a smoother continuous and non-linear process. This result is due to the greater sensitivity of the constitutive model in considering the effect of plasticity.

3.4.3 Triaxial tests comparison between models

Fig. 3.16 shows the comparison between the stress-paths on the triaxial plane (p', J) of the undrained tests with OCR=4 mentioned in the previous paragraph.

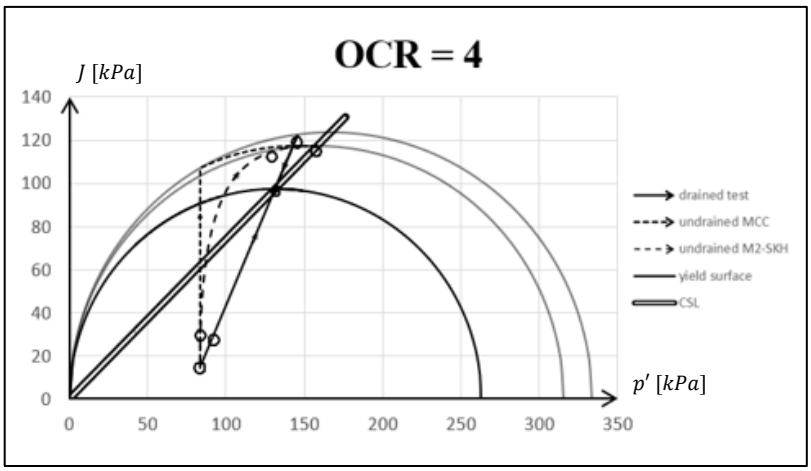

Fig. 3.16: *Comparison between the stress-paths of the MCC and M2-SKH models*

The difference between the MCC model and the M2-SKH model is even more noticeable by analysing the variation of J in relation to the evolution of the axial strain (Fig. 3.17). The paths of the drained and undrained cases of the MCC model are linearly elastic until the yield surface is reached and then deflected with the takeover of the hardening elasto-plastic phase. In the case with OCR=4 a slight softening phase follows. This phase will be marked the higher the degree of heavy over-consolidation. The path given by the M2-SKH model, as theorized, shows a markedly non-linear behaviour from the instant in which the inner 'bubble' is reached, the plasticization takes place gradually with the degradation of the elastic stiffness, as shown from the undrained case in Fig. 3.18, and a more contained softening is observed.

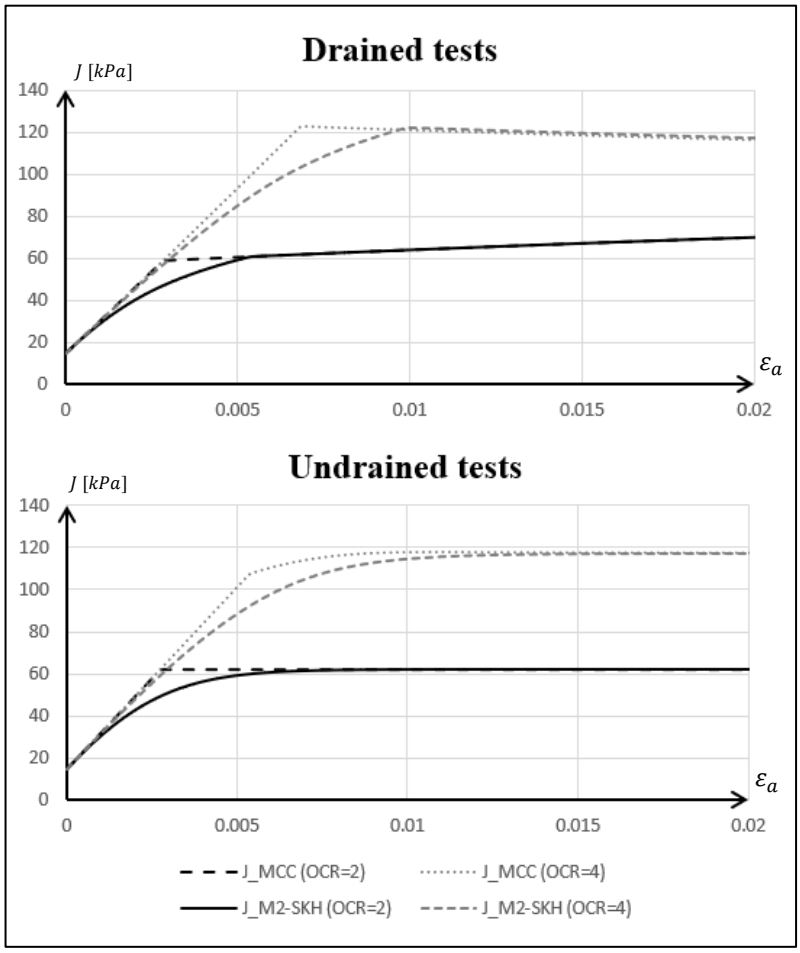

Fig. 3.18: *Comparison between the stress-strain paths of the MCC and M2-SKH model in drained and undrained conditions*

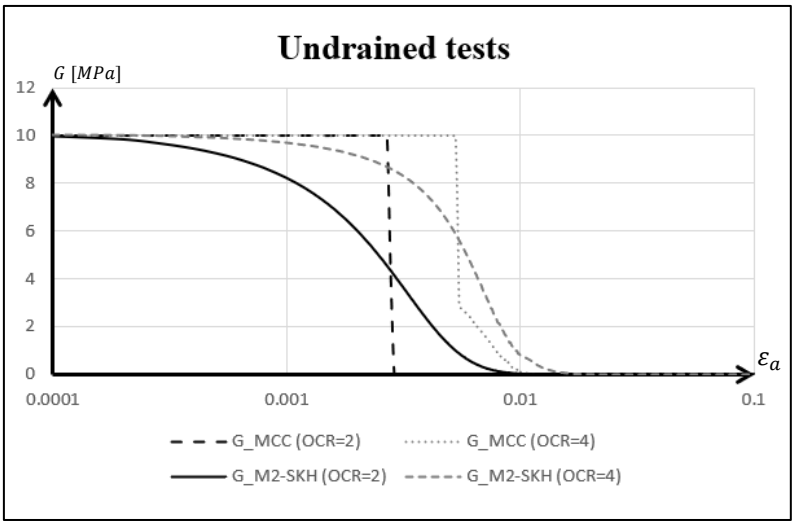

Fig. 3.17: *Scaling of the shear stiffness of the MCC and M2-SKH model in undraned condition*

The deviation between the MCC model and the M2-SKH model is longer the higher the value of the drained and undrained resistance, so the higher the degree of over-consolidation the more important it is to refer to an advanced model such as the M2-SKH. In conclusion, the M2-SKH model is more accurate than MCC model in describing the mechanical behaviour of a heavily over-consolidated clay such as London clay. According to Avgerinos (2014) the choice is due to at least three main reasons: the possibility to implement the stress history; to predict the anisotropic stiffness in relation to the loading/unloading direction; and to evoke and calibrate stiffness degradation by considering the contribution of plasticity from the early small strain stages.

Chapter 4

NUMERICAL MODELLING OF TWIN TUNNELS AT HYDE PARK SITE

This chapter refers to the numerical modelling of the excavation of the new Crossrail twin tunnels at the extensive monitored Hyde Park site. This analysis was carried out with the aim of faithfully reproducing the results of the tunnelling-induced ground movements obtained by Avgerinos *et al.* (2018), on an earlier version of ICFEP than the current v.20, using the data contained in that paper. The kinematic hardening soil model of the London clay, scanned in detail in chapter 2, has been calibrated in two different cases, the'triaxial' and the 'low both', against triaxial and oedometric tests taking into account the excellent predictive results, reported in chapter 1, obtained by Avgerinos *et al*. (2016) when used for St James's Park greenfield site predictions. The adoption of two different cases calibrations allowed to extend the predictions with a certain degree of reliability also to the long-term. While for Avgerinos *et al.* (2018) the objective was to verify the agreement between numerical results and the measures taken on the field (Wan *et al*., 2017), in this thesis the objective is to have a clear picture of the impact caused by the excavation of twin tunnels with EPBMs in order to be able to compare it later with the numerical results derived from the excavation of a DOT tunnel on the same site.

4.1 Description of the numerical model

4.1.1 General site information

The extensively monitored greenfield site of Hyde Park is located at the intersection of the existing Central Line tunnels and the new Crossrail tunnels, which are larger than the usual London underground tunnels, at the northern edge

of the park below Bayswater Road. From the site plan in Fig. 4.1 it is possible to identify the position of the instrumentation aimed at monitoring surface and subsurface displacements along the three lines X-, Y- and Z-. In particular Avgerinos *et al.* (2018) refers exclusively to X- and Y-lines as perpendiculars to the axis of the Crossrail tunnel.

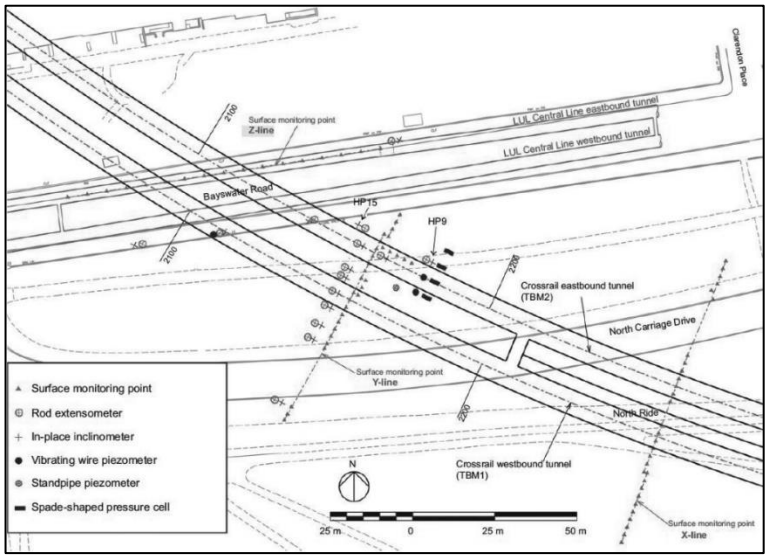

Fig. 4.1: *Instrumentation plan at Hyde Park site (Wan et al., 2017)*

As reported by Wan *et al*. (2017) vertical and horizontal surface settlements were measured through precise levelling (±0.3mm), total stations (±0.1mm) and micrometer stick measurements (±0.5mm). With regard to subsurface measurements, 38 boreholes were excavated containing a tandem of extensometers and inclinometers for vertical and horizontal displacement measurements combined with multi-level vibrating wire piezometers, a conventional stand-pipe piezometer and sword cells for measuring water pore and earth pressure variations (Fig. 4.2).

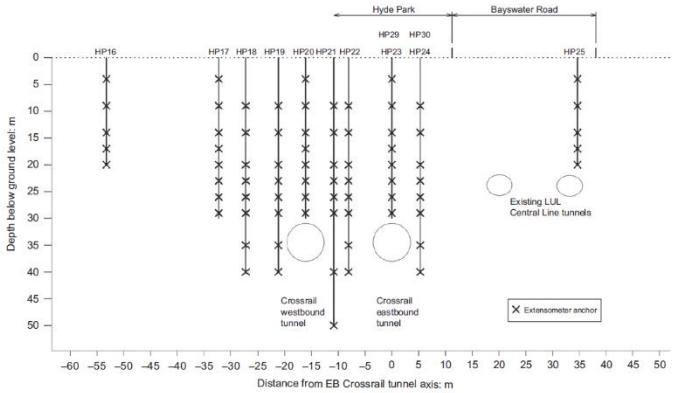

Fig. 4.2: *Cross-section A-A (looking Northwest in Fig. 4.1) with the rod extensometer boreholes on the Y-line (Wan et al., 2017)*

The soil profile that was adopted in the numerical analysis is based on surveys of the deepest inclinometer bore-holes, HP6, and is represented in Fig. 4.3. The stratigraphy is composed by a superficial 6m layer alluvial deposits and terrace gravels, that were modelled into a single layer, overlying on a 53.9m layer of London Clay within which the Crossrail tunnels were built. London Clay was subdivided into three different units (B2, A3 and A2) according to the geological distribution of King (1981) as explained at the beginning of chapter 2. The deepest layer of the model is the Lambeth Group which was also subdivided in two sublayers: the upper part with thickness of 4.7m is more clayey and less permeable while the lower part, 6m, is more granular and permeable. As already reported the tunnels were excavated by means of Earth Pressure Balance machines. The lining segments consist of conventional bolted precast concrete segments with an inner diameter of 6.2m and an outer diameter of 6.8m modelled by beam elements. The cement grade that was used is C50/60 with a steel fibre dosage of 30/40kg/m^3.

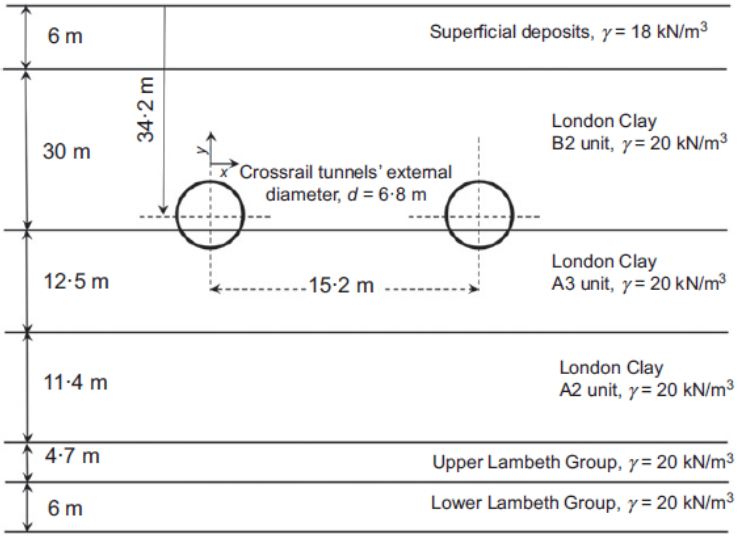

Fig. 4.3: *Soil profile and general geometry adopted for the analysis of the Crossrail tunnels at Hyde Park site (Avgerinos et al., 2018)*

4.1.2 Analysis sequences and model details

Chapter 3 mentions the importance of modelling the stress history of the site prior to tunnel excavation in order to achieve realistic predictions. Hyde Park site model simulates the erosion of 180m of overburden material in 19 increments. Subsequently, the 20th increment simulates the deposition phase of the superficial deposits in conjunction with the raising of the ground water table from the top of the London clay to the middle of the superficial depositional

layer. The underdrained profile of pore water pressures indicated by the piezometers and mainly due to the long period of water pumping from deep aquifers of London is simulated in 10 increments. The condition is assumed to be reached after 70 years in five increments (inc. 21-25), a second period of 70 years of consolidation (inc. 26-30) allows to reach a condition of equilibrium between the pore water pressure boundary condition and soil permeability, as well as giving time for the dispersion of residual loads. Excavation of each of the two tunnels takes place in 100 increments separated by a 73-day consolidation phase. The first tunnel to be excavated is the Westbound Crossrail tunnel (inc. 31-130) followed by the Eastbound one excavation (inc. 141-240). In this analysis, the lining was constructed when surface volume loss values were respectively equal to 0.87 and 1.26/1.29, really close to the values provided by Avgerinos *et al*. (2018) and in accordance with the results obtained along the X-surface monitored line, the furthest from the Central line where the results are less affected by the interaction with the pre-existing tunnels. Given the difficulty of determining the degree of permeability of the tunnels, it was decided to consider the two borderline cases of fully permeability or impermeable lining. A

Increments	**ΔT**	**Ttot after EB excavation**	**Analysis stages**
0	-	-	Deactivation of the finite elements representing the linings of the two tunnels and the superficial deposits
1 . 19	-		Erosion of 180m of overburden
20	-		Deposition of superficial deposits and rise of the groundwater table from the top of the London Clay to a 3m depth within the superficial deposits
21 . 25	70y		underdrainage of the pore water pressure profile
26 . 30	70y		
31 . 130	1d		Excavation/lining construction of westbound Crossrail tunnel
131 . 140	73d		Consolidation period of 73 days prior to the excation of the eastbound Crossrail tunnel
141 . 240	1d		Excavation/lining construction of eastbound Crossrail tunnel
241 . 250	10d	10d	Short - term consolidation period
251 . 260	40d	50d	
261 . 270	100d	150d	
271 . 275	215d	1y	
276 . 285	4y	5y	Long - term consolidation period
286 . 290	5y	10y	
291 . 295	20y	30y	
296 . 300	50y	80y	

Tab. 4.1: *Analysis sequences of twin tunnels*

detailed table of the analysis sequences is shown in Tab. 4.1.

The analyses were performed in plane-strain condition. The soil was modelled by 808 eight-noded quadrilateral isoparametric solid elements, while the two linings by 48 three-noded beam elements. The mesh dimensions, 235m

wide and 71m depth, were chosen in order to limit the influence of the boundaries conditions on the results. The finite-element mesh used in the

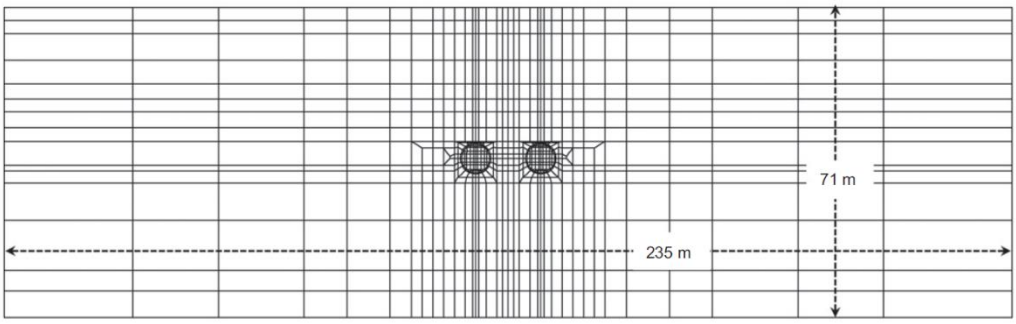

Fig. 4.4: *Finite element mesh used for the Hyde Park site Crossrail tunnel analysis*

analysis is shown in Fig. 4.4.

In the first phases, from increment 1 to increment 20, the model was run in drained conditions. Starting from the underdrainage phase, from increment 21, the analysis involves coupled consolidation. For this reason, the solid elements of London clay and of upper Lambeth Group, in addition to the 16 degrees of freedom associated with displacement, two for each of their eight nodes, have four additional pore water pressure degrees of freedom at their corners. The 3-nodes beam elements have three degrees of freedom for each node, two displacement and one rotation.

Boundary conditions fix the displacements at the base vertically and horizontally, while along the vertical boundaries horizontal displacements are prevented. London clay erosion is simulated by applying a 96.5 kPa/inc. vertical load on the top of the mesh from increment 1 to 19. A construction boundary condition has been applied to simulate the deposition of the superficial deposits.

As far as the hydraulic boundary conditions are concerned, the pore water pressure is hydrostatic and drained in the lower half of the surface deposit and in the lower Lambeth Group. From the beginning of the underdrainage phase, pore water pressure is prescribed to be 19.62 kPa at the border between the upper and the lower Lambeth Group in order to achieve the desired pore water pressure profile shown later in Fig. 4.5b. The interfaces between consolidating and non-consolidating elements are left free to drain.

For all the analyses a two-by-two integration was used, the modified Newton-Raphson technique was used as non-linear solver.

4.1.3 Constitutive models and geotechnical considerations

The constitutive models associated with the different material layers are analysed. Following exactly what reported in Avgerinos *et al.* (2018) the most

superficial alluvial and made ground layer was modelled as a unique linear elastic-perfectly plastic material having a modulus of Young E = 10000kPa and Poisson's ratio μ = 0.3 incorporating a Mohr-Coulomb yield surface with c' = 0kPa, ϕ' = 28° and υ = 12.5°. With regard to the behaviour of upper and lower Lambeth Group deposits a non-linear elastic (model J4, Jardine *et al.* (1986)) perfectly plastic (Mohr-Coulomb yield surface) model with c' = 0kPa, ϕ' = 28° and 36° and υ = 14° and 18° was adopted.

During the underdrainage phase and the consolidation period between the two tunnels excavations υ is imposed equal to zero to prevent excessive expansion and then reset to 14° during the excavation phases. Another argument is that this small-strain stiffness model is a continuously degrading model that accumulates deformations regardless of the direction of the stress-path. For this reason, the soil stiffness has been forced to increase by resetting the elastic hardening parameter to zero at each stage of the analysis.

The M2-SKH model (Grammatikopoulou, 2004) used to describe the behaviour of the London clay was discussed in detail in chapter 2. In this case, compared to Avgerinos *et al.* (2018), two different sets of calibrated parameters were used, the 'low triaxial' and the 'low both', taken from the numerical simulations contained in Avgerinos *et al.* (2016) at St. James park site. Specifically, the term 'low' refers to the initial elastic rigidity obtained experimentally after the researches on the intact properties of London clay by Heathrow terminal 5 project (Gasparre, 2005; Hight et al., 2007) which is lower than the previously available value. In the 'triaxial' the degradation of stiffness is obtained by triaxial shear tests and has proven to give very reliable predictions of displacements due to tunnelling in the short term. 'Both' calibration is obtained from a compromise between triaxial and oedometric test results. Considering the consolidation behaviour has proved to be important in obtaining good long-term predictions. Tab. 4.2 shows the different parameters associated with units A2/A3 and unit B2 for London clay.

Model parameters	'Low triaxial'	'Low both'
	(unit B2/unit A3)	
V_1	2·5/2·75	
λ	0·12/0·15	
κ	0·06/0·063	
n	0·87	
m	0·28	
A	250/180	260/190
φ'	25°/20·3°	
R	0·01/0·005	0·02/0·005
a	0·8	1·5

Tab. 4.2: *M2-SKH models parameters assumed for London clay units (Avgerinos et al., 2018)*

The model associated to the tunnel linings, consisting as mentioned of bolted precast concrete segments, is constituted by elastic linear beam elements with unit weight γ = 30kN/m^3, Young's modulus E = 40000MPa, Poisson's ratio μ = 0.15, cross sectional area per unit width of A' = 0.3m^2/m, second moment of area per unit width I = 2.25*10^-3 m^4/m and a shear correction factor, k=0.8.

The consistency between the model stress history, anisotropic permeability profile and pore water pressure distributions is verified. The trends obtained at the end of the underdrainage phase (inc. 30) coincide exactly with those reported by Avgerinos *et al.* (2018) using in-situ measurements. From the graph in Fig. 4.5a a reduction of the vertical and horizontal permeability as the depth increases is highlighted. The magnitude of the permeabilities has been multiplied by 4 in order to reach the desired underdrained pore water pressure profile (Fig 4.5b) in a shorter time frame (70 years) than the 350 years needed in reality and in the numerical analysis at St. James Park site (Avgerinos *et al.*, 2016) .

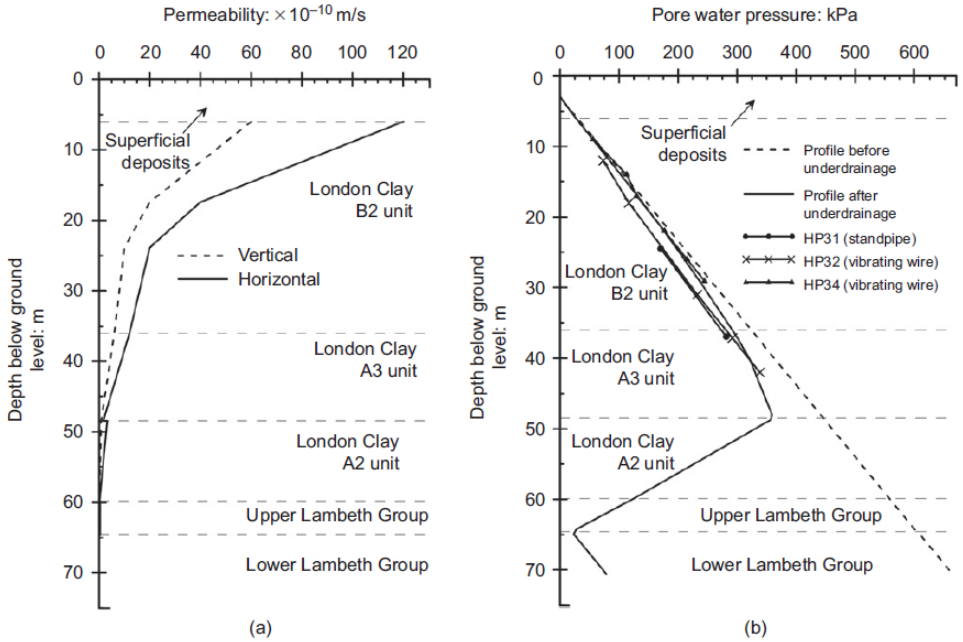

Fig. 4.5: *(a) permeability and (b) pore water pressure profile assumed in the finite-element analysis (Avgerinos et al., 2018)*

The underdrainage phase also affects the yield stress ratio (YSR) and K0 profiles represented in Fig 4.6 before and after underdrainage. The variation in terms of YSR is greater at the base of London clay where the pore water pressure profile deviates more from the hydrostatic profile. This decrease is linked to an increase in the effective vertical pressure, while the values of the effective horizontal stress remain unchanged leading to a decrease in the magnitude of K0. The kink in the K0 profile at the upper Lambeth Group is due to the adoption of a simplified constituent model that fails to accurately take into account the

effects of the previous stress history. However, since this level remains below the invert of the tunnels it was not considered to play such an important role in predicting soil displacement.

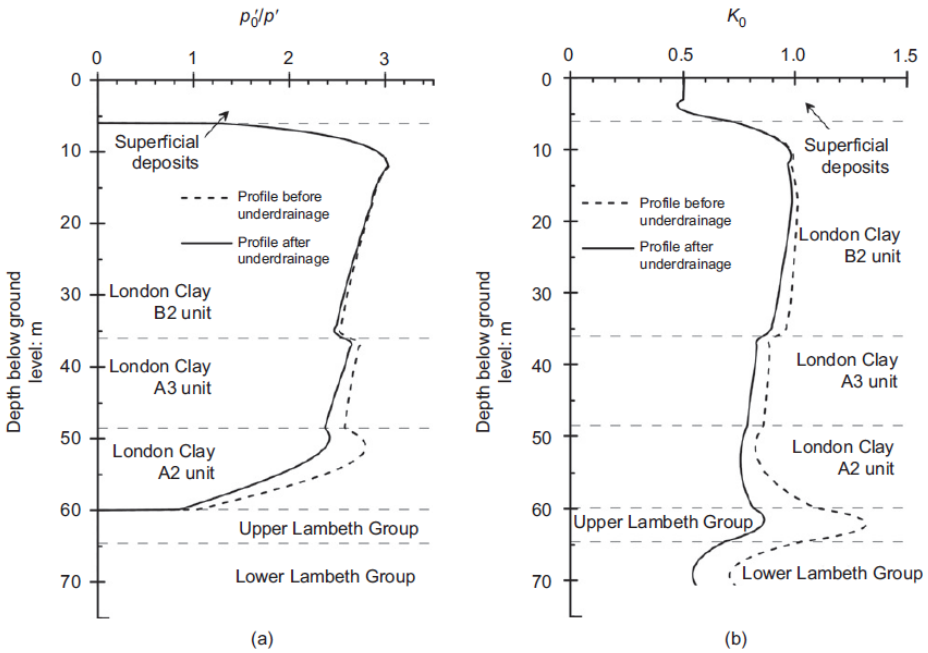

Fig. 4.6: *Effect of underdrainage phase on (a) yield stress ratio (YSR) and (b) K0 profile (Avgerinos et al., 2018)*

4.2 Soil displacement due to twin tunnels excavation

As stated above, the numerical analysis on the twin tunnels was carried out with the aim of reproducing the excellent results obtained by Avgerinos *et al.* (2018) on the most recent version of the program, v.20, and to form the basis for demonstrating the potential of the DOT tunnel technique. This paragraph compares the new results in terms of surface displacements with the previous results, demonstrating the good degree of consistency of the analyses.

4.2.1 Surface displacement due to WB Crossrail tunnel construction

The simulation of the Westbound Crossrail tunnel excavation was carefully calibrated with respect to field measurements. In particular, the trend of the vertical ground surface settlement was obtained by fitting the Gaussian function with respect to the obtained in-situ values. From these measurements a slightly wider surface trough on the northern part than on the southern one is evident. This phenomenon is attributable to the presence of the Central Line tunnels. For the same reason, another observation is the substantial difference between the ground volume losses determined along the X- and Y- lines. The measurements

along line X have higher magnitude due to the proximity of the existing underground tunnels. Avgerinos *et al.* (2018) concludes that the surface volume loss to be used as a target in the excavation of the tunnels with the volume loss-controlled method is that of the southern edge of the X-line.

The different values of surface ground volume loss are shown in Tab.4.3. The volume losses produced by the numerical analysis, obtained by integrating the Gaussian best-fit to the surface settlement part corresponding to the X-line width, are slightly higher than the desired value (0.8%).

WB Crossrail tunnel ground surface volume loss		
Y-line (*from field measurements*)	southern half-trough	northern half-trough
	0.40%	0.48%
X-line *(from field measurements)*	southern half-trough	northern half-trough
	0.78%	0.78%
integrating the surf. settl. trough (*from Avgerinos et al., 2018*)	0.86%	
integrating the surf. settl. trough (*from new numerical analysis*)	0.85%	

Tab. 4.3: *Volume loss for the WB Crossrail tunnel*

Avgerinos *et al.* (2018) to effectively compare surface settlement troughs and normalised surface settlement troughs with experimental measurements applies a correction to the real trend obtained from numerical analysis. This correction is intended to replicate the correction on the field measurements with respect to the base of the deepest boreholes considering a zero vertical displacement trend along the 50m line. The correction with respect to the value of the vertical displacement at the base of HP21 at 40m depth is not considered to be important for the objectives of this thesis. The trends obtained by Avgerinos *et al.* (2018), considering an unloading percentage of 7%, are shown in Fig. 4.7 in comparison with the new results obtained from the analysis on the most recent version of the program.

A comparison between the graphs in the first and second lines of Fig. 4.7 shows that the trend of the new analysis reproduces in a very similar way the trend of the vertical ground surface settlement and the normalised ground settlement due to the Westbound tunnel excavation compared to the trend obtained by Avgerinos *et al.* (2018) with a maximum vertical subsidence value around 7 mm. The same identical process is applicable to horizontal surface displacements obtaining, also in this case, an excellent degree of similarity between trends (Fig. 4.8).

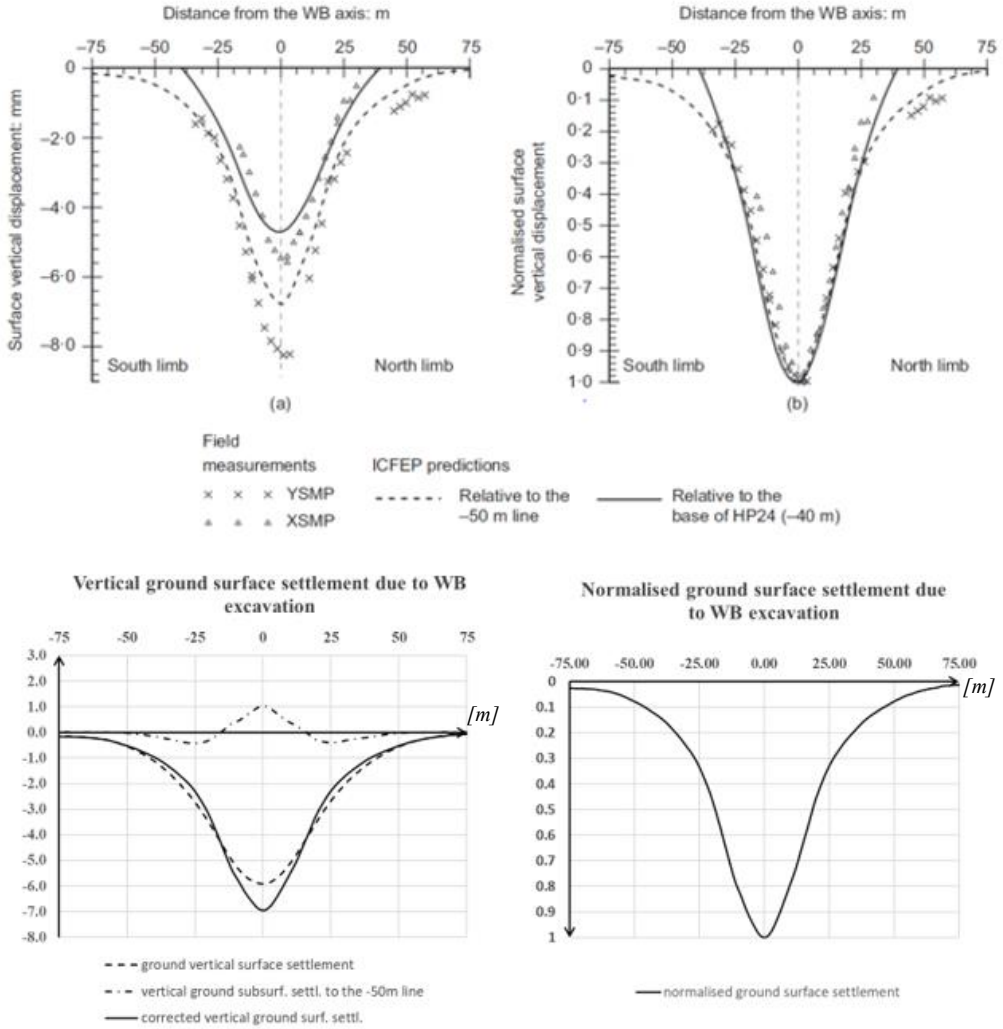

Fig. 4.8: *Comparison between the ground surface settlement and normalised ground surface settlment trends obtained by Avgerinos et al. (2018) (line 1) and the new results of v.20 (line 2)*

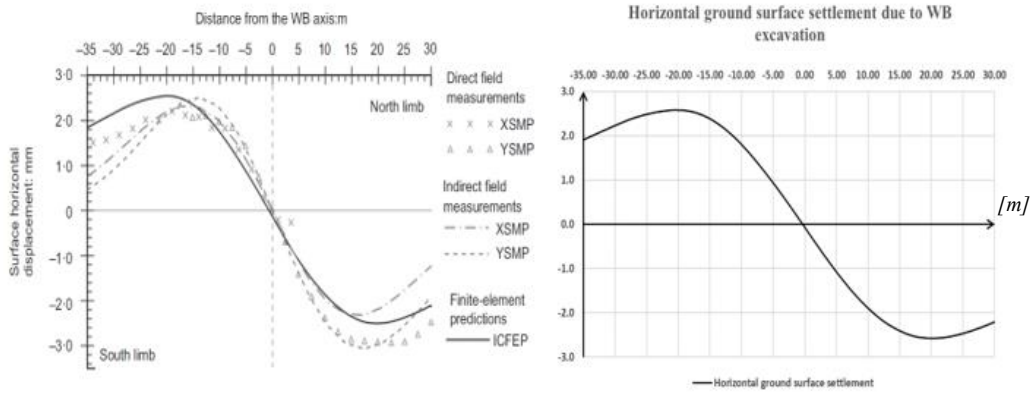

Fig. 4.7: *Comparison between the horizontal ground surface settlement and trends obtained by Avgerinos et al. (2018) (on the left) and the new results of v.20 (on the right)*

As shown in the graph on the left in Fig. 4.8. , the one showing the horizontal surface displacements reported in Avgerinos *et al.* (2018), in addition to the field measurements and numerical predictions, there are the profiles calculated indirectly based on the fitting of Gaussian curves with respect to field data in conjunction with a point sink assumption where the resultant vectors of displacement at any point of X- and Y-line is directed towards the tunnel axis.

Direct measurements reveal the asymmetry of horizontal surface displacements, the largest displacements, attributable to the Central line tunnels are on the northern side. The numerical analysis curve, instead, is symmetrical and better approximates the south side field measurement trend. Avgerinos *et. al.* (2018) concludes that both field measurements and numerical analysis predict wider curves than the indirect point-sink assumption approach. With regard to the objectives of this thesis, the new numerical results (on the right of Fig. 4.8) seem to approximate very well those obtained by Avgerinos *et al.* (2018).

4.2.2 Surface displacement due to EB Crossrail tunnel construction

Compared to the previous case, where considering the impermeability of the tunnel would have led to very similar results to the reported permeable case, the analysis of soil displacements due to EB tunnel excavation includes two different assumptions: the fully permeable or impermeable lining of the two tunnels cases. The surface volume losses obtained from field measurements and those given by the numerical analyses are reported in Tab. 4.4. The unloading percentage associated with the construction of the lining used in the volume loss control method is equal for the permeable and impermeable cases to 9% and 12% respectively.

EB Crossrail tunnel ground surface volume loss			
Y-line (*from field measurements*)		southern half-trough	northern half-trough
		0.97%	0.70%
X-line *(from field measurements)*		southern half-trough	northern half-trough
		1.39%	0.78%
integrating the surf. settl. trough (*from Avgerinos et al., 2018*)		southern half-trough	northern half-trough
	perm.	1.26%	1.21%
	imperm.	1.07%	1.18%
integrating the surf. settl. trough (*from new numerical analysis*)	perm.	1.26%	
	imperm.	1.20%	

Tab. 4.4: *Volume loss for the EB Crossrail tunnel*

Also in this case, the value given by the southern part of the troughs of the field measurements is considered more reliable in the choice of a target volume loss value (1.3%). Certainly the north side is influenced by the presence of the

Central line tunnel, but the most relevant effects are given by the presence of the WB tunnel so it was considered a slightly lower volume loss value than that obtained in the southern limb.

The comparison between the vertical ground surface settlement trends and the normalised settlement trough obtained by Avgerinos *et al.* (2018) and the results obtained in the new version are shown in Fig. 4.9.

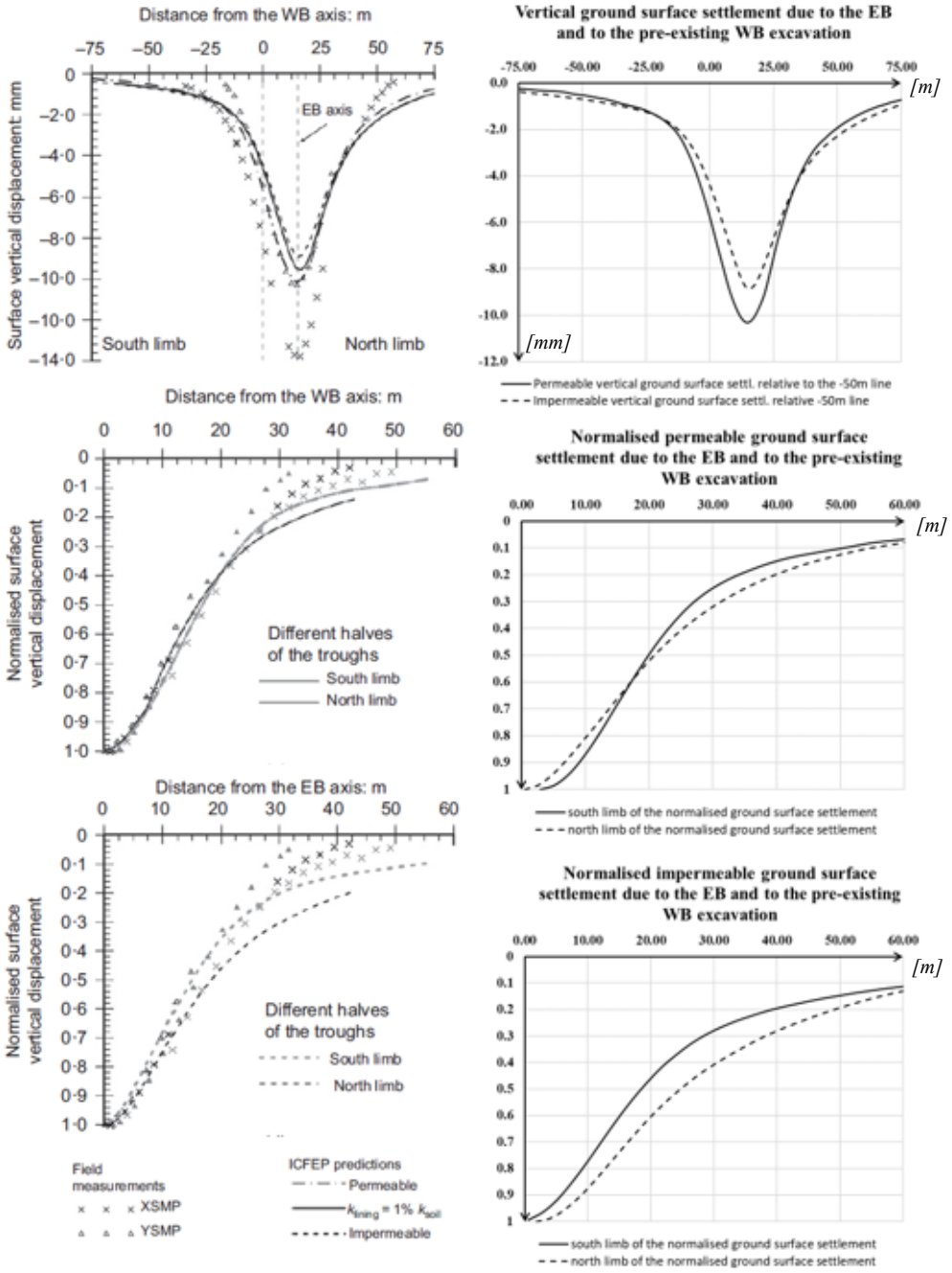

Fig. 4.9: *Comparison between the ground surface settlement and normalised ground surface settlment trends obtained by Avgerinos et al. (2018) (on the left) and the new results of v.20 (on the right)*

The comparison between the numerical data and the field measurements contained in Avgerinos *et al.* (2018) is helpful in interpreting the data. This is particularly evident at the six northernmost points of the tunnel that are affected by the presence of North Carriage Drive. In general, the numerical predictions obtained from the new version are very similar to those obtained in Avgerinos *et al.* (2018) and they approximate well the trend of the measurements on the Y-line section, the permeable case better than the impermeable case.

The northern limb of the normalised shapes predicts well field measurements up to North Carriage Drive regardless of the level of permeability. The shape of the southern limb is well predicted only for the permeable case, in fact only in this case the southern limb of the curve is wider than the northern limb as measured. As concluded by Avgerinos *et al.* (2018) this may be due to a better approximation of the changes in the pore water pressure profile in the short term of the permeable case. A correct prediction of water pore pressure changes plays a key role in the correct prediction of stress-path and thus in terms of soil stiffness response.

Finally, also with regard to the horizontal ground surface displacement due to the excavation of the EB tunnel (Fig. 4.10), using the same approach related to the excavation of the WB tunnel, there is uniformity between the results of Avgerinos *et al.* (2018) and those related to this thesis. The field results of the Y-line are quite well reproduced when the lining is simulated as fully impermeable, the maximum values are located at the same horizontal distance from the EB axis but have quite different modules.

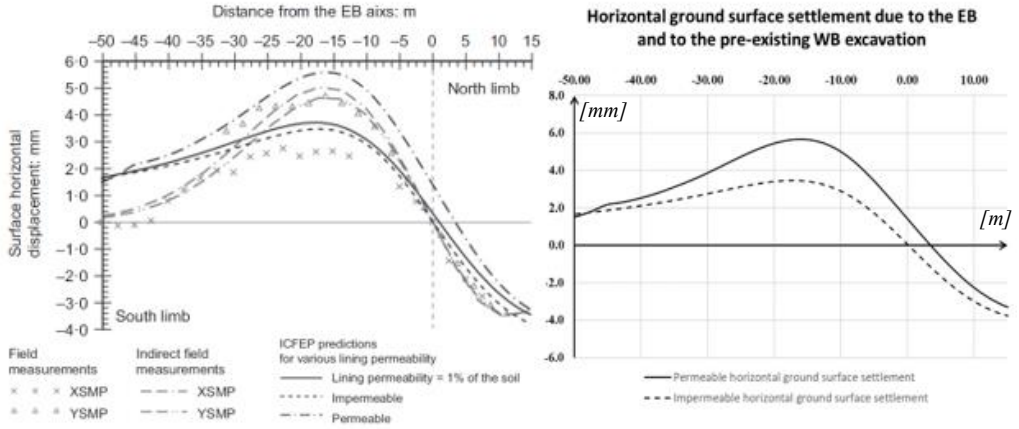

Fig. 4.10: *Comparison between the ground surface settlement and normalised ground surface settlment trends obtained by Avgerinos et al. (2018) (on the left) and the new results of v.20 (on the right)*

Taking into account the comparison of surface settlements reported in this subparagraph, it can be concluded that the analysis implemented on the most recent version of ICFEP, v.20, which is the main reference for this thesis, is consistent with the analysis of Avgerinos *et al.* (2018).

4.2.3 Short term response

Numerical analysis by Avgerinos *et al.* (2018) has demonstrated excellent predictions of tunneling-induced ground movements compared to field monitoring in Hyde Park (Wan *et al*., 2014). This paragraph reports the graphs of the surface and subsurface movements on the short period related to the excavation of the two tunnels highlighting the indications in terms of ground response provided by the new numerical results.

The identification of a boundary between long-term and short-term predictions may not be immediate and can cause potential discrepancies between different analyses, in this case it was decided to consider this boundary set at 1 year after the excavation of the EB tunnel.

The surface troughs of the calibrated permeable and impermeable vertical displacements with respect to the 'low triaxial' configuration is shown in Fig. 4.11.

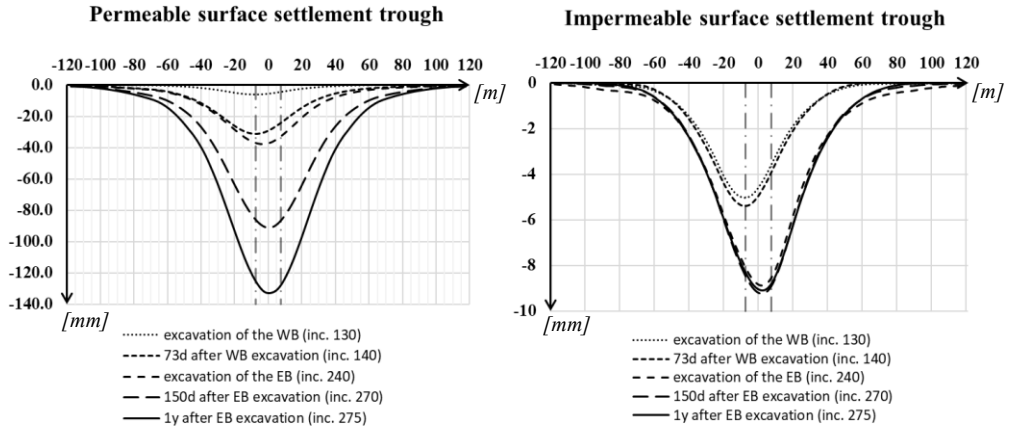

Fig. 4.11: *Permeable and impermeable 'low triaxial' surface settlement troughs centered in the symmetrical axis of the mesh*

The evolution of the predicted surface settlement reveals the importance of the parameter associated with the permeability of the lining. The fully permeable borderline trends differ greatly from the fully impermeable borderline ones.

In case the soil-lining interface is fully permeable, a first phase linked to the undrained settlement is followed by a consolidation phase that leads to deformations in the order of tens of cm. The strains given by the excavation of the two tunnels accumulate on each other. Phenomena related to the interaction followed the construction of the EB tunnel are visible from the impermeable case where the asymmetry of the curve with respect to the central and symmetrical axis of the mesh is visible. The values of maximum vertical displacement that are in the order of a few millimeters are decentralized towards the axis of the second excavated EB tunnel.

In order to ascertain the magnitude of the field of ground soil displacements, the trends of vertical subsurface displacements on different depth levels are shown in Fig. 4.12 including a whole series of graphs.

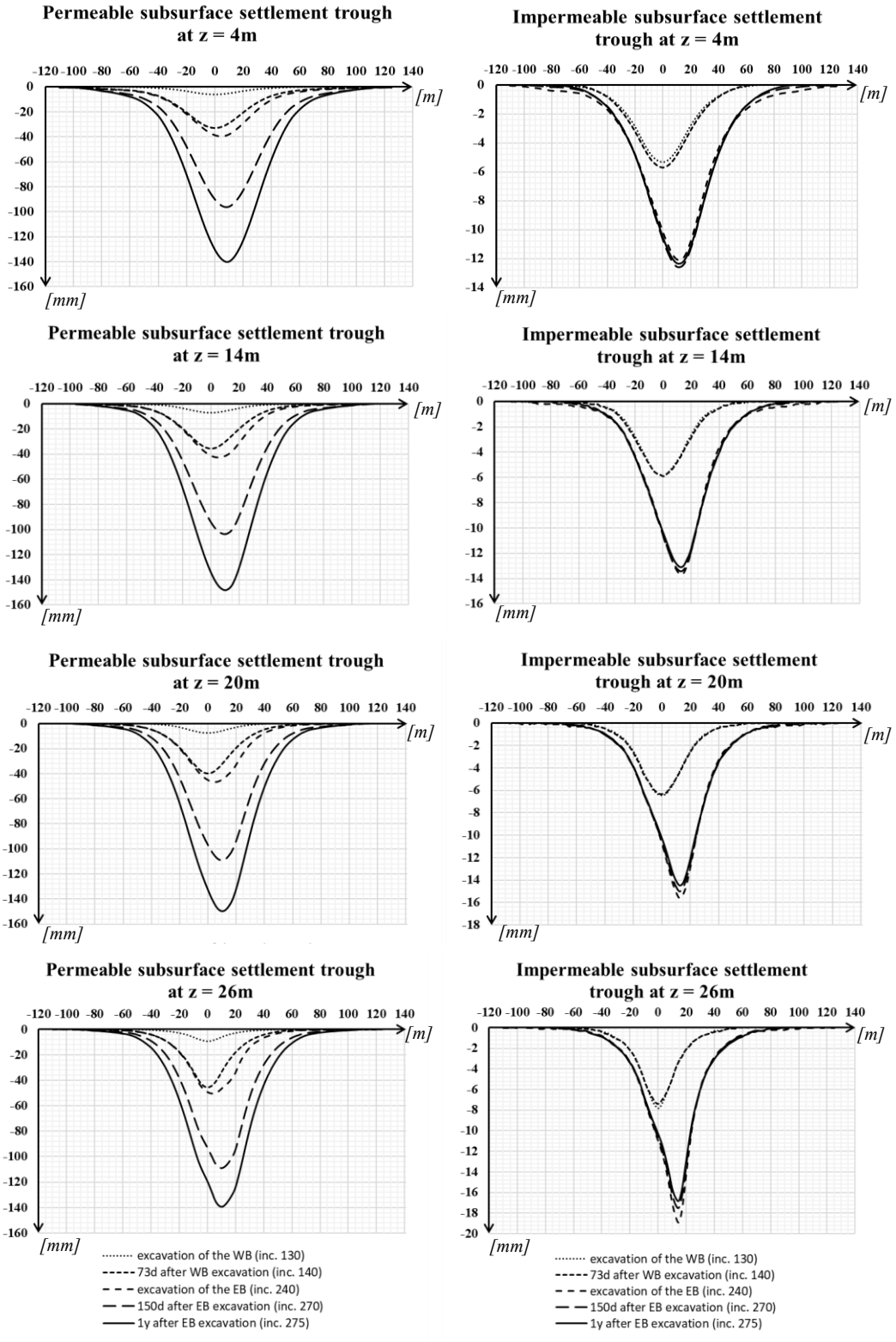

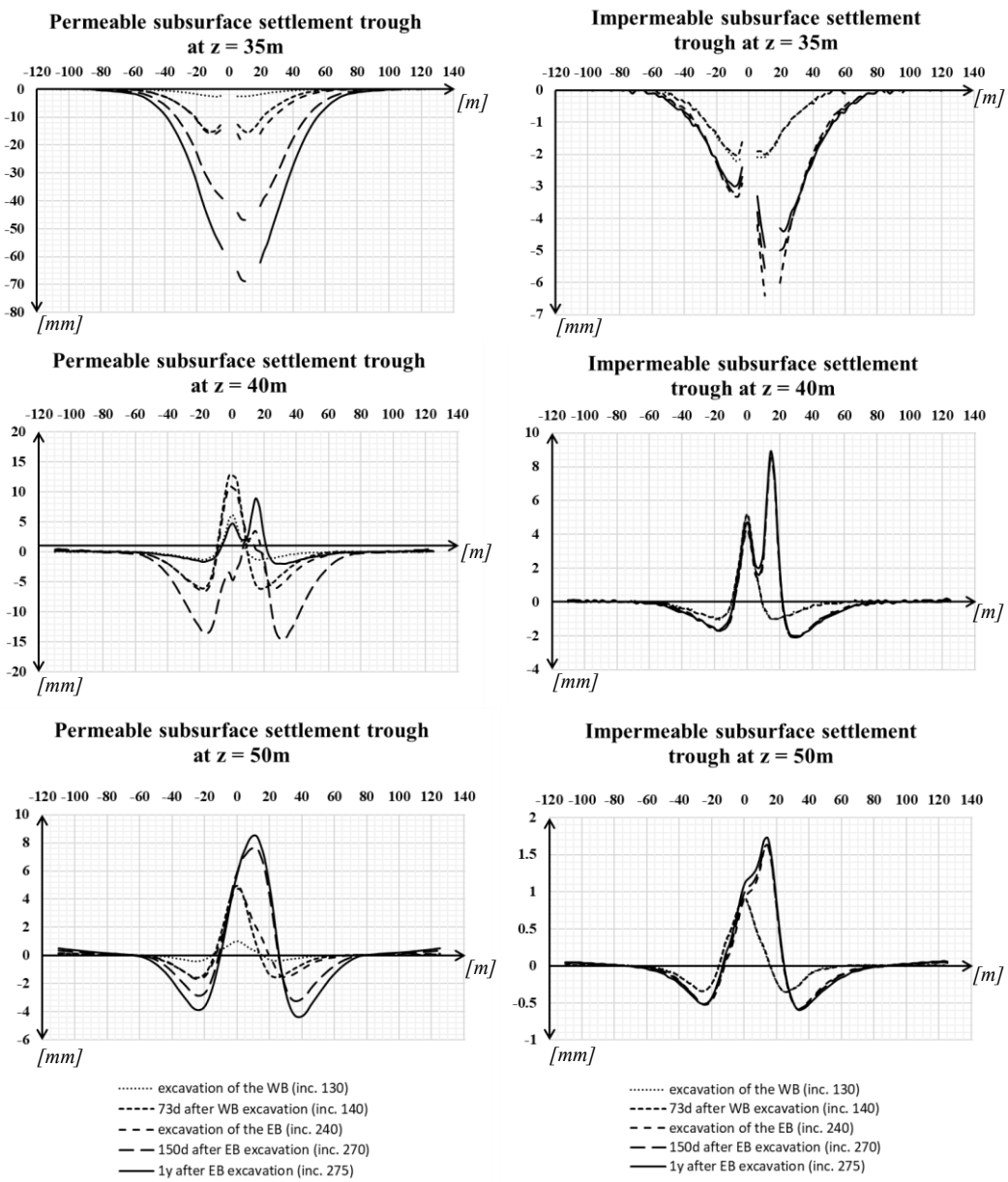

Fig. 4.12: *Permeable and impermable subsurface 'low triaxial' settlement troughs due to the WB and EB Crossrail tunnel excavation at different depths below ground level: 4m, 14m, 20m, 26m, 35m, 40m, 50m.*

The trends of the permeable vertical ground subsurface settlements show an increase in the maximum values as the depth increases above the crown level tunnel and then a decrease for greater depths. This increase is also associated with an increase in the value of the subsurface trough width parameters with the depth as reported in Fig 4.13. The variations of the settlements over time reveal, focusing on the curves in the immediate vicinity of the linings, the effect of interactions between tunnels due to the plasticization of the ground: the ground

displacements due to the excavation of the second tunnel are greater than those caused by the excavation of the first.

In the impermeable case, on the other hand, a principle of swelling of the ground can be observed after the excavation of the two tunnels. This phenomenon is evidence of how important the parameter of the permeability of the lining is on the numerical output results, especially the further the predictions go over time.

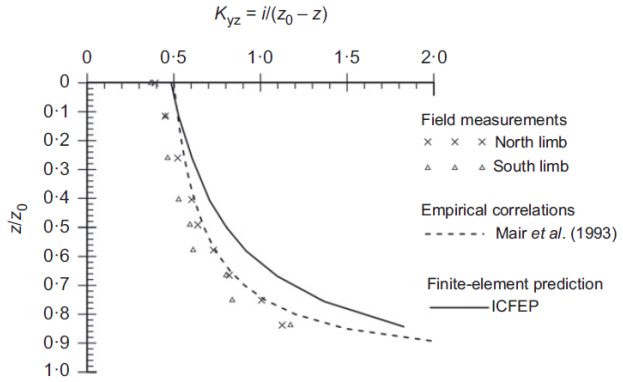

Fig. 4.13: *Subsurface trough width parameters due to the WB excation at inc. 130 (Avgerinos et al., 2018)*

4.2.4 Long term response

In the long-term the consolidation behaviour of London clay dictates the soil movements. As mentioned before, based on studies by Avgerinos *et al.* (2016) at St. James park site, the numerical predictions reveal that the bubble model needs to be carefully calibrated also against oedometer tests results using the 'low-both' calibration. The results of the long-term vertical ground surface settlement predictions using ‘low both’ calibration are shown in Fig. 4.14.

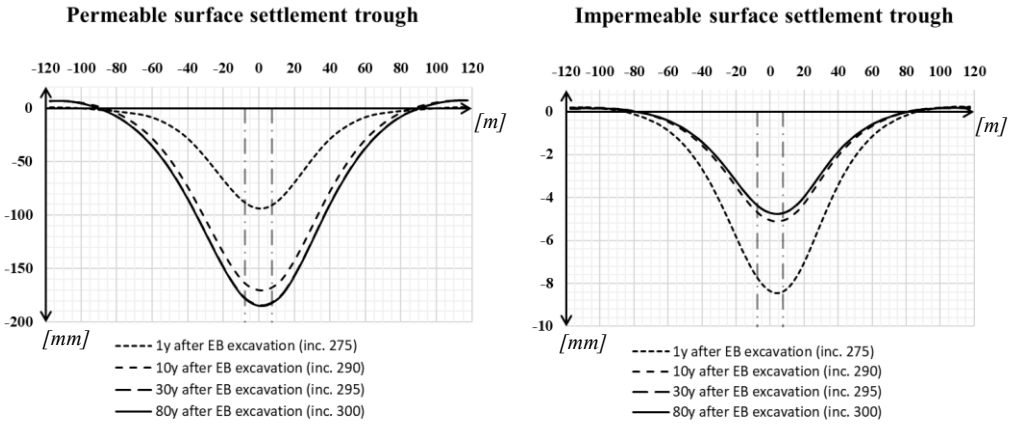

Fig. 4.14: *Permeable and impermeable ‘low both’ surface settlement troughs centered in the symmetrical axis of the mesh*

The 'low-both' calibration predicts a more rigid response compared to the ‘low triaxial’ case as can be seen from the comparison of the trend at 1 year from the EB tunnel excavation at inc. 275. Both the permeable case and the impermeable case show that the vertical ground settlement achieved after 30 years is very close to what would be achieved after 80 years so that the consolidation settlement can be considered to be completed. The swelling of the tunnels in the impermeable case is highlighted. In the entirely theoretical case of complete impermeability, in fact, the pressures exerted on the tunnel, considering the constraints imposed on the model, result in an upward movement.

For a more in-depth analysis, long-term subsurface settlements are shown in Fig. 4.15.

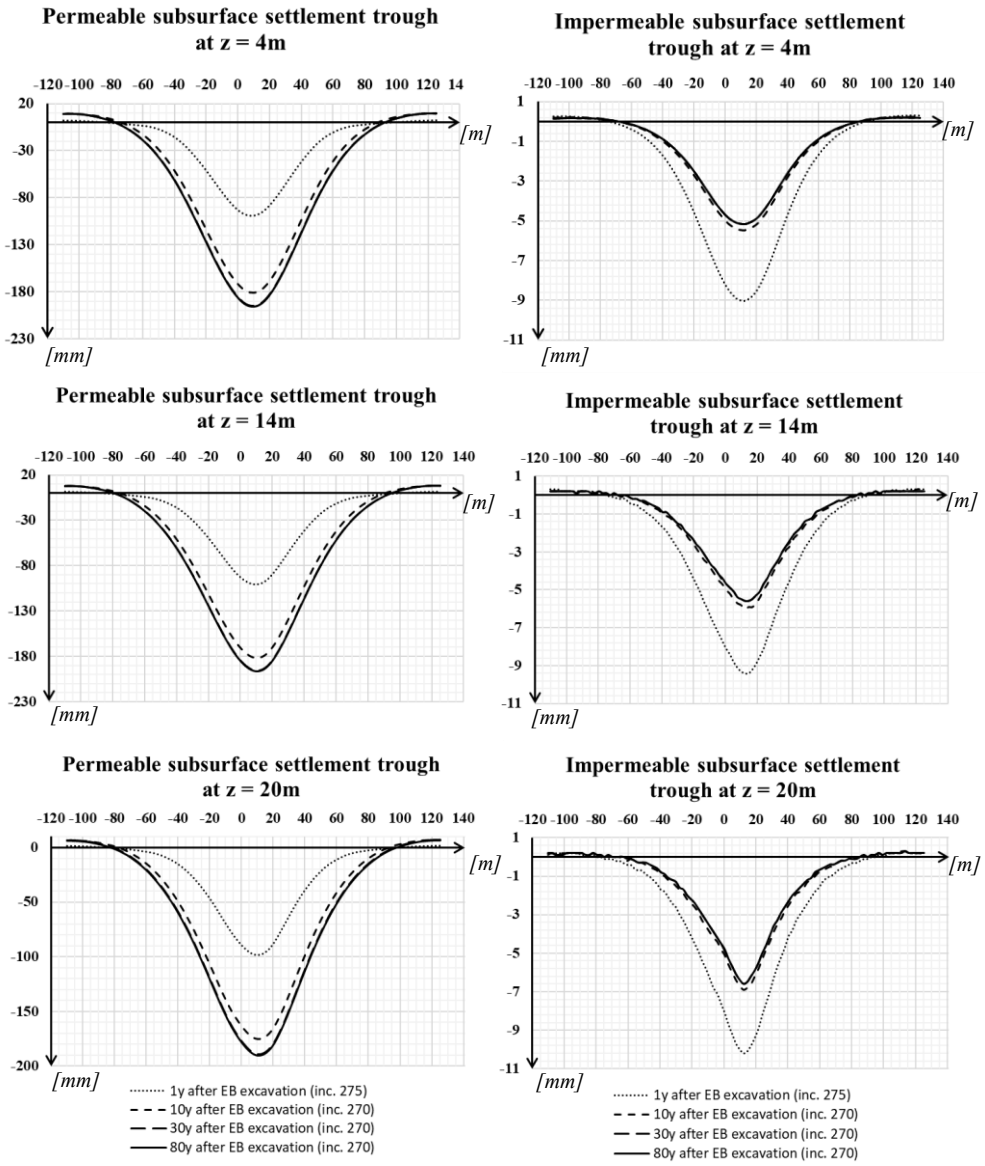

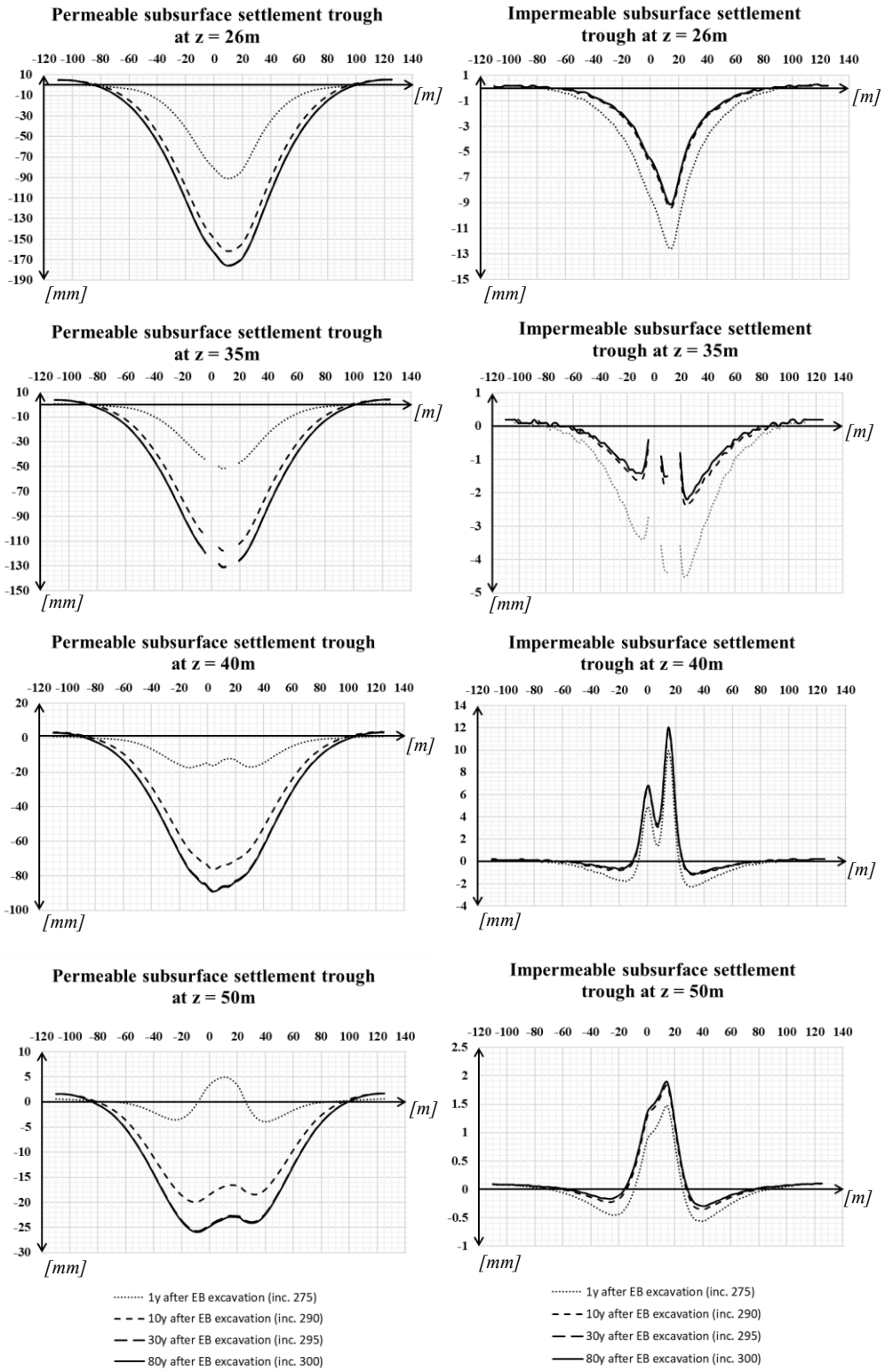

Fig. 4.15: *Permeable and impermable subsurface 'low both' settlement troughs due to the WB and EB Crossrail tunnel excavation at different depths below ground level: 4m, 14m, 20m, 26m, 35m, 40m, 50m.*

Chapter 5

NUMERICAL MODELLING OF A DOT TUNNEL AT HYDE PARK SITE

The objective of this chapter and more generally of this thesis is to test through numerical modelling the excavation of a DOT tunnel at the Hyde Park site. This analysis was performed with reference to the parameters used in Avgerinos *et al.* (2018) numerical model which was validated by field measurements (Wan et al., 2017) and reproduced on ICFEP v.20 (Potts & Zdravkovic, 1999; 2001) as reported in Chapter 4. The model of the DOT tunnel is based on the shape adopted for the construction of the Shanghai metro in China which was the subject of recent internal research (Zhou & Zdravkovic, 2020). The results are compared with those obtained from the numerical modelling of new Crossrail twin tunnels in order to measure the effectiveness of this technique in stiff London clays conditions compared to traditional excavation techniques.

5.1 Description of the numerical model

5.1.1 Model details

The Hyde Park site is extensively described in section 4.1. Each detail of the numerical analysis on the DOT tunnel related to the soil stratigraphy, the physical properties of the materials, the adoption of the constitutive models, the numerical simulation of the site's stress history and, more generally, any geotechnical considerations, faithfully reproduces what is reported in Chapter 4 for the analysis of the Crossrail twin tunnels.

The only main difference to focus on is the new mesh where instead of the two twin tunnels at a distance of 15.2m from each other there is a DOT tunnel in a central position and at a depth of 34.2m. The mesh dimensions are 70.6m in height and 213m in width. In order to be able to compare the results properly, the diameter of the two overlapping circles that make up the DOT tunnel is equal

to that of the twin Crossrail tunnels taken individually equal to 6.8m. The distance between the centres is 5m, the total area is $67.13m^2$. The outer lining consists of 26 three-noded beam elements plus the 6 elements of the central pillar. The mesh and an enlargement on the elements at the DOT tunnel are shown in Fig. 5.1.

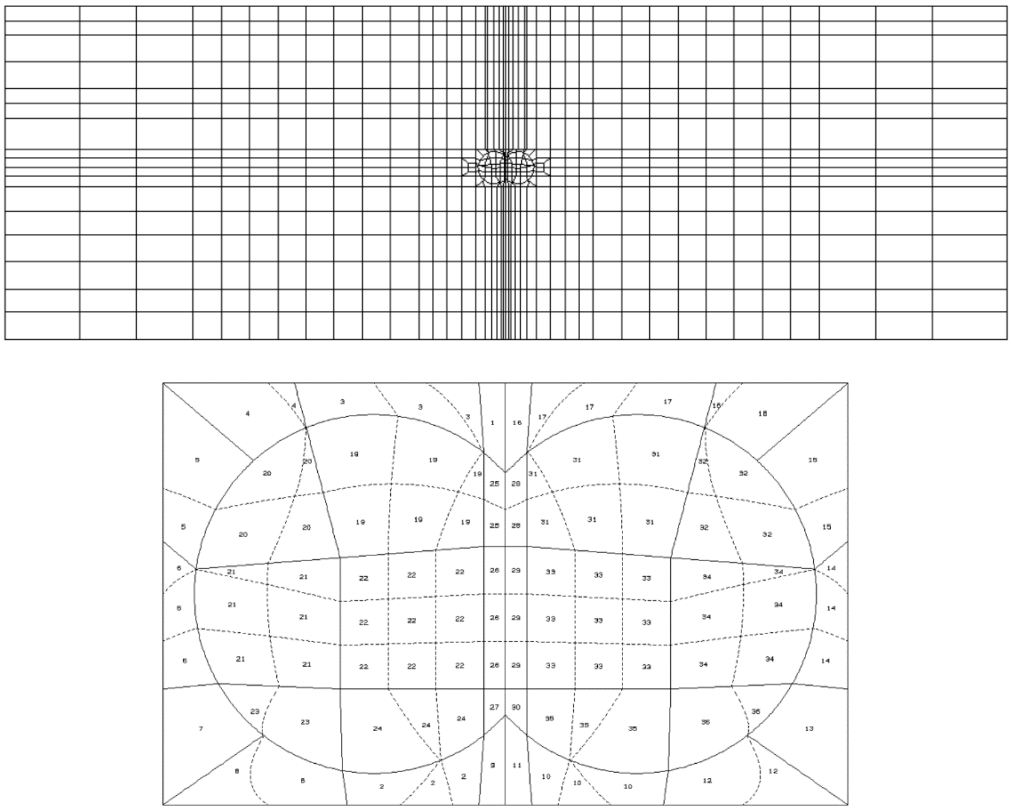

Fig. 5.1: *Finite element mesh used for the Hyde Park site DOT tunnel analysis with an enlargement on the elements at the DOT tunnel.*

5.1.2 Analysis sequences

The sequences of the DOT tunnel analysis are also adapted from those used for the Crossrail twin tunnel analysis so that the results can be effectively compared in the same time intervals in order to make the comparison as immediate as possible.

The excavation of the DOT tunnel and the construction of the lining takes place in the same range of increments associated with the excavation of the first tunnel in the numerical analysis reported in Chapter 4. The increments associated with the 73-day consolidation phase and with the excavation of the second tunnel in the twin tunnels case have been divided in order to study in detail the effects of excavation of the DOT tunnel in the temporal instants following the

construction phase (from inc. 131 to inc. 240). From increment 241 there is a return to a common overlap of the twin and DOT tunnel analyses sequences which makes it easier to compare the results.

A detailed table of the DOT analysis sequences, to be compared with those of the twin tunnel analysis (Tab. 4.1), is represented in Tab. 5.1.

Increments	**ΔT**	**Ttot after DOT excavation**	**Ttot after EB excavation**	**Analysis stages**
0	-	-	-	Deactivation of the finite elements representing the linings of the DOT tunnel and the superficial deposits
1 . 19	-			Erosion of 180m of overburden
20	-			Deposition of superficial deposits and rise of the groundwater table from the top of the London Clay to a 3m depth within the superficial deposits
21 . 25	70y			Underdrainage of the pore water pressure profile
26 . 30	70y			
31 . 130	1d			Excavation/lining construction of the DOT tunnel
131 . 140	5h	5h		74d consolidation period
141 . 159	19h	1d		
160 . 175	2d	3d		
176 . 220	10d	23d		
221 . 235	18d	38d		
235 . 240	56d	74d		
End of the excavation/lining construction of eastbound Crossrail tunnel in the twin tunnels analysis				
241 . 250	10d	84d	10d	Short - term consolidation period
251 . 260	40d	124d	50d	
261 . 270	100d	224d	150d	
271 . 275	215d	1y 74d	1y	
276 . 285	4y	5y 74d	5y	Long - term consolidation period
286 . 290	5y	10y 74d	10y	
291 . 295	20y	30y 74d	30y	
296 . 300	50y	80y 74d	80y	

Tab. 5.1: *Analysis sequences of DOT tunnel*

5.1.3 Unloading percentage calibration

The tunnel lining is constructed when a certain unloading percentage is reached. This parameter is calibrated in relation to the ratio between the ground surface volume loss and the total area of the excavated tunnel on the basis of field measurements in order to simulate as realistically as possible the excavation/construction phase of a tunnel.

In this case, no field data associated with the DOT tunnel excavation in stiff clays are available, but the volume losses caused by the DOT tunnel excavation in the soft clays of Shanghai were greater than the values obtained from the excavation of circular tunnels. Taking this into account and knowing that the volume loss value associated with the excavation of the Eastbound tunnel in the numerical analysis in Chapter 4 is higher as a result of the action of the pre-existing Westbound tunnel, the choice was to take as a reference for the permeable case an intermediate value between that caused by the excavation of

the WB and that caused by the excavation of the EB tunnel. The results of the unloading percentage calibration deriving from the application of the ground surface volume loss method are reported in Tab. 5.2 and Tab. 5.3.

unloading percentage %	LOW TRIAXIAL		LOW BOTH	
	perm	imperm	perm	imperm
WB	7	7	17	17
EB	9	12	19	23
DOT	5	5	14	14

Tab. 5.3: *Unloading percentage associated with the construction of the lining for each case of the numerical analysis*

ground surface volume loss %	LOW TRIAXIAL		LOW BOTH	
	perm	imperm	perm	imperm
WB	0.85	0.71	0.87	0.75
EB	1.26	1.20	1.29	1.25
DOT	1.03	0.72	1.06	0.81

Tab. 5.2: *Ground surface volume loss due to the excavation of the tunnels for each case of the numerical analysis*

5.2 Soil displacement due to DOT tunnel excavation

In this paragraph the results obtained from the numerical analysis simulating the excavation of a DOT tunnel are reported and analysed. The comparison with the results of the Crossrail twin tunnel analysis provides a consistent yardstick through which to make an initial assessment of the effectiveness of the use of this technique in London ground conditions. The analysis considers the two borderline cases with permeable or impermeable lining.

5.2.1 Surface displacement due to DOT tunnel construction

Compared to the excavation of a single circular tunnel with a diameter equal to one of the two circular inscribed tunnels forming a DOT tunnel, the ground volume loss due to DOT tunnel excavation is certainly greater because the excavated area is larger. Fig. 5.2 shows an overlap between the vertical ground surface settlement due to the excavation of the DOT and the two twin tunnels.

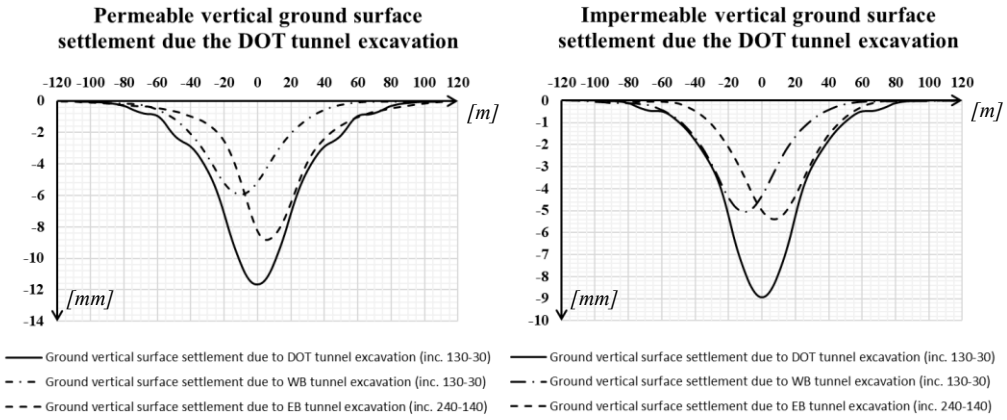

Fig. 5.3: *Overlap between the permeable and impermeable vertical ground surface settlement due to the excavation of the DOT and of the two twin tunnels*

The first observation is that the permeable case always leads to higher volume loss values than the impermeable case. The simulation of the excavation of the DOT tunnel leads to a symmetrical trend with some lateral undulations that differ from the Gaussian trend of the twin tunnels and from the asymmetry of the function associated with the EB excavation that is affected by the excavation of the pre-existing WB tunnel. The differences related to the influence of the tunnel shape on ground displacements can be consulted by comparing the normalised trends in Fig. 5.3.

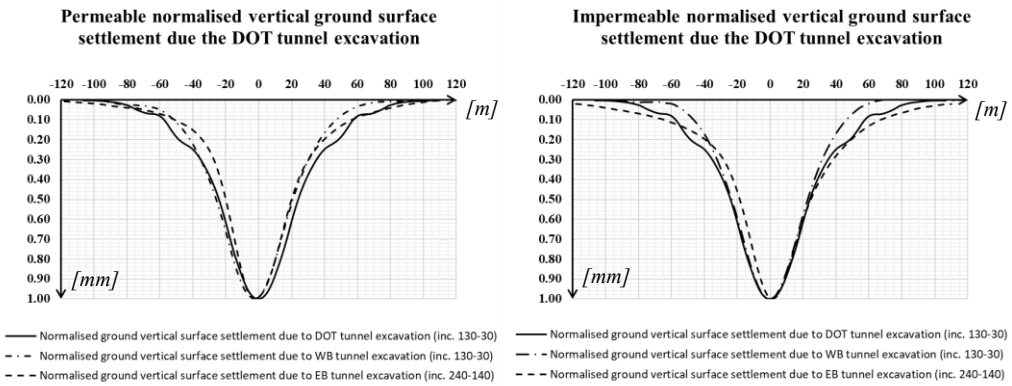

Fig. 5.2: *Overlap between the permeable and impermeable normalised vertical ground surface settlement due to the excavation of the DOT and of the two twin tunnels*

To conclude the argument in a rigorous way, Fig. 5.4 shows the comparison between the trends of horizontal surface displacements due to tunnels excavation. Horizontal displacements are limited and there is no major difference between the trend of the DOT tunnel and that of the twin tunnels. In certain ranges the horizontal displacements caused by EB tunnel excavation

exceed those caused by DOT tunnel excavation. This result can be traced back to the interaction originated by the construction of the two tunnels in different time instants.

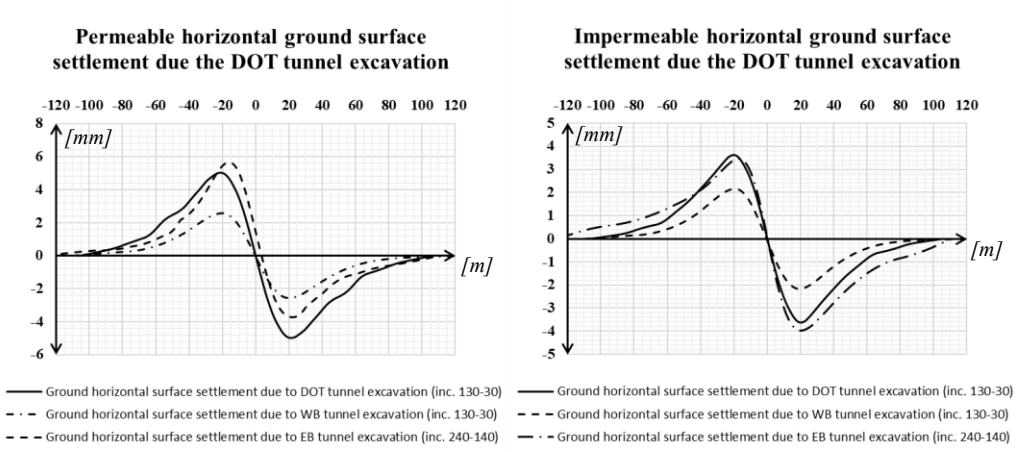

Fig. 5.4: *Overlap between the permeable and impermeable horizontal ground surface settlement due to the excavation of the DOT and of the two twin tunnels*

5.2.2 Short term response

The evaluation of the evolution of the ground vertical surface displacements due to the excavation of a DOT tunnel is the key point for measuring the effectiveness of this technique compared to the traditional twin tunnel technique from an engineering point of view.

The results of the 'low-triaxial' permeable case in Fig. 5.5 show a promising slight decrease in the maximum values for the same curve width compared to the case of twin tunnels already in the short term.

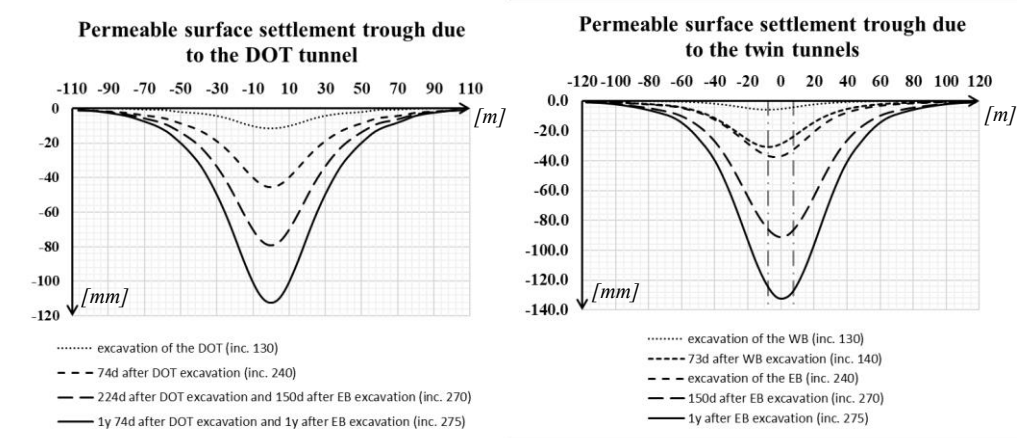

Fig. 5.5: *Permeable surface settlement trough due to the DOT tunnel (on the left) and due to the twin tunnels (on the right)*

The impermeable case in Fig. 5.6 reveals very similar trends to the final two-stage excavation of the twin tunnels. The 74 days gap between the completion of the DOT tunnel and the completion of the EB tunnel are clear and intuitive evidence that digging one tunnel is faster than digging two.

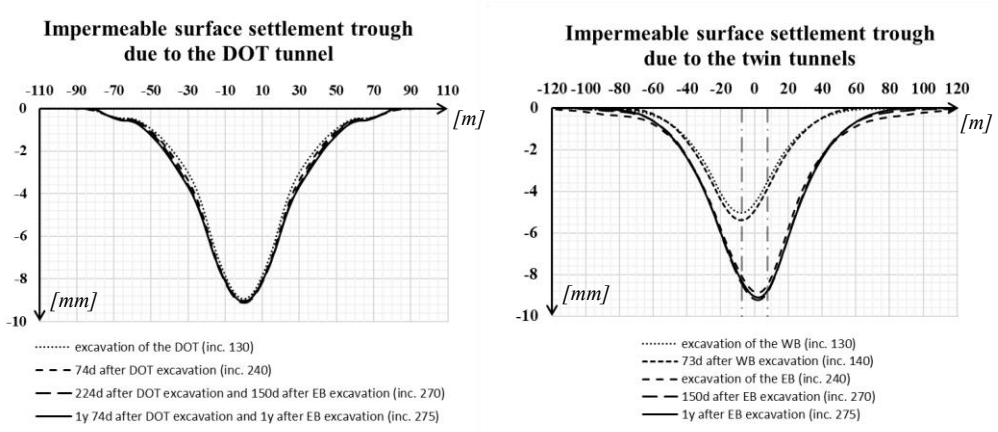

Fig. 5.6: *Impermeable surface settlement trough due to the DOT tunnel (on the left) and due to the twin tunnels (on the right)*

Fig. 5.7 shows the trends of the ground vertical subsurface displacements due to the excavation of the DOT tunnel at different depths following the same procedure reported in Chapter 4 for the twin tunnels numerical analysis. The principle of the phenomenon is very similar to that of the twin case reported in Fig. 4.12. Considering the permeable case, above the crown the magnitude of the maximum ground vertical displacement increases with the depth and the shape becomes narrower. With reference to the impermeable case, the greater the depth over the crown the more visible is the swelling phenomenon due to the gradual re-adjustment of the pore water pressure field.

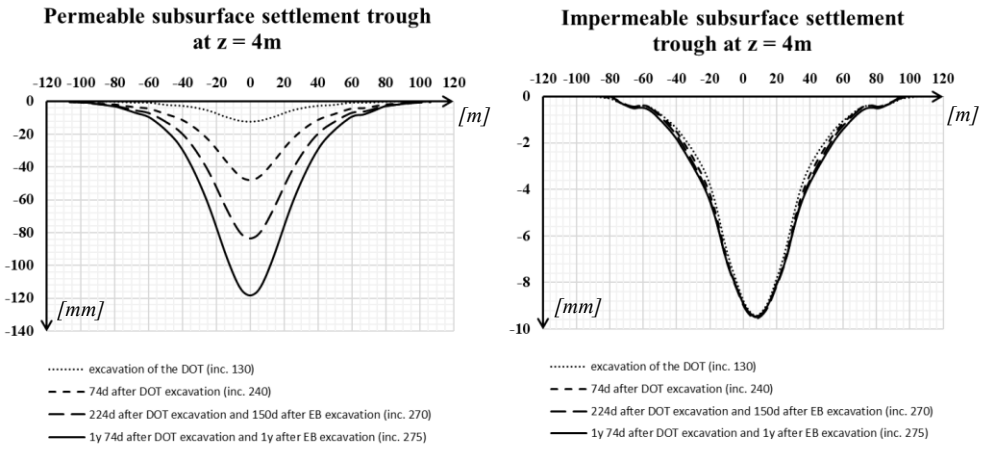

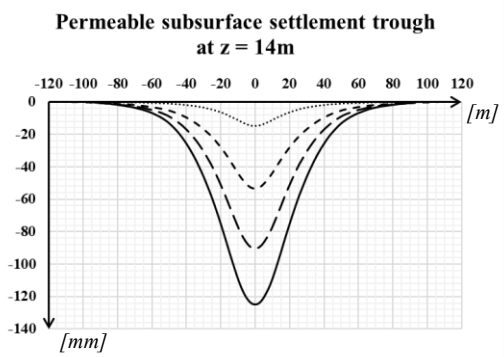
Permeable subsurface settlement trough at z = 14m
-120 -100 -80 -60 -40 -20 0 20 40 60 80 100 120
0 -20 -40 -60 -80 -100 -120 -140
[m]
[mm]

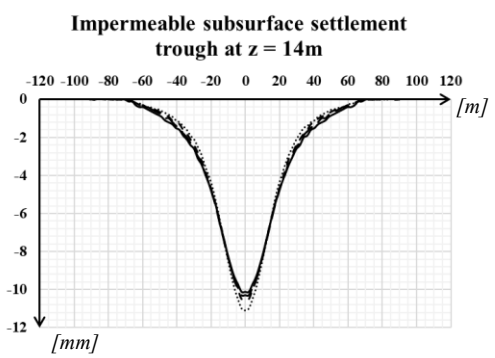
Impermeable subsurface settlement trough at z = 14m
-120 -100 -80 -60 -40 -20 0 20 40 60 80 100 120
0 -2 -4 -6 -8 -10 -12
[m]
[mm]

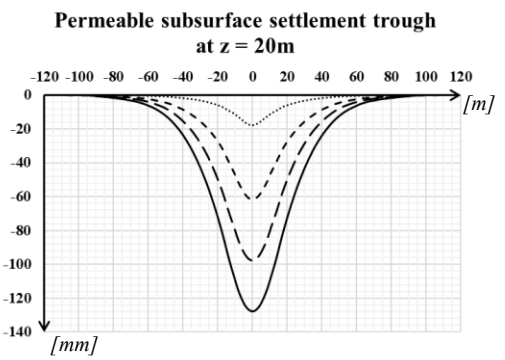
Permeable subsurface settlement trough at z = 20m
-120 -100 -80 -60 -40 -20 0 20 40 60 80 100 120
0 -20 -40 -60 -80 -100 -120 -140
[m]
[mm]

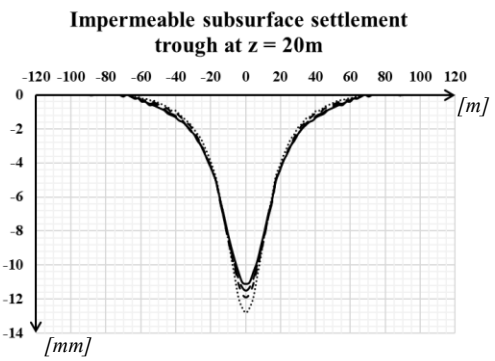
Impermeable subsurface settlement trough at z = 20m
-120 -100 -80 -60 -40 -20 0 20 40 60 80 100 120
0 -2 -4 -6 -8 -10 -12 -14
[m]
[mm]

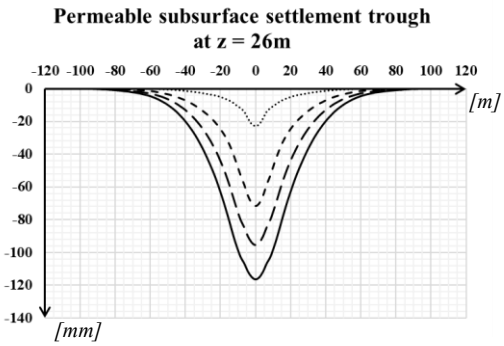
Permeable subsurface settlement trough at z = 26m
-120 -100 -80 -60 -40 -20 0 20 40 60 80 100 120
0 -20 -40 -60 -80 -100 -120 -140
[m]
[mm]

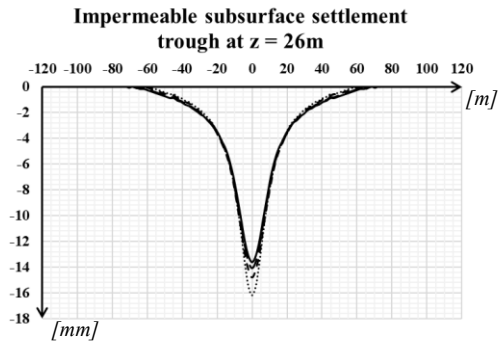
Impermeable subsurface settlement trough at z = 26m
-120 -100 -80 -60 -40 -20 0 20 40 60 80 100 120
0 -2 -4 -6 -8 -10 -12 -14 -16 -18
[m]
[mm]

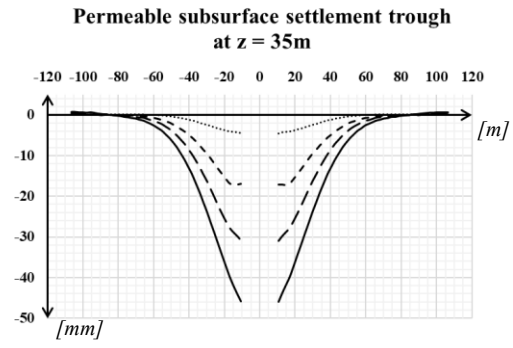
Permeable subsurface settlement trough at z = 35m
-120 -100 -80 -60 -40 -20 0 20 40 60 80 100 120
0 -10 -20 -30 -40 -50
[m]
[mm]

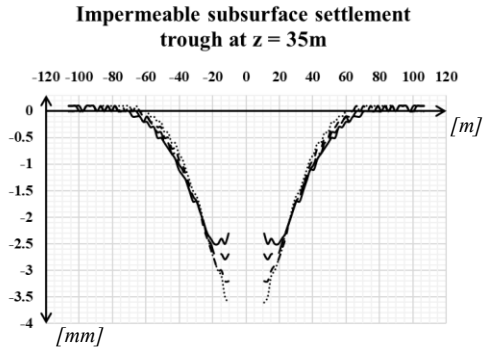
Impermeable subsurface settlement trough at z = 35m
-120 -100 -80 -60 -40 -20 0 20 40 60 80 100 120
0 -0.5 -1 -1.5 -2 -2.5 -3 -3.5 -4
[m]
[mm]

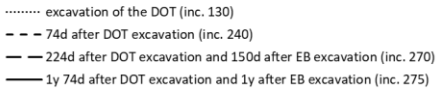
excavation of the DOT (inc. 130)
74d after DOT excavation (inc. 240)
224d after DOT excavation and 150d after EB excavation (inc. 270)
1y 74d after DOT excavation and 1y after EB excavation (inc. 275)

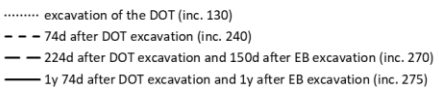
excavation of the DOT (inc. 130)
74d after DOT excavation (inc. 240)
224d after DOT excavation and 150d after EB excavation (inc. 270)
1y 74d after DOT excavation and 1y after EB excavation (inc. 275)

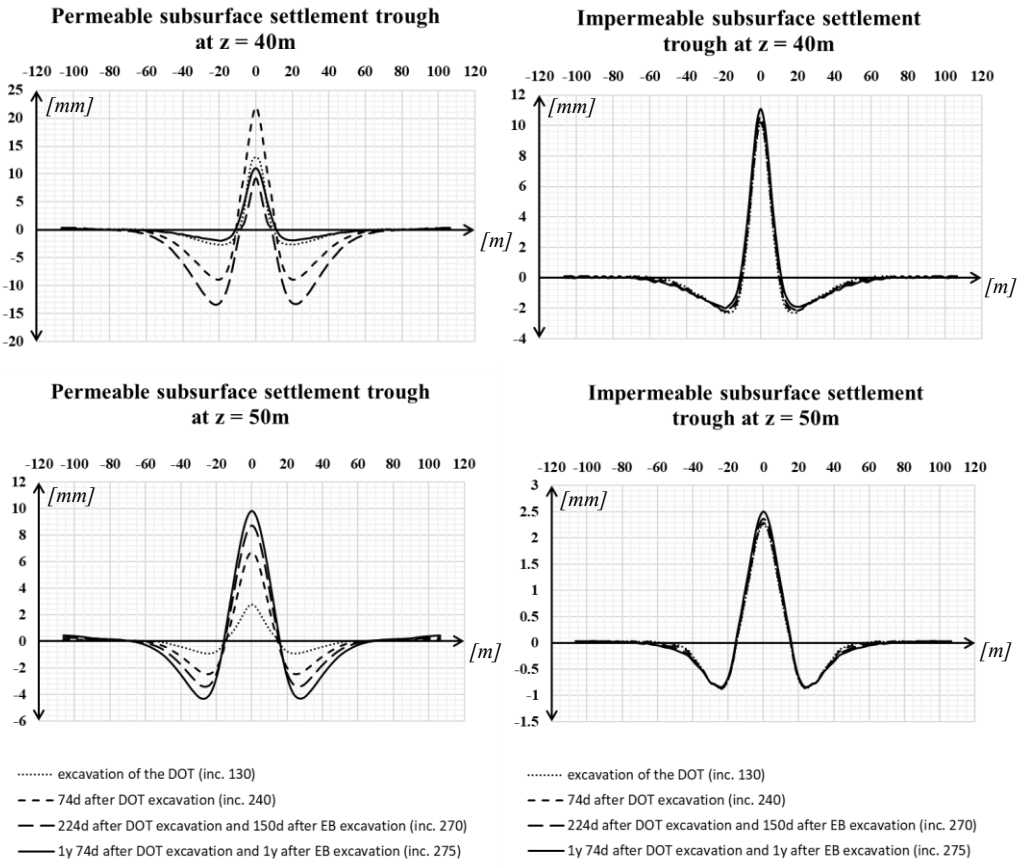

Fig. 5.7: *Permeable and impermable subsurface 'low triaxial' settlement troughs due to the DOT tunnel excavation at different depths below ground level: 4m, 14m, 20m, 26m, 35m, 40m, 50m.*

5.2.3 Long term response

For the study of the long-term effects due to the excavation of a DOT tunnel, the same procedure used in Paragraph 4.2.4 is still reported.

The evolution of the long-term permeable ground vertical surface settlement obtained from the 'low-both' numerical analysis of the DOT tunnels compared to that of the twin tunnels reveals curves with maximum values of settlement smaller than ten millimeters. Analysing the permeable case represented in Fig. 5.8, the convergence of the trends corresponding to the end of the soil consolidation phase can be considered reached 30 years after the end of the excavation.

The same can be said for the impermeable case. In this case, from about 1 year after the excavation, a swelling phenomenon similar to that which develops in the case of twin tunnels is evident. The magnitude of the vertical displacements is more contained despite the order is very small, just a few millimeters.

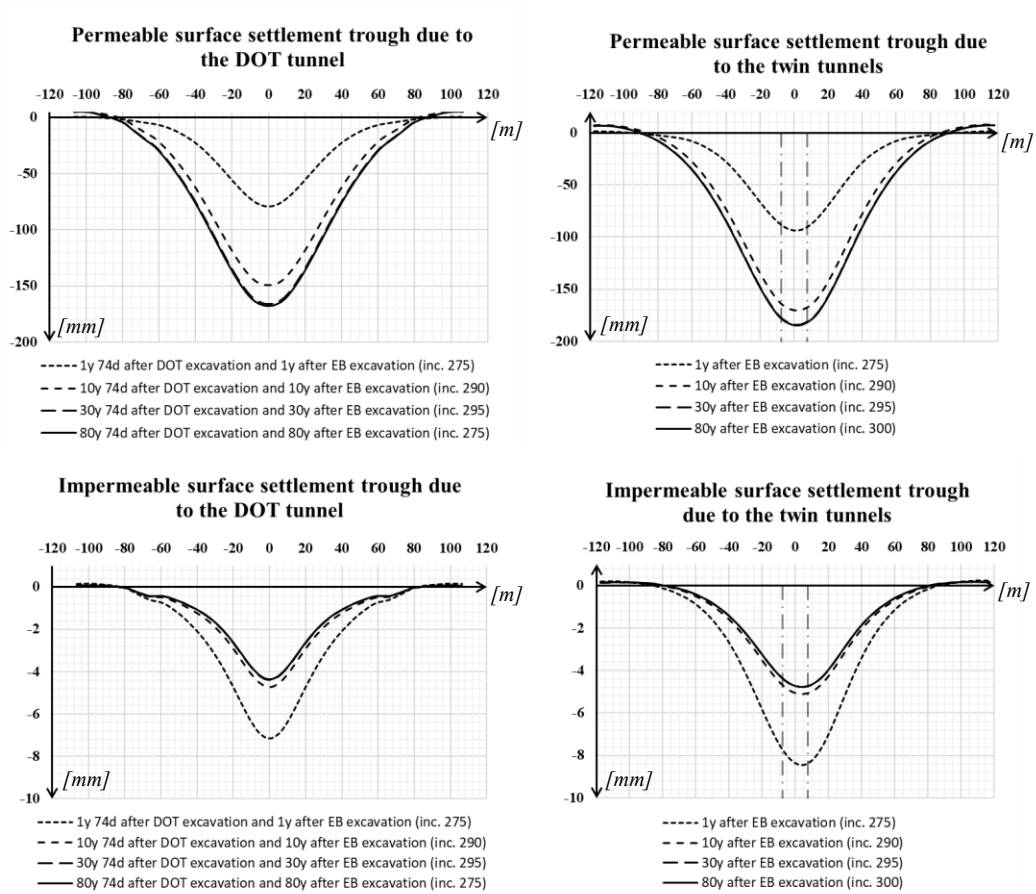

Fig. 5.8: *Permeable and impermeable surface settlement trough due to the DOT tunnel (on the left) and due to the twin tunnels (on the right)*

For the sake of completeness, the ground vertical subsurface displacements at different depths are reported as in the previous Chapter in Fig 5.9 to be compared with the results from the case of twin tunnels shown in Fig. 4.15. The main differences in the profiles are due to the particulare shape of the DOT tunnel and to the symmetry due to the lack of interaction between tunnels.

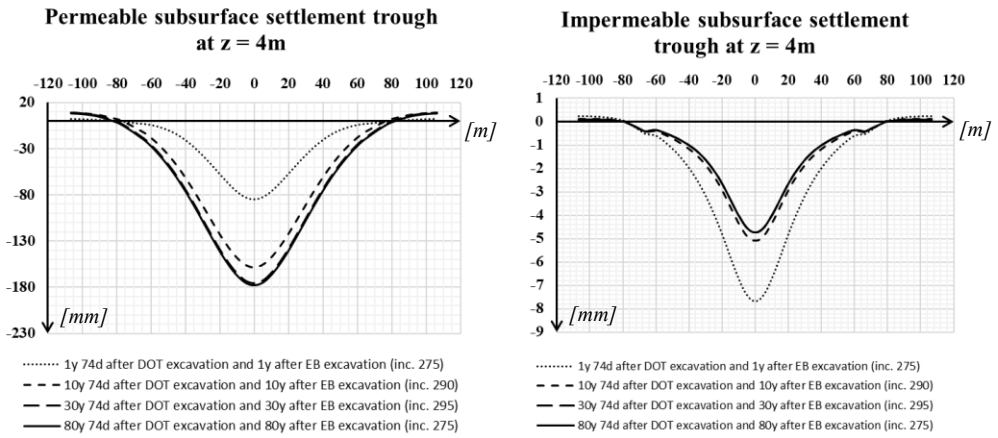

Permeable subsurface settlement trough at z = 14m

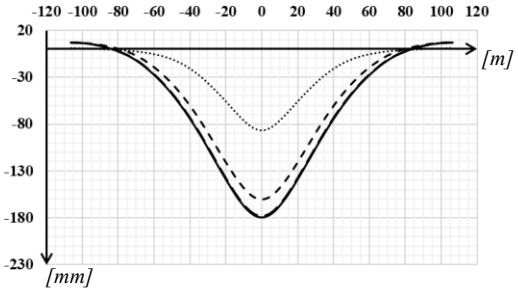

Impermeable subsurface settlement trough at z = 14m

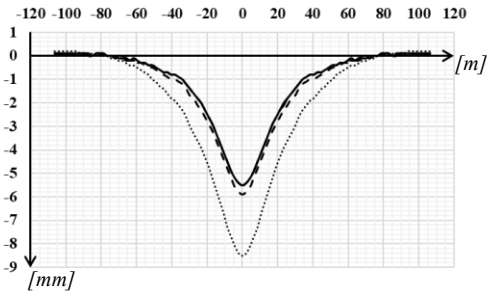

Permeable subsurface settlement trough at z = 20m

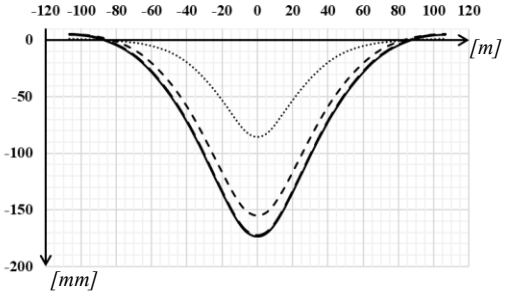

Impermeable subsurface settlement trough at z = 20m

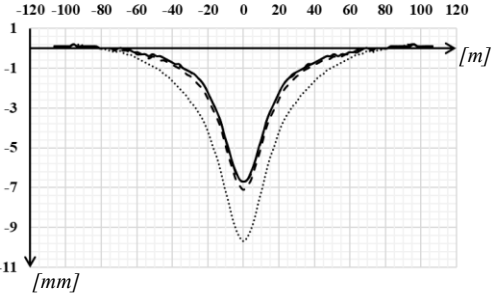

Permeable subsurface settlement trough at z = 26m

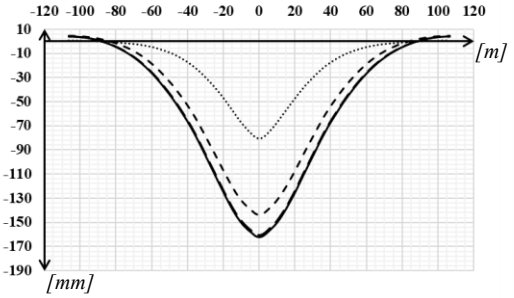

Impermeable subsurface settlement trough at z = 26m

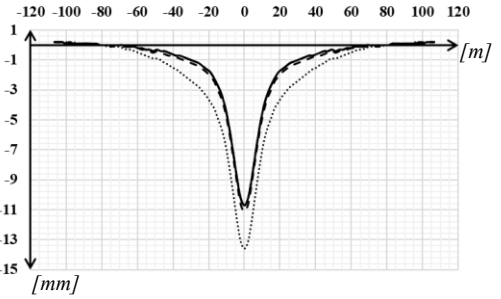

Permeable subsurface settlement trough at z = 35m

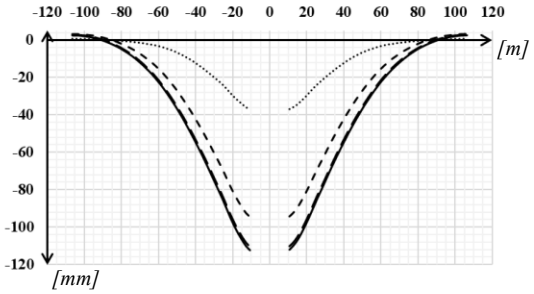

Impermeable subsurface settlement trough at z = 35m

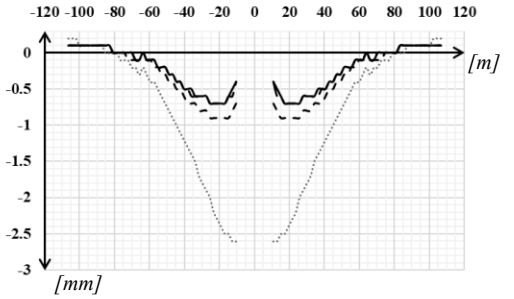

1y 74d after DOT excavation and 1y after EB excavation (inc. 275)
10y 74d after DOT excavation and 10y after EB excavation (inc. 290)
30y 74d after DOT excavation and 30y after EB excavation (inc. 295)
80y 74d after DOT excavation and 80y after EB excavation (inc. 275)

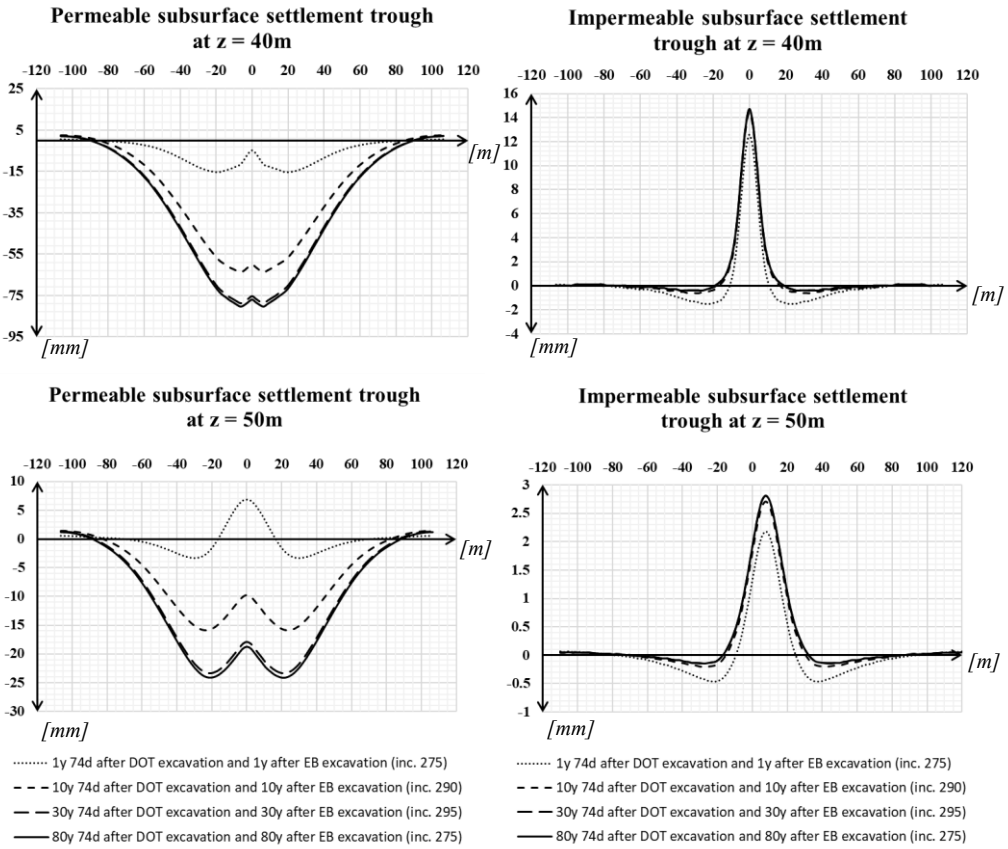

Fig. 5.9: *Permeable and impermable subsurface 'low both' settlement troughs due to the DOT tunnel excavation at different depths below ground level: 4m, 14m, 20m, 26m, 35m, 40m, 50m.*

Chapter 6

CONCLUSIONS

6.1 Summary and discussion

This research thesis represents a preliminary numerical investigation of the effects in terms of short- and long-term tunnelling-induced ground movements due to the construction of a DOT tunnel in the particular geological conditions of central London, in stiff heavily overconsolidated clays.

The available literature is still very limited, studies and measurements refer to few real cases compared to the traditional circular shield tunnelling technique and mainly in soft clay conditions such as Shanghai ones. Previous research efforts have made it possible to obtain numerical predictions of soil displacements due to tunnelling in London clay in good agreement with the values obtained in the field. To do this, it proved necessary to adopt an advanced kinematic two-surface constitutive model (named M2-SKH), to be preferred over traditional Cam clay models, which could take into account the material stress history by considering its markedly non-linear pre-yield behaviour in the small strain range and predict anisotropic stiffness values in relation to the loading/unloading direction. In view of a recent study in which it proved impossible to accurately calibrate the results of both oedometric and undrained triaxial tests using the same parameters, the model for short-term predictions was calibrated on triaxial tests and the model for long-term predictions considering the best compromise in terms of results on both tests.

The numerical analysis of the DOT tunnel was carried out superimposed on that of the new Crossrail twin tunnels on the greenfield monitored Hyde Park site in order to have a direct yardstick to quantify the results.

In both analyses the response of the ground vary greatly both in short- and long- term depending on the permeability of the lining. In the fully permeable case, the tunnel acts as a drain, causing a pore water pressure decreasing in the ground region surrounding the tunnel. This effect is associated with an increase of the deviatoric stress producing vertical displacements in the order of one

hundred and tens millimeters. On the other hand, in the impermeable case, the volume losses associated to the excavation are very small limited in the order of a few millimetres. During the consolidation phase the tunnel is pushed upwards as a result of a process of re-establishment of the pre-excavation conditions.

The construction of the second twin tunnel results in a greater volume loss than the first and leads to an asymmetric settlement trough with long-term maximum values shifted towards the second tunnel with respect to the central axis of the mesh. This phenomenon, which is the result of the plasticization of the soil following the excavation of the first tunnel reflected on the excavation of the second, is overcome by the excavation of a single DOT tunnel.

The results of this numerical research show that the use of this technique not only allows a more efficient use of underground space and faster progress in the construction of a two-way underground infrastructure without the need to build cross-passages, but at least theoretically, it is able to reduce the magnitude of ground surface settlements. The extension of the transversal surface region with respect to the direction of excavation affected by vertical settlements is as large as the region affected by the excavation of twin tunnels, so from this point of view there are no significant improvements.

Despite the potentials of DOT methodology, on a practical level controlling the trajectory in small curvature and unwanted movements such as rolling that can cause a surplus of volume losses is not easy, but as real cases in soft clays certainly prove possible and perspective for the future.

6.2 Future research

While awaiting confirmation of the good results obtained from the forthcoming research, which will also integrate considerations relating to the lining forces in particular into the modelling of the segmental nature of concrete lining under central London conditions, I believe it is appropriate to launch field tests in which to evaluate this technique at a practical level, seeking confirmation of the goodness of numerical predictions through direct measurements.

References

Addenbrooke, T. I. (1996) *Numerical analysis of tunnelling in stiff clay.* Imperial College London.

Addenbrooke, T. I. & Potts, D. M. (2001) Twin tunnel interaction: surface and subsurface effects. *International Journal of Geomechanics.* 1 (2), 249-271.

Addenbrooke, T. I., Potts, D. M. & Puzrin, A. M. (1997) The influence of pre-failure soil stiffness on the numerical analysis of tunnel construction. *Géotechnique.* 47 (3), 693-712.

Attewell, P. B. (1978) *Ground movements caused by tunneling in soil.* London, Pentech Press.

Attewell, P. B. & Woodman, J. P. (1982) Predicting the dynamics of ground settlement and its derivitives caused by tunnelling in soil. *Ground Engineering.* 15 (7), 13-22 & 36.

Attewell, P. B., Yeates, J. & Selby, A. R. (1986) Soil movements induced by tunnelling and their effects on pipelines and structures.

Avgerinos, V. (2014) *Numerical investigation of tunnelling beneath existing tunnels.* Imperial College London.

Avgerinos, V., Potts, D. M. & Standing, J. R. (2017) Numerical investigation of the effects of tunnelling on existing tunnels. *Géotechnique.* 1-15.

Avgerinos, V., Potts, D. M. & Standing, J. R. (2016) The use of kinematic hardening models for predicting tunnelling-induced ground movements in London Clay. *Géotechnique.* 66 (2), 106-120.

Avgerinos, V., Potts, D. M., Standing, J. R. & Wan, M. S. P. (2018) Predicting tunnelling-induced ground movements and interpreting field measurements using numerical analysis: Crossrail case study at Hyde Park. *Géotechnique.* 68 (1), 31-49.

Black, M., Dodge, C., Lawrence, U. & Institution of Civil Engineers (Great Britain). (2015) *Crossrail project: infrastructure design and construction. Volume one.* London, ICE Pub.

Broms, B. B. & Bennermark, H. (1967) Stability of clay at vertical openings. *Proceedings ASCE, Journal Soil Mechanics and Foundation Engineering.*

Burland, J. B. (1990) 30th Rankine Lecture: on the compressibility and shear strength of natural clays. *Géotechnique.* 40 (3), 329-378.

Burland, J. B., Standing, J. R. & Jardine, F. M. (2001a) *Building response to tunnelling: case studies from construction of the jubilee line extension, London.* Thomas Telford Publishing.

Burland, J. B., Standing, J. R. & Jardine, F. M. (2001b) *Building response to tunnelling: case studies from construction of the jubilee line extension, London.* Thomas Telford Publishing.

Diamond, R. S. & Kassel, B. G. (2018) A History of the Urban Underground Tunnel (4000 B.C.E. - 1900 C.E.). *Journal of Transportation Technologies.* 8 (1), 11-43.

EFNARC. (2015) *Specification and Guidelines for the use of specialist products for Mechanised Tunnelling (TBM) in Soft Ground and Hard Rock.*

Fang, Y. S., Kao, C. C. & Shiu, Y. S. (2012) Double-O-Tube shield tunneling for Taoyuan International Airport Access MRT. *Tunnelling and Underground Space Technology Incorporating Trenchless Technology Research.* 30 233-245.

Franzius, J. N. (2004) *The behaviour of buildings due to tunnel induced ground movements.* Ph.D. thesis, Imperial College London.

Gasparre, A. (2005) *Advanced laboratory characterisation of London Clay.* Imperial College London.

Gasparre, A. & Coop, M. R. (2008) The quantification of the effects of structure on the compression of a stiff clay. *Canadian Geotechnical Journal.* 45 1324-1334.

Gasparre, A., Nishimura, S., Coop, M. R. & Jardine, R. J. (2007) The influence of structure on the behaviour of London Clay. *Géotechnique.* 57 (1), 19-31.

Gasparre, A., Nishimura, S., Minh, N. A., Coop, M. R. & Jardine, R. J. (2007) The stiffness of natural London Clay. *Géotechnique.* 57 (1), 33-47.

Glossop, N. H. (1978) *Soil deformation caused by soft ground tunnelling.* PhD. thesis, University of Durham [referenced in Lake et al. (1992)].

Gonzalez, N. A., Rouainia, M., Arroyo, M. & Gens, A. (2012) Analysis of tunnel excavation in London Clay incorporating soil structure. *Géotechnique.* 62 (12), 1095-1109.

Grammatikopoulou, A. (2004) *Development, implementation and application of kinematic hardening models for overconsolidated clays.* Imperial College London.

He, C., Teng, L. & Yan, J. Y. (2008) The double-o-tube shield tunnel in Shanghai soil. In: Anonymous *Geotechnical Aspects of Underground Construction in Soft Ground*, CRC Press. pp. 329-334.

Hight, D. W., Gasparre, A., Nishimura, S., Minh, N. A., Jardine, R. J. & Coop, M. R. (2007) Characteristics of the London Clay from the terminal 5 site at Heathrow airport. *Géotechnique.* 57 (1), 3-18.

Hurrell, M. R. (1985) *The empirical prediction of long-term surface settlements above shield- driven tunnels in soil.* London, Pentech Press.

Jardine, R. J., Potts, D. M., Fourie, A. B. & Burland, J. B. (1986) Studies of the influence of non-linear stress-strain characteristics in soil-structure interaction. *Géotechnique.* 36 (3), 377–396.

Jardine, R. J., Symes, M. J. & Burland, J. B. (1984) The measurement of soil stiffness in the triaxial apparatus. *Géotechnique.* 34 (3), 323–340.

Kuzuno, T., Takasaki, H., Tanaka, M. & Tamai, T. (1996) Driving control and ground behaviour of triple circular face shield machine. *GeotechnicalAspects of Underground Construction in Soft Ground, Edt. R.J. Mair & R.N. Taylor, Balkama, Rotterdam.* 283-286.

Lake, L. M., Rankin, W. J. & Hawley, J. (1992) *Prediction and effects of ground movements caused by tunnelling in soft ground beneath urban areas.*

Macklin, S. R. (1999) The prediction of volume loss due to tunnelling in overconsolidated clay based on geometry and stability number. *Ground Engineering.* 32 (4), 30-33.

Mair, R. J. (2008) Tunnelling and geotechnics: new horizons. *Géotechnique,.* 58 (9), 695–736.

Mair, R. J. (1998a) Geotechnical aspects of design criteria for bored tunnelling in soft ground. *Proceedings of world tunnel congress on tunnels and metropolis.* Sao Paulo pp.183–199.

Mair, R. J. (1998b) *Recent Experiences of Tunneling and Deep Excavations in London.*

Mair, R. J., Gunn, M. J. & O'Reilly, M. P. (1981) Ground movements around shallow tunnels in soft clay. *Proceedings of the 10th International Conference on Soil Mechanics and Foundation Engineering.* Stockholm.

Mair, R. J. & Taylor, R. N. (1997) Bored tunnelling in the urban environment: State-of-the-art reportand theme lecture. *Proceedings of 14th International Conference of Soil Mechanics and Foundation Engineering. 6-12 September 1997,* Hamburg, A.A. Balkema, Rotterdam pp.2353-2385.

Mair, R. J., Taylor, R. N. & Bracegirdle, A. (1993) Subsurface settlement profiles above tunnels in clays. *Géotechnique.* 43 (2), 315-320.

Mašin, D. & Herle, I. (2005) Numerical analysis of a tunnel in London Clay using different constitutive models. *Proceedings of the 5th international symposium TC28 on geotechnical aspects of underground construction in soft ground.* Amsterdam, Netherlands pp.595-600.

Moriya, Y. (2000) Special shield tunneling methods in Japan. *Singapore. Proc. of International Conference on Tunnels and Underground Structures. 26-29 November,* pp.249-254.

Nyren, R. J. (1998) *Field measurements above twin tunnels in London clay.* Imperial College London.

O'Reilly, M. P. & New, B. M. (1982) Settlements above tunnels in the United Kingdom - their magnitude and prediction. *Tunnelling '82.* The Institution of Mining and Metallurgy, London pp.55-64.

O'Reilly, M. P. (1988) Evaluating and predicting ground settlements caused by tunnelling in London Clay. *Tunnelling '88.* Institution of Mining and Metallurgy. London pp.231-241.

Panet, M. & Guenot, A. (1982) Analysis of convergence behind the face of a tunnel. *Tunnelling '82.* The Institution of Mining and Metallurgy, London pp.197-204.

Peck, R. B. (1969) Deep excavations and tunnelling in soft ground. *Proceedings of the 7th international Conference on Soil Mechanics and Foundation Engineering.* Mexico city, State of the art Volume. pp.225-290.

Potts, D. M. & Zdravkovic, L. (2001) *Finite element analysis in geotechnical engineering - application.* Thomas Telford Publishing.

Potts, D. M. & Zdravkovic, L. (1999) *Finite element analysis in geotechnical engineering - theory.* Thomas Telford Publishing.

Puzrin, A. M. & Burland, J. B. (1998) Non-linear model of small-strain behaviour of soils. *Géotechnique.* 48 (2), 217-233.

Ren, D. J., Shen, S. L., Arulrajah, A. & Wu, H. N. (2018) Evaluation of ground loss ratio with moving trajectories induced in double-O-tube (DOT) tunnelling. *Canadian Geotechnical Journal.* 55 (6), 894-902.

Rowe, R. K., Lo, K. Y. & Kack, G. J. (1983) A method of estimating surface settlement above tunnel constructed in soft ground. *Canadian Geotechnical Journal.* 20 11-22.

Schmidt, B. (1969) *Settlements and ground movements associated with tunnelling in soil.* PhD. thesis, University of Illinois [referenced in Lake et al. (1992)].

Shin, J. H., Addenbrooke, T. I. & Potts, D. M. (2002) A numerical study of the effect of groundwater movement on long-term tunnel behaviour. *Géotechnique.* 52 (6), 391-403.

Standing, J. R., Nyren, R. J., Burland, J. B. & Longworth, T. I. (1996) The measurement of ground movement due to tunnelling at two control sites along the Jubilee Line Extension. *Proceedings of the International Symposium on Geotechnical Aspects of Underground Construction in Soft Ground.* Balkema, Rotterdam pp.751–756.

Standing, J. R. & Burland, J. B. (2006) Unexpected tunnelling volume losses in the Westminster area, London. *Géotechnique.* 56 (1), 11-26.

Sugiyama, T., Hagiwara, T., Nomoto, T., Nomoto, M., Ano, Y., Mair, R. J., Bolton, M. D. & Soga, K. (1999) *Observation of ground movements during tunnel construction by slurry shield method at the Docklands Light Railway Lewisham Extension - East London.* 3rd edition. Japanese Geotechnical Society.

Swoboda, G. (1979) Finite element analysis of the new Austrian tunneling method (NATM). 54 223-229.

Wan, M., Standing, J. R., Potts, D. M. & Burland, J. B. (2017) Measured short-term subsurface ground displacements from EPBM tunnelling in London Clay.

West, G. (1988) Innovation and the rise of the tunnelling industry: Cambridge University Press. *Tunnelling and Underground Space Technology Incorporating Trenchless Technology Research.* 3 (2), 220.

Wongsaroj, J., Soga, K. & Mair, R. J. (2007) Modelling of long-term ground response to tunnelling under St James's Park, London. *Géotechnique.* 57 (1), 75-90.

Zhang, T. L. (2007) *Research on the ground movement induced by the disturbance of multi-circular shield construction and its control technology.* Tongji university, Shanghai, China.

Zhou, D. & Zdravkovic, L. (2020) *Numerical analysis of Double-O-Tube shield tunneling in Shanghai.*

Zhou, W., Wu, W. & Gu, C. (2005) DOT shield driving technology applied in running tunnel project for Shanghai metro. *Proceedings of the 3rd Japan-China technological exchange of shield-driven tunneling in 2005.* Waseda University, Japan pp.269-276.